Thomas Hebbeker

Tests of Quantum Chromodynamics in Hadronic Decays of Z^0 Bosons Produced in e^+e^- Annihilation

TESTS OF QUANTUM CHROMODYNAMICS IN HADRONIC DECAYS OF Z^0 BOSONS PRODUCED IN e^+e^- ANNIHILATION

Thomas HEBBEKER

III Physikalisches Institut, RWTH Aachen, Germany

NORTH-HOLLAND

PHYSICS REPORTS (Review Section of Physics Letters) 217, 2 & 3 (1992) 69–157.
North-Holland

PHYSICS REPORTS

Tests of Quantum Chromodynamics in hadronic decays of Z^0 bosons produced in e^+e^- annihilation*

Thomas Hebbeker

III Physikalisches Institut, RWTH Aachen, Germany

Received April 1992; editor: R. Petronzio

Contents:

Abstract:

Hadronic decays of the Z^0 produced in e^+e^- annihilation are ideal for precise tests of Quantum Chromodynamics. A large number of measurements has been performed, based on the large data sets of more than 400 000 hadronic events observed by the each of the experiments ALEPH, DELPHI, L3 and OPAL at LEP. The most important results are: (a) the strong coupling constant is $\alpha_s(m_Z) = 0.119 \pm 0.007$. The energy dependence of the 3-jet fraction measured in e^+e^- annihilation between 14 and 91 GeV shows that α_s is running as predicted by QCD. The strong interaction is flavor-independent. (b) Second order QCD matrix element calculations reproduce all measured distributions for *jets* in 3-jet and 4-jet events. There is direct experimental evidence for the gluon self interaction. (c) All measured distributions for *hadrons* can be reproduced by QCD Monte Carlo programs or analytical calculations.

* Supported by the German Bundesministerium für Forschung und Technologie.

1. Foreword

Quantum Chromodynamics (QCD) [1–3] is *the* theory of the strong force. It can explain – at least qualitatively – all measurements of strong interaction phenomena, ranging from bound states of quarks, baryons and mesons, to asymptotic freedom at short distances [4]. However, the precision of QCD tests is limited to typically 10% for the following reasons: perturbative calculations are difficult due to the large number of diagrams involved, and the convergence of the series expansion in α_s is poor due to the large value of the strong coupling constant. In addition, non perturbative effects (hadronization, structure functions) have to be taken into account, which today must be modeled. It is important to push the accuracy of QCD tests as far as possible, and to extend the tests to many processes.

Major contributions to the establishment of QCD have come from the study of deep inelastic lepton–nucleon scattering, hadron–hadron collisions, quarkonium decays, and hadron production in e^+e^- annihilation at center of mass energies between 12 and 64 GeV.

In e^+e^- collisions the initial state is simple and completely known, therefore allowing for clean tests of Quantum Chromodynamics. The additional advantages of high energy and large event samples make the Z^0 resonance an ideal laboratory for QCD studies.

A large number of measurements of hadronic Z^0 decays have been performed at the e^+e^- colliders LEP and SLC in the years 1989–1991. A wealth of experimental results on QCD tests has been published in about fifty papers. In this review only results published or available in form of preprints by the beginning of 1992 are considered. I concentrate on those measurements for which calculations in the framework of Quantum Chromodynamics are available, in order to extract the strong coupling constant α_s, and to test the theory of strong interactions. For each of the main topics I will describe, as an example, the analysis of *one* experiment and then compare and summarize the results of all available measurements.

Here I consider mainly QCD tests based on the process $e^+e^- \rightarrow$ hadrons. As far as possible I will compare experimental results obtained for center of mass energies from above 10 GeV ($b\bar{b}$ threshold) to 91 GeV (Z^0 mass) and will also extrapolate up to 160 GeV (W^+W^- threshold). At the end of this report I will discuss possibilities for future QCD tests at LEP and SLC.

In the introduction (section 2) I briefly introduce QCD, describe the process $e^+e^- \rightarrow$ hadrons, and give an overview of the experiments at LEP and SLC. In section 3 comparisons between measurements and Monte Carlo simulations for hadron production in e^+e^- collisions are presented. Section 4 is devoted to measurements of the strong coupling constant α_s, and to related tests of Quantum Chromodynamics. This includes a comparison of α_s values obtained in different reactions (universality), for different quark species (flavor independence), and at different energies ('running'). Detailed QCD tests based on 3-jet and 4-jet events, and in particular the measurement of the three-gluon coupling, are described in section 5. "Soft" phenomena such as particle spectra and string effect are the topic of section 6. Finally the prospects for future QCD studies at the Z^0 resonance are outlined in section 7.

Throughout this report a system of units is used with $\hbar = 1$ and $c = 1$. For Dirac's γ matrices I use the conventions given in ref. [5]. If numerical values for α_s are quoted without the energy scale being mentioned explicitly, they always refer to $\alpha_s(m_Z)$. All errors and resolutions correspond to a confidence level of 68% unless stated otherwise.

For brief general introductions to QCD and related tests see for example refs. [4, 6]. References to recent books on this subject are given in ref. [7]. Theoretical reviews on QCD tests in e^+e^- collisions can be found in refs. [8–12]. Measurements in e^+e^- annihilation at center of mass energies below the Z^0 mass are summarized in refs. [13, 14].

2. Introduction

2.1. Quantum Chromodynamics

Quantum Chromodynamics (QCD) [1–3] is a nonabelian gauge theory with an SU(3) group structure describing the interaction of colored spin-1/2 quarks with colored spin-1 gluons.

Strong interactions have been discovered and investigated in detail at the level of nuclei. QCD explains strong interactions at the level of quarks, which are glued together via gluons: baryons are made out of three quarks, and mesons are quark–antiquark bound states. Today we understand the inter-nucleon forces as a kind of "van der Waals" residual interaction between color neutral 3-quark bound states. Unfortunately it is not yet possible to use this knowledge to make quantitative predictions for nucleon interactions and properties of nuclei. This will hopefully become possible with further progress of QCD lattice gauge calculations [15]. Due to the current limitations of calculations within perturbative QCD quantitative tests of the theory can be done only at the parton level.

2.1.1. History

The theory of Quantum Chromodynamics is about 20 years old. Here I review the experimental milestones and new theoretical concepts that led to the development of this theory of strong interactions and to its consolidation.

Quarks were formally introduced as constituents of mesons and baryons in the Gell-Mann–Zweig model [16]. It was realized that quarks are naturally associated with the pointlike constituents (named partons [17]) discovered in deep inelastic lepton–nucleon scattering [18].

The concept of *color* [19] was introduced in order to avoid spin statistics problems appearing for baryons made out of three quarks with the same flavor, for example the Δ^{++} resonance. Assigning to the quarks a new quantum number color, corresponding to a new symmetry SU(N_C), solves this problem. The number N_C of color degrees of freedom was measured from the partial decay width of neutral pions into photons ($\sim N_C^2$) [20]*), from the total hadronic cross section in e^+e^- collisions ($\sim N_C$) [22–24] and from other processes.

Gluons were invented to explain hadrons as dynamically bound quark states [1]. They play the role of the glue that holds the quarks together. The "invisible" particles in electron nucleon collisions [18] could be identified with the electrically neutral gluons.

Important for the development of QCD as a nonabelian gauge theory with a coupling constant decreasing with energy were the concepts of *confinement* [25] and *asymptotic freedom* [2]: free quarks do not exist, one can observe only color neutral hadrons; at high momentum transfer quarks behave as almost free particles.

Significant contributions to the establishment of QCD from e^+e^- experiments at high energies are listed in section 2.2.

*) For earlier references, in particular for the π^0 lifetime, see also ref. [21].

2.1.2. QCD Lagrangian and fundamental vertices

The QCD Lagrangian has the form [6]:

$$\mathcal{L} = \bar{q}_\alpha^{a,j}\left[\mathrm{i}\gamma^\mu_{\alpha\beta}(\delta_{ab}\partial_\mu + \mathrm{i}g_s t^r_{ab} g^r_\mu) - m_j\delta_{ab}\delta_{\alpha\beta}\right]q_\beta^{b,j} - \tfrac{1}{4}F^r_{\mu\nu}F^{r,\mu\nu}\,. \tag{2.1}$$

Over repeated indices is to be summed:

$\alpha,\beta,\ldots = 1,2,3,4,$	Dirac index,
$\mu,\nu,\ldots = 1,2,3,4,$	space time index,
$a,b,\ldots = 1,\ldots,N_C = 3,$	quark color index,
$r,s,\ldots = 1,\ldots,N_C^2 - 1 = 8,$	gluon color index,
$j,k,\ldots = 1,\ldots,N_F,$	flavor index.

The spin-1/2 quark fields are $q_\alpha^{a,j}$ and their masses are m_j. The fields F are related to the vector gluon fields g^r_μ by

$$F^r_{\mu\nu} = \partial_\mu g^r_\nu - \partial_\nu g^r_\mu - g_s f^{rst} g^s_\mu g^t_\nu\,. \tag{2.2}$$

The SU(3) generators t^r satisfy the relation

$$t^r t^s - t^s t^r = \mathrm{i}f^{rst}t^t \tag{2.3}$$

with structure constants f^{rst}. The quantity g_s is related to the QCD coupling constant

$$\alpha_s = g_s^2/4\pi\,, \tag{2.4}$$

the analogue to the fine structure constant $\alpha \approx \frac{1}{137}$ in Quantum Electrodynamics (QED). The Lagrangian also contains gauge fixing and ghost terms, which are not shown here.

The Lagrangian (2.1) is invariant under local gauge transformations

$$q^a(x) \to U_{ab}q^b(x)\,, \quad g_\mu(x) \to U g_\mu U^{-1} + \mathrm{i}/g_s U\partial_\mu U^{-1}\,, \tag{2.5}$$

with

$$U \equiv U(x) = \exp[\mathrm{i}g_s\theta_r(x)t^r]\,. \tag{2.6}$$

The first term in eq. (2.1) contains the quark–gluon interaction

$$\mathrm{qgq} \sim g_s\bar{q}t^r\gamma^\mu g^r_\mu q\,, \tag{2.7}$$

while the second term describes the three-gluon vertex

$$\mathrm{ggg} \sim g_s f^{rst} g^r_\mu g^s_\nu\,\partial^\mu g^{t,\nu} \tag{2.8}$$

and the four-gluon self interaction:

$$\mathrm{gggg} \sim g_s^2 f^{rst} f^{ruv} g^s_\mu g^t_\nu g^{u,\mu} g^{v,\nu}\,. \tag{2.9}$$

Note that the coupling strengths of all three vertices are described by the same constant. The corresponding basic Feynman graphs are shown in fig. 2.1.

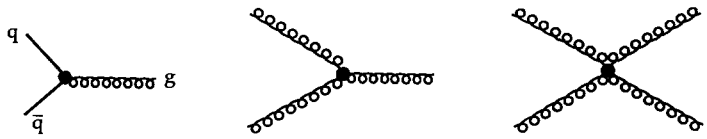

Fig. 2.1. Basic Feynman diagrams in QCD.

In QCD the so called color factors C_A, C_F and T_F are given by the relations [6]

$$f^{rst}f^{rsu} = \delta^{tu}C_A, \quad C_A = N_C = 3, \tag{2.10}$$

$$t^r_{ab}t^r_{bc} = \delta_{ac}C_F, \quad C_F = (N_C^2 - 1)/2N_C = 4/3, \tag{2.11}$$

$$t^r_{ab}t^s_{ba} = \delta^{rs}T_F, \quad T_F = 1/2. \tag{2.12}$$

They are a measure of the coupling strengths of the triple gluon vertex, of the gluon radiation off quarks and of the gluon splitting into quark and antiquark, respectively. For applications see section 5.2.2. While in an $SU(N_C)$ gauge theory and in particular in QCD the quantities N_C and C_A are equal, they describe different properties of the strong interactions. N_C is the number of color degrees of freedoms of quarks, and C_A describes the self coupling strength of gluons.

2.1.3. Running coupling constant

In Quantum Chromodynamics, as in other field theories, ultraviolet divergences must be removed by the renormalization of fields and couplings [3]. Different schemes exist. For technical reasons in QCD most often dimensional regularization is applied, and in particular the $\overline{\text{MS}}$ scheme [26], which I will use throughout this review. In this modified minimal subtraction scheme calculations are performed with $n \neq 4$ space time dimensions and divergences are expressed as poles in $\epsilon = |4-n|$. These poles, together with a constant term, are subtracted to obtain finite quantities.

The renormalization formalism leads to the running of coupling constants, described by the renormalization group equation

$$\mu^2 \partial\alpha_s/\partial\mu^2 = -(\beta_0\alpha_s^2 + \beta_1\alpha_s^3 + \beta_2\alpha_s^4 + \cdots). \tag{2.13}$$

Here the renormalization scale μ appears, which can be interpreted as an energy scale. $\alpha_s(\mu)$ is then the coupling constant describing strong interactions at an energy scale μ or distance $1/\mu$. Observables are independent of μ, see section 4.1.

The first three coefficients have been calculated [2,27,28]:

$$\beta_0 = (11 - \tfrac{2}{3}N_F)/4\pi = 0.610, \quad \beta_1 = (102 - \tfrac{38}{3}N_F)/(4\pi)^2 = 0.245,$$

$$\beta_2 = (\tfrac{2857}{2} - \tfrac{5033}{18}N_F + \tfrac{325}{54}N_F^2)/(4\pi)^3 = 0.091 \tag{2.14}$$

The numerical values have been computed using $N_F = 5$ for the number of active flavors. The lowest order coefficients of the beta function, in particular β_0, are positive, which leads to a decrease of the coupling with increasing energy μ. This is different from QED, where the beta function has the other sign, causing α to increase with μ.

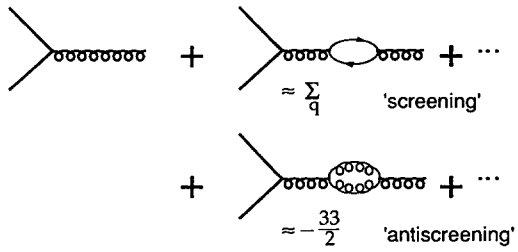

Fig. 2.2. Feynman diagrams contributing to the effective coupling strength in QCD.

The sign of β_0 in QCD is due to the gluon self coupling. Figure 2.2 shows the lowest order diagram and graphs with quark and gluon loops contributing to the coupling "seen" by a quark scattering off a gluon with momentum transfer $|q^2| = \mu^2$. The internal quark loops lead to a "screening" of the bare coupling, that is a reduction of α_s for large distances (small μ); the gluon loops however are the cause of "antiscreening". The strength of the screening effect is proportional to the number N_F of quark flavors contributing, which are those with mass below the renormalization scale μ. The gluon loops contribute a positive constant term $11/4\pi$ to β_0, which exceeds the negative contribution $-N_F/6\pi$ due to the quark loops if the number N_F of flavors does not exceed 16.

The solution to the evolution equation in lowest order,

$$\mu^2 \partial\alpha_s/\partial\mu^2 \equiv \partial\alpha_s/\partial \ln\mu^2 = -\beta_0\alpha_s^2, \tag{2.15}$$

can be written as

$$\alpha_s(\mu) = \alpha_s(\mu_0)/[1 + \beta_0\alpha_s(\mu_0)\ln(\mu^2/\mu_0^2)], \tag{2.16}$$

where μ_0 is a reference scale. Defining

$$\Lambda = \mu_0 \exp[-1/2\beta_0\alpha_s(\mu_0)] \tag{2.17}$$

leads to the equivalent expression

$$\alpha_s(\mu) = \frac{1}{\beta_0 \ln(\mu^2/\Lambda^2)}. \tag{2.18}$$

There is one free parameter, which can either be chosen as $\alpha_s(\mu_0)$, for a given scale μ_0, or as Λ. The parameter Λ indicates the boundary between non perturbative and perturbative energy ranges. It depends through β_0 on the number of flavors N_F. The parameter α_s is more directly related to measurements and is a function of the scale μ.

When comparing α_s or Λ values from different publications a great deal of caution is required [6, 29]: In practice a variety of expressions are used for the relation between Λ and α_s corresponding to different

- renormalization schemes (MOM, MS, $\overline{\text{MS}}$),
- numbers of "active flavors" N_F in the coefficients β_i (3, 4, 5),
- orders in perturbative expansion, (leading, next-to-leading, second subleading; corresponding to a truncation of the β function after the first, second or third term),
- choices of constant of integration for the solution of the evolution equation,

Table 2.1
Relation between $\alpha_s(m_Z)$ and $\Lambda^{(N_F)}$/GeV according to formula (2.19).

α_s	$\Lambda^{(5)}$	$\Lambda^{(4)}$	$\Lambda^{(3)}$	α_s	$\Lambda^{(5)}$	$\Lambda^{(4)}$	$\Lambda^{(3)}$	α_s	$\Lambda^{(5)}$	$\Lambda^{(4)}$	$\Lambda^{(3)}$
0.091	0.031	0.054	0.078	0.111	0.149	0.225	0.283	0.131	0.436	0.589	0.668
0.092	0.034	0.059	0.084	0.112	0.159	0.238	0.298	0.132	0.456	0.613	0.692
0.093	0.038	0.065	0.092	0.113	0.169	0.252	0.313	0.133	0.476	0.637	0.715
0.094	0.041	0.070	0.098	0.114	0.179	0.265	0.328	0.134	0.498	0.664	0.741
0.095	0.045	0.076	0.106	0.115	0.190	0.280	0.344	0.135	0.519	0.688	0.765
0.096	0.049	0.082	0.114	0.116	0.202	0.296	0.362	0.136	0.542	0.715	0.791
0.097	0.054	0.090	0.123	0.117	0.214	0.312	0.379	0.137	0.565	0.742	0.817
0.098	0.058	0.096	0.131	0.118	0.226	0.327	0.396	0.138	0.588	0.769	0.843
0.099	0.063	0.103	0.140	0.119	0.239	0.344	0.414	0.139	0.613	0.798	0.870
0.100	0.068	0.111	0.149	0.120	0.253	0.362	0.434	0.140	0.637	0.826	0.896
0.101	0.074	0.120	0.160	0.121	0.267	0.380	0.453	0.141	0.663	0.856	0.923
0.102	0.080	0.128	0.170	0.122	0.281	0.398	0.472	0.142	0.689	0.885	0.951
0.103	0.086	0.137	0.181	0.123	0.296	0.417	0.492	0.143	0.716	0.916	0.979
0.104	0.092	0.146	0.191	0.124	0.312	0.437	0.513	0.144	0.743	0.947	1.006
0.105	0.099	0.156	0.203	0.125	0.328	0.457	0.533	0.145	0.771	0.978	1.034
0.106	0.107	0.167	0.216	0.126	0.344	0.477	0.554	0.146	0.799	1.009	1.062
0.107	0.114	0.177	0.228	0.127	0.361	0.498	0.576	0.147	0.829	1.043	1.091
0.108	0.122	0.188	0.240	0.128	0.379	0.520	0.598	0.148	0.859	1.076	1.120
0.109	0.131	0.200	0.255	0.129	0.397	0.542	0.620	0.149	0.889	1.109	1.148
0.110	0.140	0.213	0.269	0.130	0.416	0.565	0.644	0.150	0.920	1.143	1.176

– approximations in the solution of the evolution equation (exact, expansion in inverse powers of $\ln(\mu^2/\Lambda^2)$, ...).

For a given value of Λ the numerical differences can be bigger than 10% in α_s and are therefore in general not negligible. The μ dependence of α_s also depends on the choice of the α_s formula, however the differences are small for the commonly used relations and can often be neglected [29].

In this report I use the next-to-leading order formula [20]

$$\alpha_s(\mu) = \frac{1}{\beta_0 \ln(\mu^2/\Lambda^2)} \left(1 - \frac{\beta_1}{\beta_0^2} \frac{\ln\ln(\mu^2/\Lambda^2)}{\ln(\mu^2/\Lambda^2)}\right), \tag{2.19}$$

which has been used by all LEP and SLC collaborations. The corresponding formula to second subleading order [30] agrees with expression (2.19) to about 1% for the same values of Λ and μ. Table 2.1 shows relation (2.19) in tabular form for $\mu = m_Z$.

For historical reasons most often Λ has been used as the fundamental parameter in QCD due to a lack of a "natural" scale $\mu_0 \gg \Lambda$. Today we have a convenient reference scale $\mu_0 = m_Z$ and I will express the QCD coupling strength in terms of $\alpha_s \equiv \alpha_s(m_Z)$ from now on.

The measured value for $\Lambda^{(5)}_{\overline{\text{MS}}}$ of about 0.15 GeV [4] corresponds to $\alpha_s \approx 0.11$.

Figure 2.3 shows the characteristic energy dependence of α_s, which is often referred to as the "running" of α_s. With increasing energy the coupling strength becomes smaller ("asymptotic freedom"). For high energies (say above 1 GeV) the coupling constant is sufficiently small such that perturbative calculations can be performed. For low energies, in the non perturbative region,

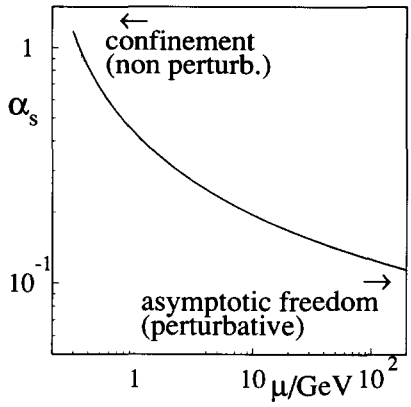

Fig. 2.3. Energy dependence of the strong coupling constant.

the coupling constant becomes large, which is believed to be the origin of confinement.

2.2. The process $e^+e^- \rightarrow$ hadrons

The process $e^+e^- \rightarrow$ hadrons at high center of mass energies is well suited for QCD tests: (a) the initial state is well defined, (b) the high momentum quarks and gluons (fig. 2.4) form jets, tight bundles of hadrons, which preserve the energy and the direction of the primary partons to a good approximation.

Figure 2.5 shows a "LEGO plot" of a hadronic event obtained at 91 GeV center of mass energy. Here the energy flow is plotted as function of the polar angle θ with respect to the e^+e^- beamline and the azimuthal angle ϕ. The figure shows nicely that the jets are narrow and well separated from each other.

The analysis of hadronic events in e^+e^- collisions at high energies has made major contributions to the establishment of QCD [13, 14]:

- The number of colors N_C has been determined from the ratio of hadronic and muonic cross sections [22–24].
- Quark jets [31] and gluon jets [32] have been discovered.
- The quark spin of 1/2 [18] has been confirmed [31, 13] and the spin of gluons has been measured [33].
- The strong coupling constant has been determined using different methods [13].

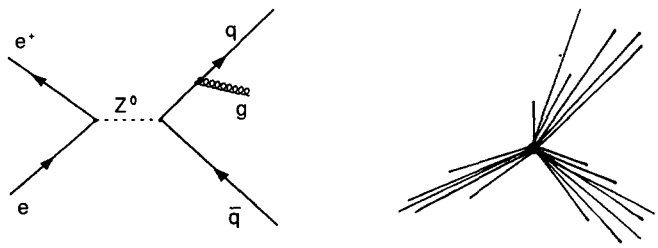

Fig. 2.4. Jet production: $e^+e^- \rightarrow q\bar{q}g$.

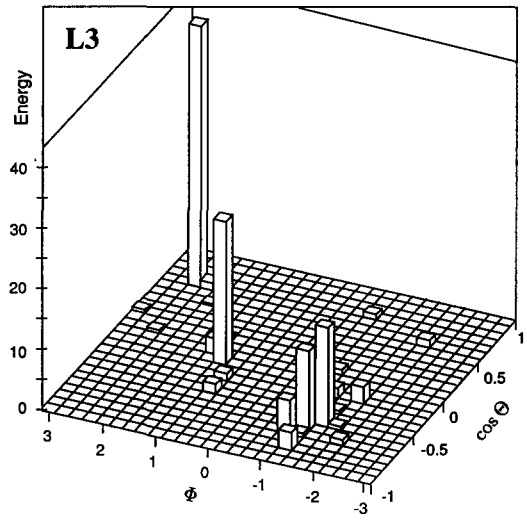

Fig. 2.5. "LEGO-plot" of a 3-jet event at 91 GeV (L3).

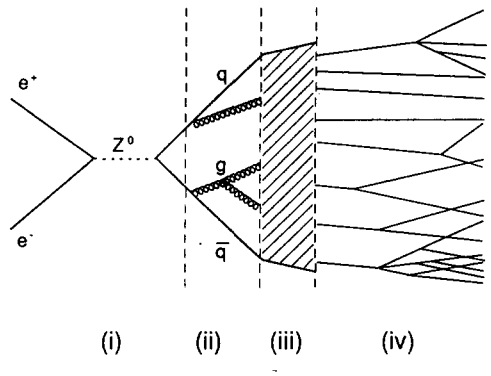

Fig. 2.6. The four phases of the process $e^+e^- \rightarrow$ hadrons.

- Indications for gluon interference effects have been found through studies of the string effect [34, 14] and of particle spectra [35].

One can distinguish four separate phases in the process $e^+e^- \rightarrow$ hadrons, corresponding to different time and length scales [11]:

(i) 10^{-17} cm: production of a $q\bar{q}$ pair (and photons) [electroweak],
(ii) 10^{-15} cm: radiation of gluons and quarks [perturbative QCD],
(iii) 10^{-13} cm: fragmentation of quarks and gluons into hadrons [non perturbative QCD],
(iv) $> 10^{-13}$ cm: decays of unstable particles [electroweak and QCD].

These subprocesses are implemented in several Monte Carlo event generators [11] and are sketched in fig. 2.6. In the following sections the four phases are described in more detail.

2.2.1. The process $e^+e^- \rightarrow f\bar{f}$

To lowest order the total cross section for fermion pair production $e^+e^- \rightarrow f\bar{f}$ at a center of mass energy $\sqrt{s}$ is given by [20]

$$\sigma(e^+e^- \rightarrow f\bar{f}) = \tfrac{4}{3}\pi(\alpha^2/s)[Q_e^2Q_f^2 + (V_e^2 + A_e^2)(V_f^2 + A_f^2)|\chi|^2 + 2Q_eQ_fV_eV_f\mathrm{Re}(\chi)] \qquad (2.20)$$

for particle masses $m_f \ll \sqrt{s}$. Here

$$\chi = \frac{1}{4\sin^2\theta_W\cos^2\theta_W}\frac{s}{s - m_Z^2 + im_Z\Gamma_Z} \qquad (2.21)$$

describes the Breit–Wigner form of the Z^0 resonance. $m_Z = 91.2$ GeV and $\Gamma_Z = 2.5$ GeV denote the mass and the total decay width of the Z^0 boson [36]. $\alpha = 0.00730$ is the fine structure constant and $\sin^2\theta_W = 0.23$ the weak mixing angle [36]. Values for the coupling constants Q_f (electric charge), $V_f = I_f^3 - 2Q_f\sin^2\theta_W$ (vector coupling to Z^0) and $A_f = I_f^3$ (axial vector coupling) are given in table 2.2. The third component of the weak isospin I^3 is $-1/2$ for fermions with negative charge and $+1/2$ for all others. The first line in eq. (2.20) describes the photon s-channel diagram

Table 2.2
Fermion couplings to γ and Z^0 for $\sin^2\theta_W = 0.23$.

Fermion	Q	V	A	Q	V	A
ν	0	1/2	1/2	0.00	0.50	0.50
e, μ, τ	−1	$-1/2 + 2\sin^2\theta_W$	−1/2	−1.00	−0.04	−0.50
u, c, t	2/3	$1/2 - (4/3)\sin^2\theta_W$	1/2	0.67	0.19	0.50
d, s, b	−1/3	$-1/2 + (2/3)\sin^2\theta_W$	−1/2	0.33	0.35	−0.50

as shown in fig. 2.7a, and the second line contains the contribution from Z^0 exchange, see fig. 2.7b. The last term describes the γ–Z^0 interference. The contribution of the Higgs exchange diagram can be neglected [37].

For $q\bar{q}$ final states an additional QCD color factor $N_C = 3$ has to be inserted. In case of electron production (f = e, Bhabha scattering) additional terms have to be added to eq. (2.20), which describe the contributions from t-channel diagrams and interference.

For unpolarized beams the only non trivial kinematical variable is the polar angle θ between incoming electron e^- and outgoing fermion f. As long as one does not distinguish between particles and antiparticles the $\cos\theta$ distribution has the simple form

$$d\sigma/d\cos\theta \sim 1 + \cos^2\theta\,. \tag{2.22}$$

For QCD corrections to this formula and for the orientation of 3-jet events see section 5.1.

Higher order electroweak and strong corrections modify the lowest order formula (2.20). Both virtual corrections and the radiation of photons in the initial state and of gluons and photons in the final state play a role [37, 38]. Figure 2.8 shows the total hadronic cross section in the center of mass energy range 10–160 GeV, once in lowest order and once including electroweak corrections to $O(\alpha)$, second order exponentiated initial state photon radiation, and QED and QCD final state corrections [39].

For these $\sqrt{s}$ values only the five flavors u, d, s, c and b contribute; the top quark mass is known to exceed 91 GeV [40]. At the Z^0 pole the biggest effect is due to QED corrections, which lead to a reduction of the peak cross section by 30%. The QCD correction $\approx \alpha_s/\pi$ is relatively small and increases σ by about 4%; for details see section 4.3 and appendix A. In fig. 2.8 and in the following graphs in this section the resonance structure in the hadronic cross section near the bottom threshold of about 10 GeV is not taken into account.

At center of mass energies below 50 GeV the contribution of the Z^0 exchange and interference diagrams to the total cross section is small, and the cross section for flavor f is proportional to the charge squared, Q_f^2. Thus the relative contribution of muons, up quarks and down quarks is to lowest order 1 : 4/3 : 1/3. Near 91 GeV, the Z^0 exchange diagram in fig. 2.7 is dominant. The cross sections are determined by the electroweak coupling constants and are proportional to $V_f^2 + A_f^2$,

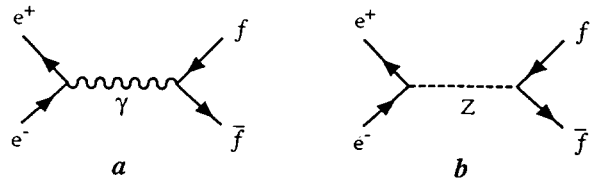

Fig. 2.7. The process $e^+e^- \to f\bar{f}$ to lowest order.

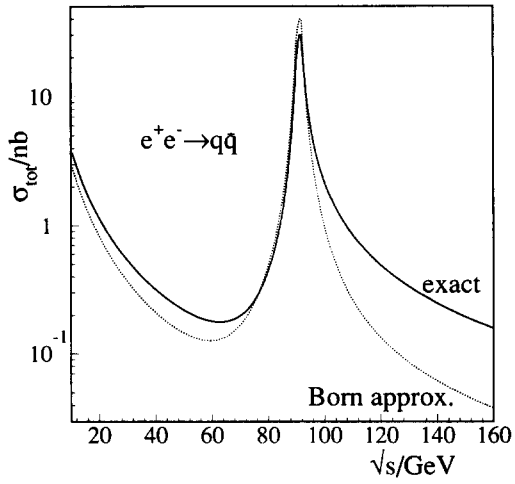

Fig. 2.8. Total hadronic cross section in e^+e^-.

leading to $\mu : u : d = 1 : 3.3 : 3.7$. Consequently the ratio of the total hadronic and muonic cross sections,

$$R = \sigma_{had}/\sigma_\mu , \tag{2.23}$$

is increased from about 4 at low energies to 20 at the Z^0 resonance, as is shown in fig. 2.9a. Also the relative contribution of the quarks u, c and d, s, b to the total hadronic cross section is changing significantly, as is illustrated in part (b) of that figure, where the ratio

$$F_f = \sigma_{ff}/\sigma_{had} \tag{2.24}$$

is plotted for the different quark species. In fig. 2.9 higher order corrections are included [39].

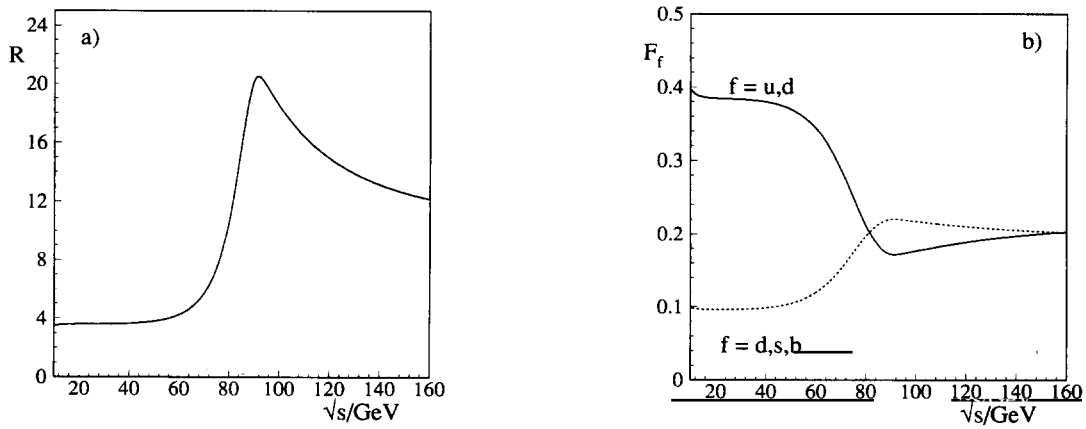

Fig. 2.9. (a) Ratio of hadronic and muonic cross section R, and (b) ratio F_f of cross sections for production of hadronic events with primary flavor f and total hadronic cross section.

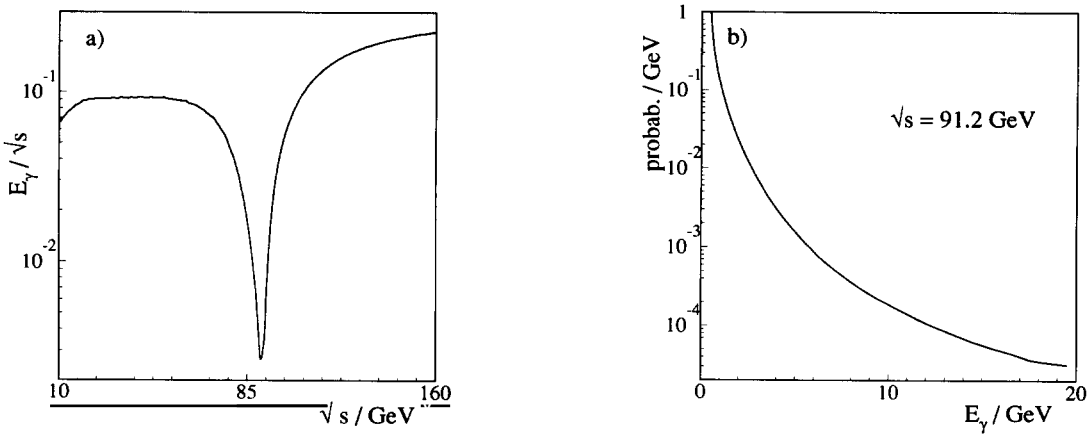

Fig. 2.10. (a) Average photon energy fraction as function of center of mass energy, and (b) photon energy spectrum at 91 GeV.

Also the effect of initial state radiation in the process $e^+e^- \rightarrow$ hadrons has a strong center of mass energy dependence. Due to the radiation of photons with energy E_γ from the electrons the hadronic system is boosted and the energy in its rest frame reduced:

$$s'/s = 1 - 2E_\gamma/\sqrt{s}. \tag{2.25}$$

The photons are emitted preferentially in the direction of the incoming electron or positron and escape often undetected. The probability for photon radiation increases with the ratio $\sigma(s')/\sigma(s)$. Therefore initial state radiation is very small on the Z^0 pole but large in particular at center of mass energies above 100 GeV. This is illustrated in fig. 2.10a, where the average photon energy normalized to the center of mass energy is shown between 10 and 160 GeV*). At 91 GeV the mean value is $\langle E_\gamma \rangle = 1.3$ GeV. The steeply falling photon energy spectrum at the Z^0 pole is shown in fig. 2.10b.

The probability for final state photon radiation from quarks is small for all center of mass energies. At $\sqrt{s} = 91$ GeV a photon with energy above 10 GeV is emitted in 1 event out of 200 [41]. These events are of special interest for QCD studies: they allow a comparison between $q\bar{q}\gamma$ and $q\bar{q}g$ events and can probe the parton shower evolution, see section 3.6. Interference between initial and final state radiation is small in the vicinity of the Z^0 [38].

2.2.2. Gluon radiation

Phase (ii) of fig. 2.6 is of primary interest in this article. It describes the radiation of gluons off the primary quarks and the subsequent parton cascade due to gluon splittings into quarks or gluons, and gluon radiation of secondary quarks. It can be calculated approximately within QCD and allows for quantitative tests. There are two approaches:

- "matrix elements" (ME) [exact order by order calculation],
- "parton showers" (PS) [(next-to) leading log approximation].

The classes of corresponding Feynman diagrams are shown in fig. 2.11 (from ref. [11]). The two methods are complementary and both widely used. The first one provides a more accurate

*) The curves shown in fig. 2.10 are calculated with the program JETSET [41], where photon radiation is generated according to the first order formula.

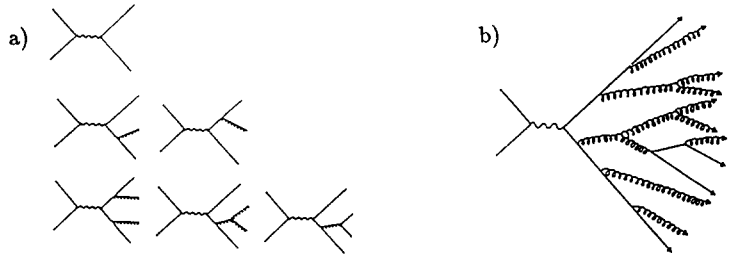

Fig. 2.11. Feynman diagrams describing $e^+e^- \rightarrow$ quarks + gluons. (a) Matrix element calculation to $O(\alpha_s^2)$. Virtual corrections are not shown. (b) Parton shower approach, one possible configuration.

description of hadronic events on the jet level, while the PS generators are better suited to describe the structure of jets. The ME approach is needed to determine α_s and to test QCD in 3-jet and 4-jet events, while the parton shower programs are used to analyze gluon coherence and fragmentation effects, to study detector responses, etc.

Full *Matrix Element* calculations [42] exist only to second order in α_s [43–46]. Therefore the final state consists of at most four partons. Only in ME computations α_s has a well defined meaning, and the hard parton kinematics is calculated exactly. The first order ME for massless quarks has the simple form [47]

$$\frac{d\sigma}{dx_q\, dx_{\bar{q}}} \sim \alpha_s \frac{x_q^2 + x_{\bar{q}}^2}{(1-x_q)(1-x_{\bar{q}})}. \tag{2.26}$$

Here x_q, $x_{\bar{q}}$ and $x_g = 2 - x_q - x_{\bar{q}}$ denote the parton momenta (divided by the beam energy) of the quark, antiquark and gluon, respectively. The cross section has infrared (e.g. $x_g \rightarrow 0$) and collinear (e.g. $x_q \rightarrow 1$, corresponding to the case where the $\bar{q}$ and g are collinear) divergences. These singularities are canceled by corresponding poles in the first order vertex and propagator corrections, so that the total cross section is finite.

To first order also parton mass corrections have been calculated [48], while this is not the case for the second order matrix element. The angular orientation of events with respect to the beam line has been computed to $O(\alpha_s^2)$ [49], but not yet included in any matrix element generator. Also terms related to the axial vector coupling of the Z^0 [50] are not yet evaluated. All three effects are presumably small at the Z^0 pole*). Tree-level calculations for n-parton final states with $n > 4$ exist [52], but have so far not been compared with experimental results.

There are different methods of calculating observables such as event shape distributions. The necessary integrations can be performed in one of the three following ways:

(i) with Monte Carlo techniques inside an event generator,

(ii) analytically,

(iii) numerically (other than (i)).

In (second order) ME Monte Carlo programs (i) configurations with two, three and four partons are generated. In order to separate these topologies a parton resolution criterion has to be used, for example the smallest invariant mass m_{ij} of any two partons. For massless three-parton configurations m_{ij} is related to the energy of the third parton k by $y_{ij} \equiv m_{ij}^2/s = 1 - x_k$. The quarks and gluons are then transformed into hadrons using a fragmentation model. Then the event shape distributions can be calculated. The disadvantage of this approach is that the probabilities for producing an n-parton

*) For the influence on the orientation see ref. [51].

final state must be positive. This implies that the invariant mass of two partons must exceed ≈ 10 GeV (corresponding to $y_{\min} = 0.01$) at the Z^0 resonance [11]. Even then in some regions of phase space the three- or two-jet cross section can become negative, depending on the value of α_s and the renormalization scale [53]. All softer (perturbatively calculated) contributions are cut out by the hard $y_{\min} = 0.01$ cut and must be effectively put back in the "hadronization" step!

The problem of negative cross sections is avoided in analytical or numerical calculations of an event shape distribution [8, and references therein], since the sum of the n-jet contributions is always positive. They correspond to the limit $y_{\min} \to 0$. The numerical approach (iii) has the advantage that the calculations can be repeated relatively easily for a modified or new observable. In the analytical formulas (ii) explicit dependences on QCD color factors and the number of quark flavors are retained. The problem with the perturbatively calculated distributions using methods (ii) or (iii) lies in the hadronization correction. Those are always calculated using Monte Carlo methods and depend on the initial parton configurations, which are different for the MC ME approach and the analytical calculations, and also for PS generators. Therefore a certain ambiguity exists on how to *define* the hadronization correction. Often the solution suggested in ref. [8] is adopted: the parton shower Monte Carlo generators should be used with a low invariant mass cutoff of $m_{ij} \approx 1$ GeV to determine hadronization corrections. The shower programs produce on average significantly more than four partons (about nine in JETSET). However, this difference in the parton configuration between PS generators and second order calculations is due to higher order corrections and has to be distinguished from non perturbative fragmentation effects.

Parton shower generators [54, and references therein] are based on calculations in the framework of the (next-to) leading logarithmic approximation [55]*). As in the case of the ME approach many observables can be calculated analytically in the LL framework. Examples will be discussed in section 6. Here I describe briefly the basics of PS generators.

In LL calculations only leading terms of the perturbative expansion are retained and resummed to all orders (corresponding to multiple parton splittings). PS programs are based on a probabilistic picture of successive parton branchings (fig. 2.11b). Starting from the first order matrix element (2.26) the differential cross section can be written approximately as

$$\frac{\mathrm{d}\sigma}{\mathrm{d}m^2\,\mathrm{d}z} \sim \alpha_s \frac{1}{m^2} \frac{1+z^2}{1-z}, \tag{2.27}$$

where $z = x_q/(x_q + x_g)$, and m is the mass of the qg system. Equation (2.27) is exact only in the limit of collinear kinematics. Integrating (2.27) over m^2 (for fixed z) or $(1-z)$ (for fixed m^2 and assuming $z \approx 1$) gives

$$\frac{\mathrm{d}\sigma}{\mathrm{d}z} \sim \ln(m^2) \frac{1+z^2}{1-z}, \quad \frac{\mathrm{d}\sigma}{\mathrm{d}m^2} \sim \ln(1-z) \frac{1}{m^2}. \tag{2.28}$$

This explains the name "leading log approximation".

The probability for the branching process $q \to qg$ as sketched in fig. 2.12 is then given by

$$\frac{\mathrm{d}p}{\mathrm{d}z}(q \to qg) \sim \frac{1+z^2}{1-z}. \tag{2.29}$$

Similar expressions exist for the parton splitting processes $g \to q\bar{q}$ and $g \to gg$. They are known as Altarelli–Parisi splitting functions [56].

*) In the following I will use the acronym "LL" as a generic name for leading, next-to-leading, modified leading, ... logarithmic approximations.

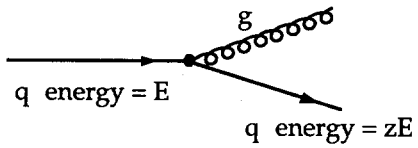

Fig. 2.12. Branching process q → qg.

The probability ΔP for a branching to take place during a small change Δt of the "evolution variable" t is given by the Altarelli–Parisi equations [56],

$$\Delta P(t) \sim \int \alpha_s(t) \frac{dp}{dz} dz \, \Delta t . \tag{2.30}$$

The evolution parameter can be written in the form $t = \ln(Q^2/\Lambda^2)$. In leading order different choices for Q are possible, one of them being the mass m of the branching parton.

Equations (2.29) and (2.30) are used in Monte Carlo programs to generate a sequence of parton branchings, a "parton shower". When Q approaches Λ perturbative QCD is no longer applicable and therefore a cutoff parameter $Q_0 = O(1\ \text{GeV})$, which corresponds to an effective gluon mass, is introduced to terminate the showering.

In general the various parton shower programs use different kinematical approximations, evolution variables, α_s formulas and energy scales. For details see ref. [11].

Calculations beyond leading log predict coherence effects [57, 9], influencing soft gluons inside a jet and the particle flow in between jets. An important prediction is, that the intrajet interference leads to an effective decrease of emission angles in subsequent parton branchings ("angular ordering"). This allows the simulation of coherence phenomena also in (probabilistic) PS programs.

The consequences of coherence effects as predicted by analytical QCD calculations and PS programs are discussed and compared with experimental results in section 6.

2.2.3. Hadronization

The fragmentation of quarks and gluons, phase (iii), can be modeled quite successfully by string and cluster fragmentation schemes, which will be explained briefly. A very detailed review of these and other hadronization models and event generators can be found in ref. [11], which I follow closely. Here I use the expressions "fragmentation" and "hadronization" as synonyms. Before describing the two models it is important to define what hadronization stands for.

Hadronization describes the conversion of colored quarks and gluons into hadrons. How big this step is, depends on the initial parton configuration. In case of $O(\alpha_s^2)$ ME generators at most four partons at an energy scale (invariant mass of two partons) exceeding 10 GeV are created at the Z^0 resonance. This implies that hadronization models have to bridge a big gap from the parton to the hadron level which is governed by multiplicities of 15–20 (before decays) and mass scales of 1 GeV or less.

The situation is better for PS Monte Carlo generators, where one can go down to a parton energy scale Q_0 (virtuality of gluons) of about 1 GeV. The average parton multiplicity of 9 at the Z^0 pole (JETSET PS) is much closer to the number of hadrons produced than in the matrix element case. This means that the task fragmentation models have to accomplish is relatively smaller for the PS generators. Consequently the hadronization model dependence is much reduced in comparison with the ME programs.

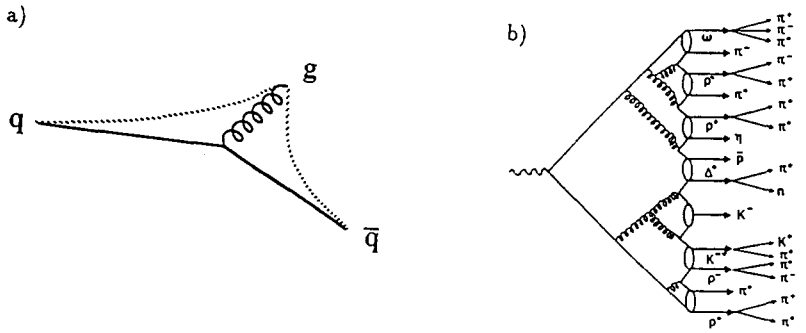

Fig. 2.13. (a) String fragmentation (first step), (b) cluster fragmentation.

It has to be stressed that the notion of hadronization used here, in particular for the ME case, refers both to non perturbative effects and to missing higher order terms in the perturbative calculation of the parton configuration.

The *string fragmentation* model [58] as used in the JETSET Monte Carlo program [41] is based on the QCD inspired idea, that a "color flux tube" (= "string") is stretched between the quark and antiquark produced for example in e^+e^- annihilation. A gluon is a kink on the string as depicted in fig. 2.13a. When the partons move apart the potential energy of the string increases, the string breaks up and a $q\bar{q}$ pair is created. The remaining string pieces may break up, too. The quarks and antiquarks from adjacent breakings can then form mesons. Also baryon formation is possible, for example via diquark production.

The details of the fragmentation process can be adjusted by a rather large number of free parameters. Two important ones influence the longitudinal component of the hadron momenta, and a third one determines the transverse component. The production yields of different hadron species can be steered by parameters defining the strange quark content, the spin probabilities (pseudoscalar and vector mesons), the number of diquarks created etc.

The *cluster fragmentation* [59] as implemented in the HERWIG program [60] should be used only for "developed" parton configurations as obtained in PS generators. First all gluons are split into $q\bar{q}$ pairs, see fig. 2.13b (from ref. [11]). Adjacent quarks and antiquarks form colorless clusters, which decay further into hadrons, according to flavor content and phase space.

There is basically only one free parameter, the maximum cluster mass. Clusters with a higher mass first decay into smaller clusters, which subsequentially decay into hadrons.

Independent fragmentation models [61] have been used extensively at PEP and PETRA [62,63] some ten years ago, but were gradually phased out after the discovery of the string effect [34], which they fail to reproduce (see section 6.5).

To illustrate the number and kinds of hadrons produced, I use the JETSET PS Monte Carlo program with string fragmentation, which reproduces measured particle fractions quite well [64]*). JETSET predicts, that at the Z^0 resonance on average 17 hadrons are created which decay into a total of about 45 particles with an average lifetime exceeding 3×10^{-10} s.

The ten most frequently produced "primary" hadrons (string decay products) are listed in table 2.3 for events with light (u, d, s) primary quarks. Their production rates (number of hadrons per event) as predicted by the JETSET parton shower program, and their lifetimes and dominant decay

*) Several parameters in JETSET are tuned to optimize the agreement with measured particle yields at lower center of mass energies.

Table 2.3
Primary hadrons produced in u, d and s events at the Z^0 resonance.

Hadron	Mass (MeV)	τ (s)	No./event	Principal decay modes
$\pi^{\pm}$	140	3×10^{-8}	3.0	$\mu^{\pm}\nu$
$\rho^{\pm}$	768	10^{-24}	2.8	$\pi^{\pm}\pi^0$
π^0	135	8×10^{-17}	1.5	$\gamma\gamma$
ρ^0	768	10^{-24}	1.4	$\pi^+\pi^-$
ω	782	10^{-22}	1.4	$\pi^+\pi^-\pi^0(89\%)$
$K^{*\pm}$	892	10^{-23}	1.1	$K^{\pm}\pi^0(67\%), K^0\pi^{\pm}(33\%)$
K^{*0}	896	10^{-23}	1.1	$K^+\pi^-(67\%), K^0\pi^0(33\%)$
η	549	6×10^{-19}	0.8	$\gamma\gamma(39\%), \pi^0\pi^0\pi^0(32\%), \pi^+\pi^-\pi^0(24\%)$
$K^{\pm}$	494	10^{-8}	0.8	$\mu^{\pm}\nu(64\%), \pi^{\pm}\pi^0(21\%)$
K^0	498	$9 \times 10^{-11}, 5 \times 10^{-8}$	0.8	$K^0_S \rightarrow \pi^+\pi^-(69\%), \pi^0\pi^0(31\%)$

modes are shown [20]. For the production and decay of hadrons containing charm and bottom quarks see ref. [65]. Due to their high mass they contain almost exclusively a primary charm or bottom quark. Therefore one finds exactly two charmed hadrons per $c\bar{c}$ event and two bottom hadrons per $b\bar{b}$ event.

2.2.4. *Particle decays*

For the well established light hadrons their masses, decay modes, lifetimes and branching fractions as measured are built into the Monte Carlo generators [20]. For heavier particles, in particular charm and bottom hadrons, not all exclusive branching fractions have been measured. Therefore statistical models have to be invoked. For weak decays of heavy quarks the known matrix elements are taken. Particle polarization is in general not taken into account.

The principal decay modes of the most frequently produced light hadrons are shown in table 2.3 in the previous section. Table 2.4 shows the average number of all "stable" particles (those with an average lifetime bigger than 3×10^{-10} s, corresponding to flight paths of 10 cm and more) observed in hadronic Z^0 decays. These numbers are calculated with the JETSET PS program plus string fragmentation using default parameters. The difference between the numbers for $\mu^{\pm}$ and $e^{\pm}$

Table 2.4
"Stable" particles produced in hadronic events at the Z^0 resonance.

Neutral		Charged	
particle	no./event	particle	no./event
γ	21.5	$\pi^{\pm}$	17.1
n, $\bar{n}$	1.1	$K^{\pm}$	2.2
K^0_L	1.1	p, $\bar{p}$	1.2
$\nu, \bar{\nu}$	0.3	$e^{\pm}$	0.4
		$\mu^{\pm}$	0.1

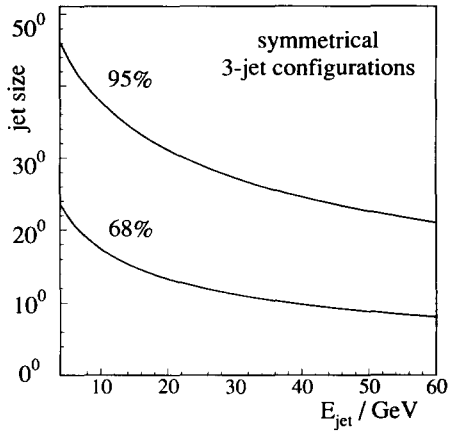

Fig. 2.14. Jet size for symmetrical 3-jet events as function of the jet energy.

is due to Dalitz decays $\pi^0 \to \gamma e^+ e^-$. In section 6.3, measured yields for some hadrons are given.

2.2.5. Energy dependence of hadron event topology

The electroweak properties of fermion pair production depend strongly on the center of mass energy, in particular in the neighborhood of the Z^0 resonance. The properties of the events determined by the strong interactions vary only slowly with $\sqrt{s}$, typically as $\sim 1/\ln\sqrt{s}$ (strong coupling constant) or $\sim 1/\sqrt{s}$ (hadronization effects). Figure 2.14 shows as an example the variation of the jet size with jet energy. Here the effects of parton showering, hadronization and decays are included. The jet size is defined as the half opening angle of a cone around a jet axis including a certain fraction (e.g. 68%) of the total jet energy. Figure 2.14 is obtained from symmetrical 3-jet events where the three jets all have the same energy within 15%*). The decrease of the jet size with increasing center of mass energy is mainly due to hadronization effects: fragmentation is characterized by a transverse momentum scale of about 300 MeV, which is independent of $\sqrt{s}$. Therefore the size of a jet is to first approximation proportional to $1/E_{jet}$. When taking into account also the effects of parton showering, increase of particle multiplicities and decays, the jetsize variation with $\sqrt{s}$ is reduced, as is shown in fig. 2.14.

2.2.6. Background processes

Apart from beam related background and cosmics the main background to hadronic final states in e^+e^- reactions comes from τ's and two-photon interactions:

$$e^+e^- \to \tau^+\tau^- \to \text{hadrons}, \tag{2.31}$$

$$e^+e^- \to e^+e^-\text{hadrons}. \tag{2.32}$$

The corresponding cross sections at the Z^0 peak are about 0.01 nb for the τ background and ≈ 0.1 nb for the two-photon process, to be compared with the cross section of 30 nb for $e^+e^- \to$ hadrons. These values are calculated assuming that all $\tau^+\tau^-$ events for which both leptons decay into at

*) 3-jet events are pre-selected applying the LUCLUS jet algorithm [66] in the JETSET program with a jet resolution parameter of $d_{join} = 4.5$ GeV.

least three charged hadrons contribute. The two-photon background has been extrapolated from measurements in e^+e^- collisions at $\sqrt{s} = 29$ GeV [67, 68]. The acceptance was calculated [69, 41] assuming an ideal detector and by selecting all events with a total hadronic energy E_{vis} above $0.5\sqrt{s}$ and a hadronic energy imbalance below $0.5E_{vis}$. The exact magnitude of the background depends of course on the detector features and on the selection criteria. For most QCD studies at the Z^0 pole the small background can be neglected.

Another potential background is Bhabha scattering,

$$e^+e^- \to e^+e^-, \tag{2.33}$$

at small angles. As long as hadron jets and single electromagnetic showers can be separated efficiently, as is the case for most e^+e^- detectors, this background is negligible.

In summary, one can say that the Z^0 resonance is an ideal laboratory for QCD studies. One finds at the Z^0 pole a large number of events with 2, 3 and 4 well collimated jets with an energy exceeding 10 GeV. These "clean" topologies allow for a precise determination of α_s and for many tests of QCD.

Important advantages in comparison with e^+e^- collisions at $\sqrt{s} \approx 30$ GeV (PEP, PETRA) are:

(i) large cross section and negligible background,

(ii) relatively small fragmentation effects,

(iii) suppressed initial state photon radiation.

Increasing the center of mass energy beyond 91 GeV leads to a small further reduction of hadronization effects, however the advantage of a large cross section is lost and initial state radiation becomes important.

2.3. Accelerators and detectors

Six detectors installed at the two e^+e^- accelerators LEP and SLC have taken data at center of mass energies close to the Z^0 mass.

2.3.1. LEP and SLC

The "Large Electron Positron" collider LEP [70] is located at CERN, Geneva. It is a (nearly) circular machine, into which electrons and positrons are injected in $4 + 4$ bunches at a beam energy of 20 GeV. Currently they can be accelerated to energies up to 50 GeV. The integrated luminosity delivered in the years 1989–1991 to each of the four detectors ALEPH [71], DELPHI [72], L3 [73] and OPAL [74] amounts to about $25\,pb^{-1}$. In total approximately two million Z^0 decays have been recorded.

In the next years the number of events is expected to rise to several million per detector. From 1994 onwards center of mass energies close to 180 GeV will be achieved. The possibilities of transversal and longitudinal beam polarization are under study.

The "SLAC Linear Collider" SLC [75], the first e^+e^- linear collider, has only one interaction region. In 1989 and 1990 the MARK II detector [76] recorded a few hundred Z^0 events. In 1991 some 400 events were measured by the SLD detector [77]. Starting in 1992 SLC will operate with longitudinally polarized beams.

2.3.2. The detectors

The general structure of the six detectors is quite similar. Starting at the interaction point they are composed of

Table 2.5
Features of the LEP detectors relevant for the analysis of hadronic events.

		ALEPH	DELPHI	L3	OPAL
Tracking	coverage $\lvert\cos\theta\rvert$	0.96	0.96	0.98	0.98
	double track resolution (deg)	0.6	1	(0.1)	(0.1)
	$p_\perp$ resolution at 3 GeV (%)	0.4	0.5	8	2
Calorimetry	$\lvert\cos\theta\rvert$ electrom.	0.98	0.98	0.98	0.98
	granularity electrom. ($\deg^2$)	0.8×0.8	0.1×1	2×2	2×2
	E resolution 3 GeV π^0, γ (%)	10	20	1	4
	$\lvert\cos\theta\rvert$ hadron.	0.99	0.98	0.996	0.99
	granularity hadron. ($\deg^2$)	3.7×3.7	3.8×3	2.5×2.5	7.5×5
	E resolution 30 GeV jet (%)			17	25
Muons	$\lvert\cos\theta\rvert$ muon det.	0.98	0.96	0.8	0.98
	p resolution at 10 GeV (%)	1	2	3	2
Hadron identification	method	dE/dx	dE/dx, RICH	–	dE/dx

- vertex and tracking chambers,
- an electromagnetic detector,
- a hadron calorimeter,
- a muon detector.

In addition, luminosity counters are installed close to the beam pipe. The inner tracking chambers (in case of L3 the whole detector) are placed in a magnetic field in order to be able to measure particle momenta. The angular coverage of most of the detector components is close to 4π.

Table 2.5 summarizes some features of the four LEP detectors ALEPH [71], DELPHI [72], L3 [73] and OPAL [74] which are relevant for analyses of hadronic Z^0 decays. The two SLC detectors are not included, since they can so far not contribute very much to QCD studies due to their small event samples.

Here θ denotes the polar angle with respect to the beam axis. The symbols E, p and $p_\perp$ stand for energy, momentum and transverse momentum with respect to the beam line, respectively.

The momenta of the charged tracks and neutral pions of 3 GeV correspond to the average hadron energy at the Z^0 resonance. The jet energy of 30 GeV is a representative number for 3-jet events. Muons of 10 GeV are typical for semileptonic B meson decays.

The double track resolutions quoted for L3 and OPAL are only valid for the projections onto a plane perpendicular to the beam axis. The calorimetric jet energy resolution is not given for ALEPH and DELPHI, since for these detectors tracking information is always included when reconstructing jets. The L3 detector is not designed to identify charged hadrons of different kinds.

Table 2.5 shows the complementarity of the LEP detectors: L3 has a very precise electromagnetic calorimeter, while ALEPH, DELPHI and OPAL measure charged tracks with high accuracy. A special feature of the DELPHI detector is the Ring Image Cherenkov detector (RICH) for particle identification.

3. QCD models for $e^+e^- \rightarrow$ hadrons

To be able to interpret measurements one has to use models to describe the hadronization process and also the subsequent decays. Therefore tuning and testing of fragmentation models is the first step in any analysis. However, the study of the non perturbative hadronization process does not allow for a quantitative QCD test. Therefore hadronization models and experimental constraints are not discussed in detail here. In this context the word "model" refers to Monte Carlo programs which simulate hadronic events. These generators always include all four phases in the process $e^+e^- \rightarrow$ hadrons ($q\bar{q}$ production, gluon radiation, hadronization and particle decays) as described in section 2.2.

3.1. Monte Carlo generators

The most popular Monte Carlo programs are:
- JETSET 7.3 [41]. Both parton shower and $O(\alpha_s^2)$ matrix element options are available [43, 45]. Most often the string fragmentation model is used (see section 2.2.3), however, also independent jet fragmentation models [61] can be selected. The parton shower is based on leading logarithmic calculations and incorporates angular ordering and azimuthal correlations (see section 6.1). The first gluon branching is modified using the first order matrix element to improve the predicted rates with hard acollinear gluon radiation. In case of the $O(\alpha_s^2)$ matrix element option most often the calculations from ref. [43] are used.
- HERWIG 5.3 [60]. This parton shower generator incorporates a detailed simulation of QCD interference phenomena and spin effects. Hadronization is simulated by cluster fragmentation (section 2.2.3).

Other programs being used are
- ARIADNE 3.3 [78]. In this parton shower generator gluon radiation is modeled as coherent emission from color dipoles formed by a parton system. Coherence effects including azimuthal correlations are automatically incorporated.
- NLLJET 2.0 [79]. The first three letters stand for next-to-leading logarithmic approximation [80]. This parton shower generator includes also three-body-parton splittings such as $q \rightarrow qgg$ and $g \rightarrow ggg$.
- ERT-E_0 matrix element generator [43, 81]. This $O(\alpha_s^2)$ matrix element program is based on the "E_0" recombination scheme, see section 4.4.1. The renormalization scale is a free parameter.
- COJETS 6.12 [82]. Also COJETS is based on leading log calculations, however the branchings in the parton shower are incoherent. The hadronization step is based on an independent jet fragmentation model.

In the programs ARIADNE, NLLJET and ERT-E_0 the JETSET routines are used for hadronization and decays. In some cases older versions than those indicated above have been used by the LEP and SLC experiments. Since the differences are small they shall not be discussed here.

3.2. Parameter fitting

To fit the parameters of the various models the following analysis steps have to be made:
- Out of many free parameters in the model the relevant ones have to be identified. For the perturbative part there is first of all the (effective) coupling strength α_s^{eff}. This parameter is not exactly equal to the value of α_s in the $\overline{\text{MS}}$ scheme, due to the approximations made in the programs. For shower programs there is a cutoff parameter which determines the termination of the parton

cascade. In JETSET this is the minimum parton virtuality and in HERWIG the effective gluon mass. In the matrix element case the minimal scaled invariant mass $y_{\min}$ of two partons is usually set to the smallest value compatible with a positive 2-jet rate. At the Z^0 a good value is 0.01 [11]. Another free parameter is the renormalization scale μ. The parameters to be fitted in the hadronization step obviously depend on the model used. Typically one to three parameters are included in the fit. In JETSET two variables are used. One describes the longitudinal hadron momenta and the other one determines the transverse momentum distribution of hadrons with respect to the primary parton. In HERWIG the only free parameter is the maximum cluster mass.

- The distributions to be used in the fit have to be chosen. Event shape variables like thrust and oblateness or inclusive distributions such as particle momenta are suitable [8]. Such measurements have been performed by ALEPH [83,84], DELPHI [85–87], L3 [88,89], OPAL [90,53] and MARK II [91].
- A global fit to the event shape distributions is performed. The data, corrected for detector effects, are directly compared with the Monte Carlo predictions, and the relevant parameters are determined. Such fits have been done by ALEPH [84], DELPHI [86]*), L3 [89] and OPAL [90,53].

In some programs, in particular JETSET, a variety of options are implemented and many free parameters exist. Some of them, for example the ratio of the numbers of spin-1 and spin-0 mesons or the strange quark content, have been determined in e^+e^- experiments at lower energies [64, and references therein] and need not to be readjusted. L3 [93] and ALEPH [94] use the fragmentation function as given in ref. [95] for the hadronization of the heavy quarks charm and bottom inside the JETSET program.

The fitted parameters are in general correlated. A comparison between the results of the LEP experiments is difficult since the parameter sets used in the fits and the values of fixed parameters are different. However, the agreement between model predictions (after parameter tuning) is found to be quite similar by the four LEP collaborations.

The parameters in the programs NLLJET and COJETS so far have not been fitted by the LEP and SLC experiments**).

3.3. *Measurements and Monte Carlo predictions*

After the models are tuned they can be tested by comparing the predictions for event shape variables, in particular for those not used in the parameter fit, to the measurements. Here the results of such comparisons for global event properties are summarized. Special distributions such as the particle flow in 3-jet events or intermittency will be discussed in section 6.

Figure 3.1a shows as an example the ALEPH thrust distribution in comparison with the predictions of the JETSET (both parton shower and matrix element) and HERWIG event generators [84]. The observable thrust T [96] is defined as

$$T = \max\left(\left|\sum \boldsymbol{p}_i \cdot \boldsymbol{n}_T\right| / \sum |\boldsymbol{p}_i|\right), \tag{3.1}$$

where the $\boldsymbol{p}_i$ is the momentum vector of hadron i in one event. The thrust axis $\boldsymbol{n}_T$ is varied as to maximize the above expression. The thrust values can vary between 0.5 (spherical event) to 1 (two back-to-back partons). All models investigated can reproduce the measurements, however the

*) See also ref. [92].

**) The authors of COJETS have determined the free parameters in their program by a fit to OPAL data.

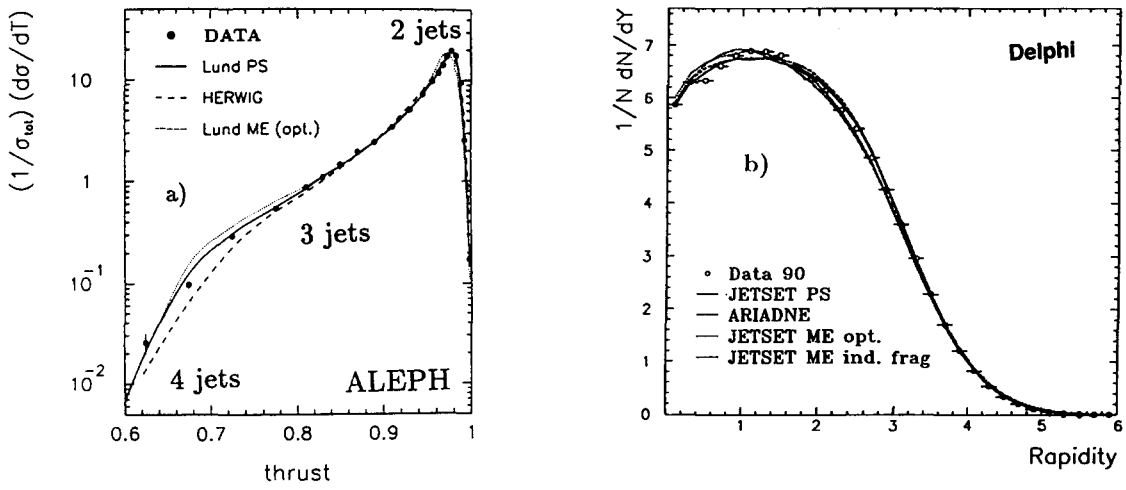

Fig. 3.1. (a) Distribution of thrust T as measured by ALEPH [84] in comparison with QCD models, (b) rapidity distribution measured by DELPHI [86] together with model predictions.

HERWIG program somewhat underestimates the production of low thrust events. In case of the matrix element a value of the scale $\mu \approx 3$ GeV is used, as obtained in a fit to the data.

In fig. 3.1b the inclusive rapidity distribution as measured by DELPHI [86] is compared with the predictions of JETSET (different options) and ARIADNE. The rapidity value is calculated for all charged particles:

$$y = 0.5 \ln[(E + p_{\parallel})/(E - p_{\parallel})], \tag{3.2}$$

where E is the particle energy and $p_{\parallel}$ its longitudinal momentum with respect to the thrust axis. All models describe the rapidity distribution.

The different studies [84, 86, 92, 89, 90, 53] arrive at similar results, which can be summarized this way:

- All parton shower models using string or cluster fragmentation as listed above can be tuned to give a fair overall description of hadronic Z^0 decays. JETSET performs best. HERWIG underestimates the number of events with hard gluon radiation. Versions with independent jet fragmentation (as for example COJETS) have not yet been compared with the full set of measured event shape distributions.
- Matrix element based programs with string fragmentation can describe the data only for a rather small value for the renormalization scale of the order of a few GeV. This increases the fraction of 4-jet events which is apparently underestimated in the second order calculation when using a value of $\mu = \sqrt{s}$. Even with a small scale μ the matrix element generators describe the data not as well as parton shower programs do. The independent jet fragmentation option cannot reproduce the measured energy and particle flows in 3-jet events.

3.4. Energy dependence of event shape variables

As an example I show the dependence of the mean thrust value $\langle T \rangle$ on the center of mass energy in e^+e^- collisions in fig. 3.2. The data below the Z^0 resonance are taken from ref. [97]. In some cases

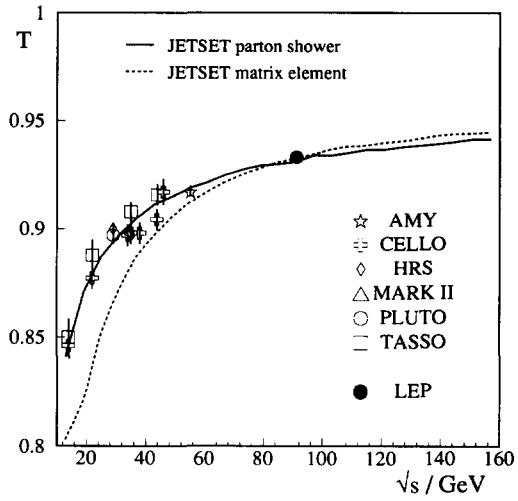

Fig. 3.2. Evolution of mean thrust value with center of mass energy.

only statistical errors are published. The weighted average of the measurements by ALEPH [84], DELPHI [85] and OPAL [90] is $\langle T \rangle = 0.933 \pm 0.002$ at 91 GeV*). The predictions of JETSET are calculated for the parameters given in ref. [86] for the case of string fragmentation. Figure 3.2 shows that the JETSET parton shower program can reproduce the $\sqrt{s}$ dependence between 12 and 91 GeV, while the matrix element generator with $y_{\min} = 0.01$ does not describe the measurements. The latter result is expected, since for a fixed value of $y_{\min}$ (similar parton configuration) the hadronization correction must vary with center of mass energy.

The increase of thrust with energy is due to two effects: The decrease of the strong coupling constant, which for massless partons in first order perturbation theory is proportional to $1 - T$, and the narrowing of the jet structure, see fig. 2.14 in the previous section.

The studies of the center of mass energy dependence of event shape variables arrive at the following conclusions:
- The parton shower models JETSET, HERWIG and ARIADNE can describe the $\sqrt{s}$ dependence in the interval 12–91 GeV.
- Matrix element based programs need to be retuned at different center of mass energies.

3.5. *Fragmentation properties of heavy quarks*

So far I have considered event properties obtained by analyzing the full hadron data sample with contributions from all flavors. For the heavier quarks charm and bottom, which can be tagged via their semileptonic decays, measurements of their fragmentation properties have been made at the Z^0 resonance [94, 98, 93, 99]. Charm and bottom quarks are produced almost exclusively as primary partons and not in the fragmentation process because of their high masses.

The theoretical foundations to heavy quark physics at the Z^0 resonance are summarized in ref. [65], and the experimental results are reviewed in ref. [100]. The main results are:
- The energies of hadrons containing charm or bottom quarks are large, as expected due to their

*) The MARK II result [91], for which only the statistical error is published, is compatible with the LEP average.

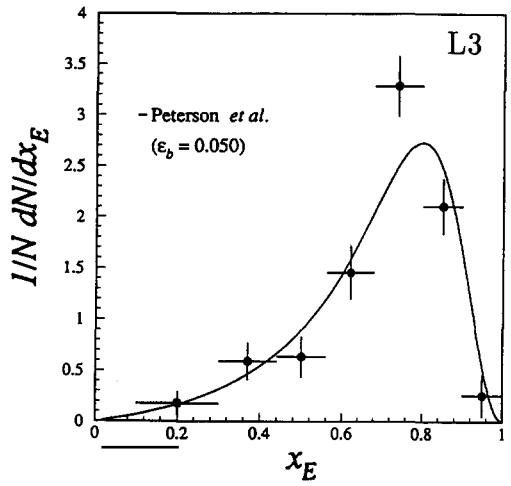

Fig. 3.3. x_E spectrum for bottom hadrons measured by L3 [93].

high masses:

$$\langle x_E^{\text{charm}} \rangle = 0.51 \pm 0.02 \quad (\text{for } D^* \text{ mesons}), \quad \langle x_E^{\text{bottom}} \rangle = 0.71 \pm 0.01, \tag{3.3}$$

where x_E denotes the energy of the hadrons divided by the beam energy. This is in qualitative agreement with QCD calculations, which predict a suppression of gluon radiation from heavy quarks [101].

- The shape of the energy spectrum for bottom hadrons can be described by a function of the form [95]

$$f(x_E) \sim \frac{1}{x_E}\left(1 - \frac{1}{x_E} - \frac{\epsilon}{1 - x_E}\right)^{-2}, \tag{3.4}$$

as is shown in fig. 3.3 for the L3 data [93] and a value of $\epsilon = 0.05$. The form of the measured spectrum can be reproduced by QCD calculations [102, 103].

- The decrease of the mean energies $\langle x_E \rangle$ in the center of mass energy range between 10 and 91 GeV can be attributed to the growth of the energy fraction radiated off in form of gluons before the heavy quarks hadronize.

3.6. Final state photon radiation from quarks

Quarks produced in e^+e^- collisions can radiate not only gluons but also photons [104]. The relative probabilities are given by

$$p(q \to q\gamma)/p(q \to qg) = O(\alpha Q_q/\alpha_s C_F) = O(\tfrac{1}{100}). \tag{3.5}$$

The first measurements of the cross section for $q\bar{q}\gamma$ final states have been done based on a few hundred events per LEP detector [105, 106]. These results have been compared with predictions from parton shower programs and analytical QCD calculations. While the parton shower programs

JETSET and ARIADNE can describe the global features of hadronic events, the number of highly energetic and isolated photons predicted by ARIADNE is about 30% higher than the corresponding JETSET cross section. The measured rates lie in between the predictions of the shower programs and agree with an $O(\alpha_s\alpha)$ matrix element calculation [107]. The differences between ARIADNE, JETSET and two new programs, HERWIG 5.4 [108] and SPLASH 1.2 [109], seem to be related to different choices of the evolution parameter, of the energy scale used in the α_s formula, and of kinematical approximations [110, 111, 108, 109]. Therefore final state photon radiation provides a powerful tool to probe the parton shower development. Further progress requires more statistics and detailed comparisons between measured and generated $q\bar{q}\gamma$ events.

4. Strong coupling constant

There are many compelling reasons for measuring the strong coupling constant: (1) α_s is the only free parameter in perturbative QCD, (2) many tests of QCD require α_s to be known, (3) for a large number of electroweak tests strong corrections must be calculated precisely, (4) grand unification theories can be tested by extrapolating the different coupling constants to very high energies [112, and references therein].

Apart from *measuring* the fundamental parameter α_s several *tests* of QCD can be made by comparing α_s values obtained from different variables (*consistency*), in different reactions (*universality*), for different quark species (*flavor independence*), and at different energies (*running*).

In sections 4.1 to 4.5 the measurements of the strong coupling constant in $e^+e^- \to Z^0 \to$ hadrons are described and an average for α_s is computed taking into account all available results. The QCD tests as listed above are discussed in sections 4.5 to 4.8.

4.1. How to measure the strong coupling constant

An observable V sensitive to the strong coupling constant can be expressed symbolically in the form [113]

$$V(\alpha_s) = v^{\text{pert}}(\alpha_s) \otimes v^{\text{non pert}}. \tag{4.1}$$

The perturbatively calculable part v^{pert} may depend also on electroweak parameters, which are assumed here to be known exactly. The perturbative part has to be "convoluted" with non perturbative corrections $v^{\text{non pert}}$. In principle also this part depends on the strong coupling strength, but often α_s does not appear explicitly, for example in fragmentation models, or the dependence is negligible, in particular if the non perturbative corrections are small.

It has to be stressed that the classification into "perturbative" and "non perturbative" parts is ambiguous, as was illustrated in section 2.2.3. Often $v^{\text{non pert}}$ is simply defined to contain all those contributions which are not (yet) included in v^{pert}. This implies that the full theoretical uncertainty is hidden inside $v^{\text{non pert}}$. Using those definitions, improved perturbative calculations (by including higher order corrections) reduce the role of the "non perturbative" corrections.

In this article I define $v^{\text{non pert}}$ to contain only effects not accessible with perturbation theory, i.e. the soft gluon region with $Q < Q_0 \approx 1$ GeV [8]. This implies a distinction between the term "hadronization correction" as used in connection with matrix element generators and $v^{\text{non pert}}$ (see section 2.2.3). Corresponding to eq. (4.1) two theoretical errors have then to be taken into account when extracting α_s from a measurement of V, an uncertainty due to missing higher order corrections in v^{pert}, and the uncertainty related to the non perturbative part.

The perturbative calculation can be done in a leading logarithmic approximation or as an order by order matrix element computation. To measure α_s the latter approach is the preferred one, since here the strong coupling constant is well defined, and since the kinematics, in particular for hard processes, calculated exactly (in the limit of vanishing masses). Then v^{pert} of eq. (4.1) can be expanded in powers of α_s in the form

$$v^{\text{pert}} = a_0^0 + a_1^0\alpha_s + a_2^0\alpha_s^2 + a_3^0\alpha_s^3 + \cdots, \tag{4.2}$$

where the coefficients a_i^0 have been calculated in a given renormalization scheme at an energy scale $|q|$ assuming a certain number of quark flavors N_F.

For a renormalization scale μ different from $|q|$ the strong coupling α_s has to be evaluated at the scale μ instead of $|q|$, and also the above coefficients a_i are μ dependent. The complete series (4.2) remains unchanged, as it must, since μ is not a physical parameter.

If the expansion is truncated after the ith term, a renormalization scale dependence of $O(\alpha_s^{i+1})$ remains. This causes an uncertainty for the determination of α_s, since the renormalization scale is not predicted by QCD. The problems of scale dependence and unknown higher order terms are therefore closely related. To estimate the latter one often explores the former, as described in section 4.4, where also other estimates of uncalculated higher order effects are discussed. In second order perturbation theory a change of the renormalization *scheme* (for example from $\overline{\text{MS}}$ to MS) is equivalent to a change in the renormalization *scale* μ [114], and is therefore not discussed here.

The new coefficients $a_i(f)$, where $f \equiv \mu^2/q^2$, can be written in the form

$$a_i = \sum_{j=0}^{i-1} c_i^j (\ln f)^j, \tag{4.3}$$

where the numbers c_i^j can be calculated from the sets of numbers a_i^0 and β_j using a recursive relation [115]. Here the β_j are the coefficients of the QCD β function, as introduced in section 2.1.3. For the terms up to α_s^3 (so far no full QCD calculation beyond that order exists) one obtains:

$$\begin{aligned} v^{\text{pert}} &= a_0^0 + a_1^0\alpha_s + (a_2^0 + a_1^0\beta_0 \ln f)\alpha_s^2 \\ &\quad + [a_3^0 + (a_1^0\beta_1 + 2a_2^0\beta_0)\ln f + a_1^0\beta_0^2(\ln f)^2]\alpha_s^3. \end{aligned} \tag{4.4}$$

Figures 4.1a and 4.1b illustrate the renormalization scale dependence. In part (a) the scale dependence is shown when truncating the series expansion (4.2) after the first, second and third order terms. In this example the coefficients a_i^0 are taken from the QCD correction to the total hadronic Z width (section 4.3.1). One can see nicely how the dependence on the scale parameter f is reduced when higher order terms are included in the calculation.

Figure 4.1b shows the scale dependence for second order calculations as a function of the relative size of the second order coefficient. The values 3 and 1 chosen for the ratio a_2^0/a_1^0 are typical for event topology variables (in particular jet fractions and asymmetry of energy–energy correlations, see section 4.4). For small values of f the coefficients $a_2, a_3, \ldots$ can become very large. This regime has to be avoided since the convergence of the series expansion (4.2) cannot be expected to be fast in that case. It seems that observables with a small second order correction (and consequently a modest scale dependence) result in small theoretical uncertainties and are thus suited best for a determination of α_s. However, a small coefficient a_2^0 does not necessarily imply that also the third order coefficient is small! Therefore one should determine the scale uncertainty from several observables V and compute the average. This gives an estimate of the theoretical error for any of

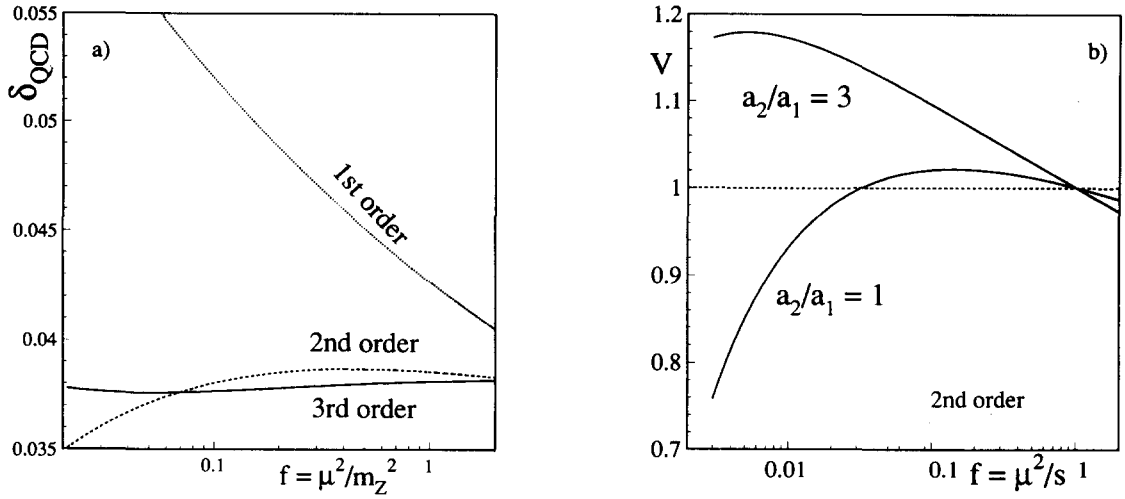

Fig. 4.1. Scale dependence for (a) δ_{QCD} and (b) typical event shape variables.

those quantities V. It is not justified to declare one variable to be better than another one on the basis of the numerical value of a_2^0.

Different recipes have been suggested for a choice of μ^2 in e^+e^-:

- *Physical scale* [116]: $\mu^2 \approx m_{qg}^2$, where m is the invariant mass of the quark–gluon system, assuming that the gluon g was radiated from a primary quark q.
- *PMS* (principal of minimal sensitivity) [117]. Here the scale μ_{PMS} is determined from the requirement $dV/df \equiv 0$, which is automatically fulfilled if V is calculated to all orders. The resulting value for the scale depends only on the ratio of the second and first order coefficients. For $a_2^0/a_1^0 = 1$ the best scale parameter is of the order of $f = 0.1$, which corresponds to $\mu_{PMS} \approx 30$ GeV for $|q| = 91$ GeV. This value becomes smaller than 10 GeV for $a_2^0/a_1^0 = 3$, as can be seen from fig. 4.1b.
- *FAC* (fastest apparent convergence) [118]. The scale μ_{FAC} is determined from the requirement $a_2 \equiv 0$.
- *BLM* (Brodsky–Lepage–Mackenzie scheme) [119]. Here the scale is shifted such that a flavor dependent part in a_2^0 is absorbed in the running coupling constant.

None of those prescriptions is a priori better than the others. However, the range of α_s values obtained by applying the different procedures is probably a good estimate of the theoretical error. All suggested recipes suggest μ^2/s to be smaller than 1 for most event shape variables (with a positive second order correction).

Some collaborations have tried to determine both α_s and the scale μ from a fit to jet data [120–122]. This is possible only when the regime of low jet-jet invariant masses is included in the fit. However, in this domain second order perturbation theory is known to fail [123]. Therefore the meaning of the resulting scale values, which turn out to be quite small (of the order of a few GeV), is not clear.

4.2. *Measuring α_s in $e^+e^- \to Z^0 \to$ hadrons*

There are two different methods to determine α_s:

Table 4.1
Relative uncertainties (in percent) for α_s.

Method	Theoretical error		Experim.	Total
	higher order	fragmentation	error	uncertainty
(1) hadronic Z^0 width	2	-	10–15	10–15
(2) event topology	5–10	3	3	5–10

(1) Measurement of the hadronic partial Z^0 width Γ_{had} or, equivalently, of the hadronic cross section at the Z^0 pole. This determination of α_s implies counting of hadron events, independent of their structure. The QCD correction to the hadronic width has been calculated to third order in α_s [124], and the uncertainty due to missing terms of $O(\alpha_s^4)$ is presumably small. There are no hadronization uncertainties, since the fragmentation process can only change the shape of an event, but cannot make it disappear [113, and references therein]. Since the QCD correction ($\approx \alpha_s/\pi \approx 4\%$) is small, a very high experimental precision is required: in order to reach $\Delta\alpha_s = 0.01$ an accuracy of $\Delta\Gamma_{had}/\Gamma_{had} = 0.3\%$ is needed.

(2) Analysis of the event topology, in particular a study of events with hard gluon bremsstrahlung. The fraction of those events is to lowest order proportional to α_s. A large number of variables exist to measure the hard gluon content in hadronic events [8]. Here I will describe jet fractions, the heavy jet mass distribution and the asymmetry of energy–energy correlations. From these observables the strong coupling constant can be obtained with relatively small hadronization uncertainties. Since the matrix element calculations for the 3-jet fraction and other event shape variables have been performed only to $O(\alpha_s^2)$, the uncertainty due to unknown higher order corrections is the dominant contribution to $\Delta\alpha_s$ in this method.

These two methods are largely independent and therefore complementary. The theoretical and experimental uncertainties are quite different in both cases, as is shown in table 4.1. The theoretical error has two contributions: missing higher order terms in the perturbative expansion and non perturbative effects (fragmentation). The experimental uncertainty corresponds to the combined LEP measurements, based on the 1990 data samples.

4.3. Determination of α_s from $\Gamma_{had}/\Gamma_{lep}$

4.3.1. Standard Model prediction

The QCD correction to the hadronic width can be measured best from the ratio of the hadronic and leptonic partial widths of the Z^0 boson. In the Standard Model of electroweak and strong interactions it is given by

$$R_Z \equiv \Gamma_{had}/\Gamma_{lep} = F_Z(1 + \delta_{QCD}) . \tag{4.5}$$

The factor F_Z contains the electroweak coupling constants of leptons and quarks. Including electroweak radiative corrections one obtains for $m_t = 124^{+32}_{-36}$ GeV [36]*) and $m_H = 300$ GeV [39]

$$F_Z \equiv \Gamma^0_{had}/\Gamma_{lep} = 19.97 \pm 0.02 . \tag{4.6}$$

*) Here the value for m_t is used which is obtained from a fit to LEP, $p\bar{p}$ collider and neutrino data with α_s being a free parameter.

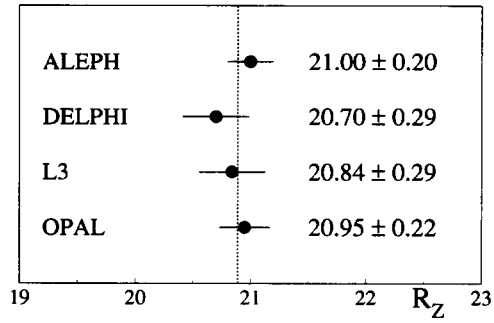

Fig. 4.2. Measured values for $R_Z = \Gamma_{had}/\Gamma_{lep}$.

Most m_t and m_H dependent corrections are common to Γ^0_{had} and Γ_{lep}. The remaining dependence stems mainly from the vertex corrections to $b\bar{b}$ production. Here Γ^0_{had} stands for the hadronic width without QCD corrections ($\alpha_s = 0$). The error of $\Delta F = \pm 0.02$ corresponds to a variation of m_t within the errors given above and m_H in the range 50–1000 GeV. The result (4.6) is reproduced by other calculations [125, 126, 38, 37] within ≈ 0.01. Instead of R_Z also the ratio of the peak cross sections

$$R \equiv \sigma^{peak}_{had}/\sigma^{peak}_{lep} = F(1 + \delta_{QCD})$$

can be used to derive α_s [39]. The factor $F = 19.77$ is slightly smaller than F_Z because of the photon exchange diagram, which contributes to the cross sections but not to the partial Z^0 widths. The quantity R can be measured directly, without need for off-peak data, knowledge of luminosity or line shape fitting.

The QCD correction can be cast in the form [127]

$$\delta_{QCD} = 1.05\alpha_s/\pi + 0.9(\alpha_s/\pi)^2 - 13(\alpha_s/\pi)^3, \tag{4.7}$$

where the recently calculated third order correction [124]*) and charm and bottom mass effects and the top mass dependence [129–131] are taken into account. The relative theoretical uncertainty for δ_{QCD} is estimated to be 2%. This corresponds to an uncertainty of the strong coupling constant of $\Delta\alpha_s \approx 2\%$. For more details see appendix A.

The uncertainty in the electroweak part of the calculation of $\Delta R_Z = \pm 0.02$ translates into $\Delta\alpha_s = 3\%$ and is therefore currently the biggest theoretical uncertainty in the determination of the strong coupling constant from the hadronic Z width. However, this error will shrink to about 2% as soon as the top mass is known to some 10 GeV, and to about 1% if also the Higgs mass is known.

4.3.2. Experimental results

Figure 4.2 summarizes recent LEP measurements of R_Z, based on 1989 and 1990 data samples [132–135]. The statistical and systematic errors are not shown separately, since they are not published individually by all LEP collaborations. Typically the statistical error is about twice as big as the systematic one [133]. Since both the Z^0 branching ratio into hadrons and the acceptance for hadronic final states are larger than for Z^0 decays into electrons, muons and taus, the experimental uncertainty in R_Z is dominated by the leptonic channels.

*) The first calculation of the third order coefficient as published in ref. [128] was found to be incorrect.

From the average value [36]

$$R_Z = 20.89 \pm 0.13 \tag{4.8}$$

one gets

$$\delta_{QCD} = 0.0461 \pm 0.0065 \tag{4.9}$$

and

$$\boxed{\alpha_s(m_Z) = 0.136 \pm 0.019,} \tag{4.10}$$

where the error is dominated by experimental uncertainties. Without including the third order term in eq. (4.7) the α_s value would be 0.133.

Apart from the hadronic partial width the *total* width of the Z^0 can be used to measure the strong coupling constant. However, Γ_{tot} depends not only on α_s, but also strongly on the top quark mass. From a combined fit of all LEP cross section and asymmetry data, including the m_W measurements in $p\bar{p}$ collisions [136, 137], and the electroweak mixing angle determined by neutrino experiments [138, 139], one can determine m_t and α_s simultaneously, leading to a value of the strong coupling constant of 0.138 ± 0.015 [36], consistent with the result (4.10). The errors are somewhat smaller, but the result is more model dependent than the α_s value derived above.

4.4. Measurements of α_s from event topology

Many variables sensitive to the radiation of hard gluons from quarks have been defined [8]. In the context of this article all observables describing the topology of hadronic events are called event shape variables. Examples are jets, thrust, or energy–energy correlations. I consider here only quantities for which QCD predictions exist, so that the strong coupling constant α_s can be determined from a measurement of those event shape variables. We must use "infrared and collinear safe" variables [140]. This means that a variable should change only little when adding a soft parton or splitting one parton into two collinear ones (such that energy and momentum are conserved). Apart from these theoretical arguments "infrared and collinear safe" variables are also preferred for experimental reasons, since they allow a "calorimetric" measurement: adding a soft particle or splitting a particle into two with half the energy changes the measurement in a continuous way.

Why are so many different event shape variables needed, since they all measure the same hard gluon bremsstrahlung? Would it not be enough to analyze hadronic events in terms of jets? The concept of jets has the advantage of relating the measurable event structure directly to the hard primary partons and gluons. Furthermore hadronization corrections are of modest size and known with small uncertainties. The reason why also other event shape quantities are used to extract α_s is that they have a different sensitivity to higher order corrections and to hadronization effects. Therefore an important estimate of theoretical uncertainties can be made by comparing α_s values derived from different observables.

QCD calculations of the various event shape parameters as a function of the strong coupling constant can be done in several ways, as explained in section 2.2.2. Here I consider only calculations based on the second order matrix element (ME).

The QCD predictions in fixed order perturbation theory cannot take into account the effect of multiple gluon emission. In second order α_s at most two gluons can be emitted. For variables like thrust, jet fractions, etc. this leads to a singular behavior of the distributions in kinematic regions

where multi-gluon emission becomes dominant. This is a direct consequence of the collinear and infrared divergence of the gluon emission cross section.

Recently leading and next-to-leading contributions due to soft and collinear gluons have been exponentiated, i.e. resummed to all orders, and combined with the second order ME calculations [141]. One thus obtains a meaningful result for all regions of phase space, and does no longer need to introduce very small values of the renormalization scale for describing the region of high thrust T and small jet–jet invariant masses [121, 122]. These calculations are done analytically, so far only for the e^+e^- event shape variables thrust and heavy jet mass. Also the average jet multiplicity has been computed, however some terms have not yet been included in the resummation. Up to now the LEP collaborations have not yet made use of these important improvements; this will certainly be done in the near future.

Resummation techniques have been applied also in refs. [142, 143], however without combining these results with a second order ME calculation.

The different event shape variables can be classified formally according to the kind of numbers associated to each event:

(a) One integer number. Example: number of jets.

(b) One real number, as for thrust ("global event shape variables").

(c) A one-dimensional distribution, e.g. energy–energy correlations EEC [144].

(d) Multi-dimensional distributions, as for example triple energy correlations TEC [145].

This classification is not very rigid, since one can also study e.g. differential jet distributions (class (b)) or integrate over distributions. An example for the latter case are Fox–Wolfram moments [146] (class (b)) which are defined as integrals over energy correlations.

In the following sections three examples of measurements of α_s at LEP will be described, corresponding to the cases (a)–(c): the jet rate analysis by L3 [147], the measurement of the heavy jet mass distribution by ALEPH [148], and the determination of α_s from the asymmetry of energy correlations by OPAL [53]. For those three event shape distributions hadronization uncertainties are comparatively small.

In section 4.4.4 a value for the strong coupling constant will be determined combining all available measurements of event topologies.

4.4.1. Jets

Jets [149] can be defined in various ways. Most often invariant mass jet algorithms or variants are used, which depend only on one jet resolution parameter, y_{cut}. One of these jet finders is the JADE jet algorithm [150] which works in the following way: for each pair of particles i and j the scaled invariant mass squared,

$$y_{ij} = 2(E_iE_j/s)(1 - \cos\theta_{ij}), \tag{4.11}$$

is evaluated. E_i and E_j are the particle energies and θ_{ij} is the angle between particles i and j. $\sqrt{s} = \sum_i E_i$ denotes the total energy of the event. The pair for which y_{ij} is smallest is replaced by a pseudoparticle k with four-momentum

$$p_k = p_i + p_j. \tag{4.12}$$

This procedure is repeated until all y_{ij} exceed the jet resolution parameter y_{cut}. The remaining (pseudo)particles are called jets. Increasing y_{cut} lowers the fraction of multi-jet events but increases the separation of the jets.

Table 4.2
Definitions of jet algorithms.

Scheme	"Distance" y_{ij}	Particle recombination
"JADE"	$2E_iE_j(1-\cos\theta_{ij})/s$	$p_k = p_i + p_j$
E_0	$(p_i + p_j)^2/s$	$E_k = E_i + E_j$ $\boldsymbol{p}_k = (E_k/\lvert\boldsymbol{p}_i + \boldsymbol{p}_j\rvert)(\boldsymbol{p}_i + \boldsymbol{p}_j)$
E	$(p_i + p_j)^2/s$	$p_k = p_i + p_j$
p	$(p_i + p_j)^2/s$	$\boldsymbol{p}_k = \boldsymbol{p}_i + \boldsymbol{p}_j$ $E_k = \lvert\boldsymbol{p}_k\rvert$
$k_\perp$	$2\min(E_i^2, E_j^2)\,(1-\cos\theta_{ij})/s$	$p_k = p_i + p_j$

Other jet algorithms based on an invariant mass criterium can be defined using slightly different expressions for y_{ij} and p_k [8]. The recombination scheme and the distance measure are logically independent and can be combined in different ways. In the recently proposed $k_\perp$ algorithm [151, 152] y_{ij} measures the transverse momentum of the softer particle with respect to the other one. Table 4.2 shows the definitions for "distance" (y_{ij}) and recombination for the most popular algorithms.

For up to four massless partons the JADE scheme is equivalent to the E_0 scheme with respect to jet counting. The schemes differ from each other in their sensitivity to hadronization corrections. This is illustrated in fig. 4.3, where the ratio of the number of 3-jet events after and before hadronization (and decay) corrections is shown as a function of $\sqrt{s}$ for the algorithms JADE, E, p and $k_\perp$.

The correction of the E_0 scheme (not shown) is very close to that of JADE. The number of 3-jet events is calculated for y_{cut} values of 0.08 (JADE), 0.10 (E), 0.06 (p) and 0.03 ($k_\perp$). These values are chosen such that the 3-jet fraction is about 20% at 91 GeV for the four jet clustering schemes. The hadronization correction factors are determined using the parton shower (PS) option in the

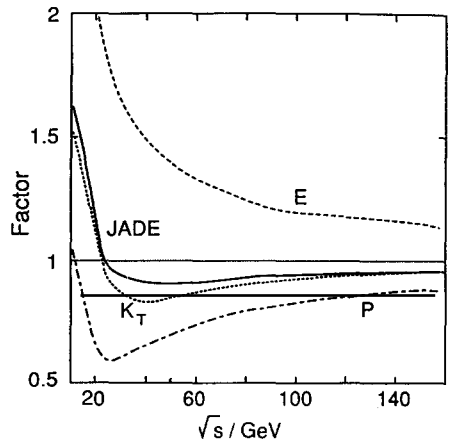

Fig. 4.3. Hadronization correction factor, defined as fraction of 3-jet events after and before hadronization.

Fig. 4.4. A 3-jet event, as "seen" by (a) the JADE algorithm and (b) the $k_\perp$ clustering scheme.

JETSET generator. For high center of mass energies the correction is small both for the JADE and the $k_\perp$ scheme, but substantially larger for the E and p algorithms. The probability that a 3-jet event at the parton level remains a 3-jet event at the hadron level is about 85% at 91 GeV for all the algorithms studied here at the y_{cut} values listed above. At energies below 25 GeV the effect of fragmentation and decays becomes large for all algorithms. Consequently QCD tests in that energy domain cannot be very precise.

The disadvantage of the JADE algorithm lies in the fact that two soft (pseudo)particles with a small invariant mass can be clustered together, even if their angular distance is very large. This is illustrated in fig. 4.4a, showing which particles are clustered together into jets. One of the jets (dashed lines) contains particles in opposite hemispheres. This feature of the JADE scheme prevents the resummation of the contribution of soft and collinear gluons [152].

This problem is avoided in the new $k_\perp$ algorithm, as is illustrated in fig. 4.4b. Here the same 3-jet event is shown as in part (a) of that figure, but now the three $k_\perp$-jets consist only of particles which are "close" to each other. Since for this new jet clustering scheme the resummation techniques can be applied [141], it will probably become the standard jet algorithm for QCD tests.

So far all experiments taking data at the Z^0 have used the JADE jet algorithm [148, 122, 147, 121, 153], since the hadronization uncertainties are smallest. L3 and in particular OPAL have studied jet rates also using other schemes such as the E algorithm.

The L3 analysis is based on 37 000 hadronic Z^0 decays at a center of mass energy of 91.2 GeV. Charged and neutral particles are measured in the electromagnetic detector and the hadron calorimeter, which covers the polar angular range $|\cos\theta| < 0.996$. The jet rates obtained with the JADE algorithm are corrected for detector effects, resolution and acceptance, and also for initial state photon radiation. All these corrections (individually and combined) are smaller than 10%. The measured jet fractions are compared with the analytical second order QCD calculation for the E_0 scheme [8, 43]. A small hadronization correction is included.

The measured 3-jet fraction at a particular value of y_{cut}, $y'_{cut} = 0.08$ is

$$f_3 = (18.4 \pm 0.9)\%. \tag{4.13}$$

The value of 0.08 was chosen so that the 4-jet fraction is negligible ($\approx 0.1\%$) while the 3-jet rate is still large. The corresponding QCD prediction is

$$f_3 = c_3 \cdot 1.08[\alpha_s(\mu) + (3.20 + \beta_0 \ln(\mu^2/s)\alpha_s(\mu)^2)], \tag{4.14}$$

where the hadronization correction factor c_3 is given in fig. 4.3. For the central value of the renormalization scale $\mu^2/s = y'_{cut} = 0.08$ [116], the strong coupling constant is determined to be:

$$\alpha_s(m_Z) = 0.115 \pm 0.005(\text{exp.})^{+0.012}_{-0.010}(\text{theor.}). \tag{4.15}$$

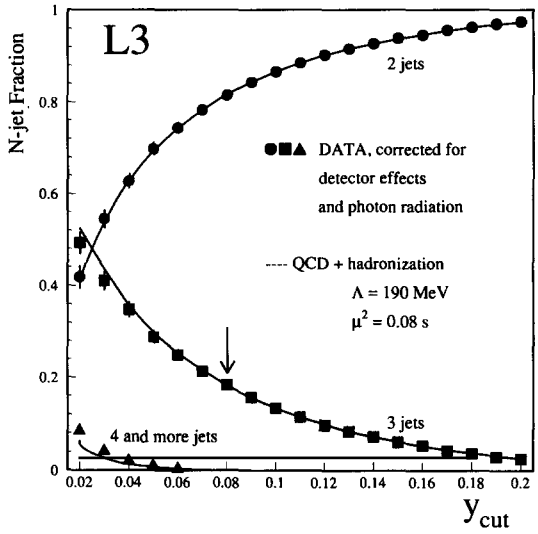

Fig. 4.5. Jet fractions measured by L3 [147].

The theoretical error is dominated by unknown higher order corrections, which have been estimated from a variation of the renormalization scale μ in the range 3–91 GeV [117]. Figure 4.5 compares the measured jet fractions as a function of y_{cut} with the QCD predictions for $\alpha_s = 0.115$ (corresponding to $\Lambda = 190$ MeV) and $\mu^2 = 0.08s$ [147]. The deviation in the jet rates at low values of y_{cut} is due to higher order corrections which are not yet calculated.

Similar results on jet fractions and α_s have been obtained by ALEPH [148], DELPHI [122], OPAL [121] and MARK II [153].

4.4.2. Heavy jet mass

The heavy jet mass [154, 8] is calculated in the following way: the event is divided into two hemispheres which are defined by the plane orthogonal to the thrust axis $\boldsymbol{n}_T$. The two invariant masses M_1, M_2 are calculated from the particles in the two hemispheres. The larger one is the heavy jet mass

$$M_h = \max[M_1(\boldsymbol{n}_T), M_2(\boldsymbol{n}_T)]\,. \tag{4.16}$$

For three massless partons there is a simple relation between thrust T and the heavy jet mass:

$$M_h^2/s = 1 - T\,. \tag{4.17}$$

The observable M_h has the advantage that the second order correction is smaller than for thrust [8], resulting in a relatively small estimated renormalization scale dependence. Also hadronization corrections are smaller than for thrust [8].

The ALEPH analysis [148] uses the charged track information from the time projection and inner tacking chambers in 53000 hadronic events. The measurements are corrected for detector effects, unseen neutral particles and initial state photon radiation. The resulting M_h distribution is compared with the theoretical predictions in ref. [8], convoluted with a hadronization correction function $p(M_h^{\text{parton}}, M_h^{\text{hadron}})$, where p is the probability to observe a heavy jet mass value M_h^{hadron}

at hadron level, if the parton level value is M_h^{parton}. The probability function is studied in different fragmentation models, based on ME and PS parton configurations. Also the renormalization scale dependence is analyzed. The final result is given for a scale $\mu = 0.5\sqrt{s} = 45$ GeV:

$$\alpha_s(m_Z) = 0.136 \pm 0.004(\text{exp.}) \pm 0.012(\text{hadr.})^{+0.008}_{-0.011}(\text{scale}). \tag{4.18}$$

The scale uncertainty corresponds to a variation of μ between m_{bottom} and m_Z. Note that the hadronization uncertainty is rather large. Therefore the ALEPH collaboration uses for their final result for α_s only the value obtained from jet fractions, due to its smaller fragmentation error.

Also DELPHI has measured the strong coupling constant from the heavy jet mass distribution and arrives at a result which is consistent with the ALEPH α_s value.

4.4.3. Energy–energy correlations

The energy–energy correlation [144] is the distribution of all angles between particles i, j in hadronic events weighted with the product of their energies. Using an angular bin width Δ_{bin} one can write

$$\text{EEC}(\chi_{\text{bin}}) = \frac{1}{\Delta_{\text{bin}} N} \sum_{\text{events}}^{N} \sum_{i,j} \frac{E_i E_j}{s} \delta_{\text{bin}}(\chi_{\text{bin}} - \chi_{ij}). \tag{4.19}$$

$\delta_{\text{bin}}(\chi_{\text{bin}} - \chi_{ij})$ is 1 for angles χ_{ij} inside the bin around χ_{bin} and 0 otherwise. $\sqrt{s} = \sum_i E_i$ is the total energy of the event. For 2-jet events most angles are close to 0° or close to 180°, while events with hard gluon radiation contribute to the central region. The integral of the EEC distribution in a range of 30° to 150° is a measure of the strong coupling constant. Events with hard gluon radiation contribute asymmetrically to the EEC distribution such that the asymmetry in the energy–energy correlation

$$\text{AEEC}(\chi) = \text{EEC}(180° - \chi) - \text{EEC}(\chi) \tag{4.20}$$

is positive for $\chi > 30°$. While the second order correction to EEC is of about the same size as for jet fractions, it is quite small for AEEC.

Figure 4.6 shows the AEEC distributions measured by OPAL [53] in comparison with the predictions of the Monte Carlo generators HERWIG 5.0 and COJETS 6.12. The data, based on 130 000 events, are corrected for resolution, acceptance and photon radiation. The JETSET PS curve is not shown, since it is nearly indistinguishable from the data points. COJETS can not describe the low χ region and HERWIG underestimates AEEC for large values of χ.

To extract α_s two methods have been used: once the JETSET PS program is used to calculate the hadronization correction which is applied to the data. Then the integral of the AEEC distribution in the range $30° \leq \chi \leq 90°$ is computed, and the result is compared with an analytical calculation [8]. In the second method the hadronization correction is determined with fragmentation parameters tuned for the JETSET ME generator using a value of $y_{\text{min}} = 0.01$ to define resolvable parton jets. The experimental result, corrected for hadronization, is compared with the predictions of the ME generator as a function of α_s. For a value of $\mu = m_Z$, OPAL obtains the result

$$\alpha_s(m_Z) = 0.118 \pm 0.003(\text{exp.})^{+0.009}_{-0.004}(\text{theor.}). \tag{4.21}$$

The theoretical error includes estimates of hadronization uncertainties and the effect of unknown higher order corrections. The second contribution, which is largest, has been estimated by comparing

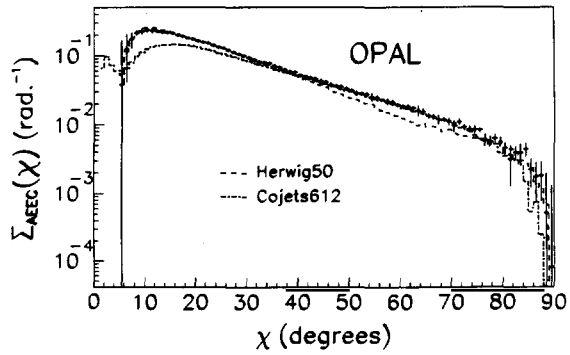

Fig. 4.6. Asymmetry of energy–energy correlations measured by OPAL [53].

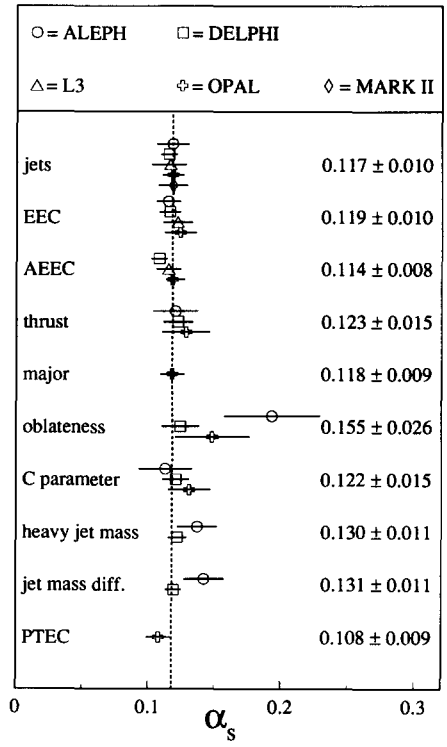

Fig. 4.7. α_s from event topology.

the results of the two methods (PS and ME) and by a variation of the scale μ between 18 and 91 GeV.

The second order terms for EEC and AEEC have been calculated by several authors who arrive at different results [155–157, 8]. This introduces an uncertainty for the strong coupling constant of $\Delta\alpha_s = ^{+0.005}_{-0.002}$, which is not included in the above result. Hopefully these discrepancies will soon be understood and eliminated.

Also DELPHI [158, 87] and L3 [89] have measured α_s from the AEEC distribution and arrive at similar results.

4.4.4. Global α_s value from event structure

Values for α_s have also been derived from the study of energy–energy correlations (EEC) and from distributions of global event shape variables like thrust, C parameter, etc. [8, and references therein]. All those results obtained by the five experiments ALPEH [148, 159], DELPHI [122, 158, 87], L3 [147, 89], OPAL [121, 160, 53, 161–163] and MARK II [153] are summarized in fig. 4.7. The combination of all these results into one global α_s value is difficult for two reasons: (1) the errors are dominated by theoretical uncertainties, which can only be estimated, (2) the values of α_s derived from the various quantities are correlated.

In order to derive a combined value, first the experimental and theoretical uncertainties need to be estimated, as I will describe in the following paragraphs.

As an example for the agreement between different measurements fig. 4.8a compares the 3-jet

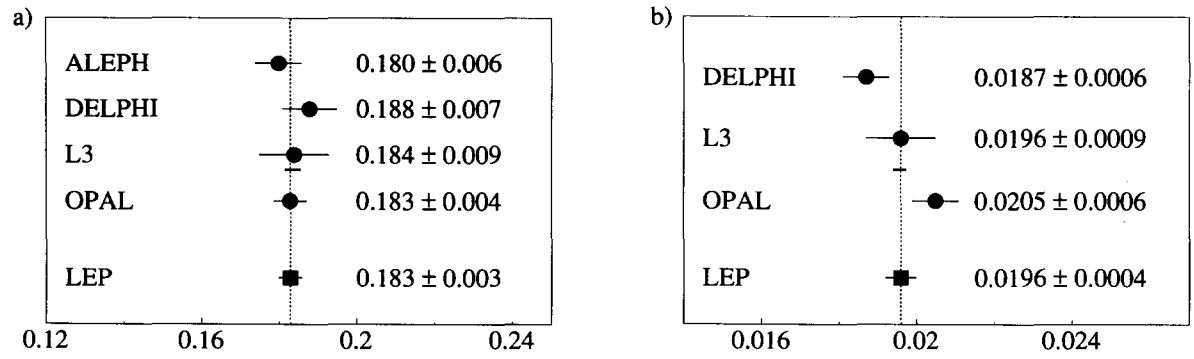

Fig. 4.8. (a) 3-jet fraction with $y_{cut} = 0.08$ and (b) AEEC, integral between 36° and 90°.

fractions for a jet resolution parameter of $y_{cut} = 0.08$ as measured by the four LEP experiments [148, 122, 147, 121]. All errors are dominated by systematic uncertainties. The relative statistical errors are of the order of 1%, since the measurements are based on samples with 10000 or more 3-jet events. The weighted average has a relative error of about 1.5%.

A similar comparison of experimental results is shown in fig. 4.8b for the integral of the asymmetry of energy–energy correlations between 36° and 90° [158, 89, 53]. Also in this case the different measurements agree. The precision of the weighted average is 2% in this case.

Also for the other event shape variables sensitive to the strong coupling constant the different LEP measurements are consistent with each other. The experimental accuracy is variable-dependent. The relative *experimental precision* of the combined LEP results for α_s can be conservatively estimated to be $\approx 3\%$.

The *theoretical uncertainties* for α_s from event topology are due to (a) missing higher order (> 2) corrections in the perturbative expansion, and (b) our limited knowledge about non perturbative effects (hadronization). Theoretical uncertainties of type (a) turn out to be the dominant ones. They can be estimated in several ways [164]:
- variation of the strong coupling constant with renormalization scale, see above,
- analysis of spread of α_s values for different variables,
- study of effects of higher orders in parton shower Monte Carlo generators.

The three methods lead to similar numerical estimates of 5–10% for the theoretical uncertainties due to uncalculated higher order corrections.

In this context it is interesting to study if the series expansion in α_s exhibits convergence: the OPAL data [90] have been used to derive α_s in first and second order from five different event shape variables [163]. While the lowest order results scatter between 0.007 and 0.205, the agreement becomes much better when next to leading corrections are included (0.098–0.142). This indicates the convergence of the series expansion.

Hadronization errors (b) can be estimated by
- the variation of fragmentation parameters of a given hadronization model,
- using different fragmentation models (see section 3).

For "good" variables (like the 3-jet-fraction) the hadronization uncertainty is found to be of the order of 3%.

To compute a global value for α_s from event topology analyses two alternative recipes can be applied:

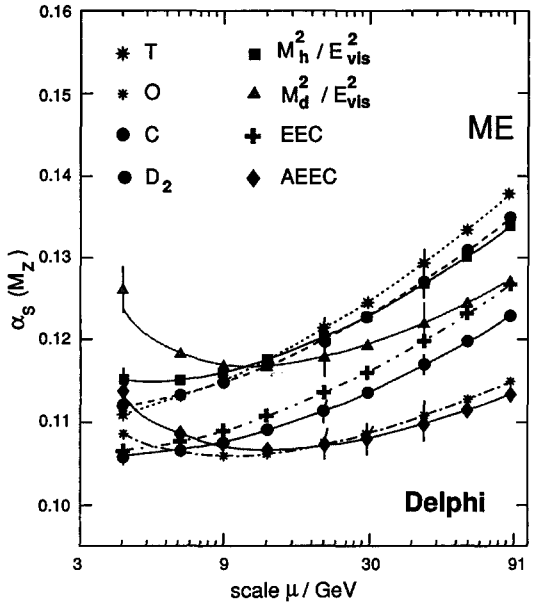

Fig. 4.9. α_s values determined by DELPHI [87].

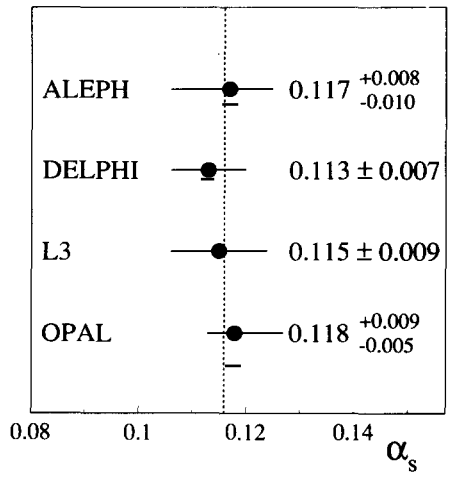

Fig. 4.10. α_s values from event topology.

(i) First average α_s values derived from jet-fractions, energy correlations etc. over experiments, then combine results from the different variables.

(ii) First calculate combined α_s value for a single experiment, then derive global average.

Method (ii), which will be applied here, has the advantage that correlations within one experiment can be taken into account better. In addition, due to the smallness of the experimental errors, a comparison of the different LEP values of α_s and corresponding error estimates is effectively a comparison of the different analysis methods applied by the four LEP collaborations. Method (i) has been used previously, for example in refs. [165, 164], with results similar to those derived here.

As an example for an α_s analysis combining several observables I will describe briefly the results of the DELPHI method [87]. This analysis is based on eight event shape variables, among them jet rates, thrust and AEEC. The measured distributions in these variables are corrected for detector effects and hadronization and then compared with the second order QCD calculations. To determine α_s, a fit is performed in a range of the shape variables where the 3-jet contribution is dominant and where the corrections are small.

Figure 4.9 shows the values of $\alpha_s(m_Z)$ as function of the renormalization scale μ for the eight variables [87]. Indicated are some typical experimental errors. The difference in α_s values obtained from the different quantities as well as the μ dependence indicate that higher order effects are not negligible. For small scales μ the spread of the α_s values is substantially reduced. The average α_s value corresponding to fig. 4.9 is found to be $\alpha_s = 0.111 \pm 0.002$ (exp.) ± 0.006 (theor.). Here correlations between the variables are taken into account. The theoretical error is estimated from the spread of α_s values as a function of shape variable and renormalization scale. Also hadronization uncertainties are included.

The whole analysis is performed twice. Once the QCD prediction is calculated using the ERT matrix element (ME) [43] option in JETSET and string fragmentation with parameters tuned for

this case. The results are shown in fig. 4.9. In a second analysis the hadronization corrections are calculated using the parton shower option in JETSET. In this case the parton level distributions as calculated numerically in ref. [8] are used. The second method leads to a slightly higher average α_s value. Combining the results of the two methods leads to an average value of the strong coupling constant from event topology of

$$\alpha_s(m_Z) = 0.113 \pm 0.007 . \tag{4.22}$$

Also the other LEP experiments have derived an "average" or "best" value for α_s and an estimate of the uncertainty. The results are shown in fig. 4.10.

The ALEPH value [159] is obtained from a combined analysis of energy–energy correlations and the global event shape variables thrust, C parameter and oblateness for pre-clustered events [166]. L3 has measured the strong coupling constant from jet rates [147], energy–energy correlations and their asymmetry [89]. The value given in fig. 4.10 is that from the AEEC analysis. This one has a slightly smaller error than the other two α_s values, which are consistent with the former one. Also the OPAL result for the strong coupling constant in fig. 4.10 is obtained from AEEC [53], see previous section. This result is consistent with an average of α_s values [167] as measured from jet rates [121], planar triple energy correlations [161] and global event shape variables [162]. The values and also the error estimates in fig. 4.10 are consistent with each other. Since the errors are dominated by theoretical uncertainties, which are common to all four α_s values, I combine the results of the figure by calculating the unweighted means, both for the central value and the error. The final result for the α_s value measured from the event structure at the Z^0 resonance becomes

$$\boxed{\alpha_s(m_Z) = 0.116 \pm 0.008 .} \tag{4.23}$$

The result from MARK II [153], which has a large statistical error, is compatible with the LEP average.

In ref. [168] a scheme of exponentiation of the leading terms in the perturbative expansion (corresponding to infrared divergences) for event shape variables is proposed. This method does not rely on explicit calculations of the contributions of soft and collinear gluons to certain event shape distributions. It assumes that the second order coefficient in (4.2) can be separated into two terms, of which one is common to all event shape variables and which can be exponentiated. This ansatz has been applied to LEP event shape measurements. The result on α_s and its error are similar to the one given in (4.23) [168].

4.5. Comparison and summary of α_s results

Figure 4.11 compares the α_s values obtained from R_Z and from the event shape. It has to be stressed that these two determinations are independent and that in one case (R_Z) the error is dominated by experimental uncertainties, while in the other case (event shape) the theoretical error is larger.

The weighted mean value of

$$\boxed{\alpha_s = 0.119 \pm 0.007} \tag{4.24}$$

is dominated by the result from the event topology. The value given in (4.24) corresponds to [20]

$$\Lambda^{(5)}_{\overline{\mathrm{MS}}} = 240^{+110}_{-80}\ \mathrm{MeV} . \tag{4.25}$$

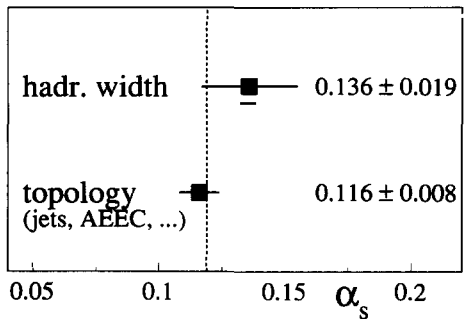

Fig. 4.11. Summary of α_s values measured at LEP.

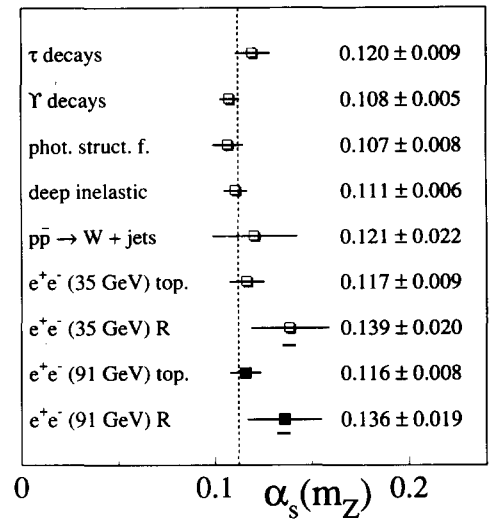

Fig. 4.12. α_s values at the scale $\mu = m_Z$.

With a relative precision of about 6% the α_s measurement at LEP is a very precise determination of the strong coupling strength. In the next section the result will be compared with α_s measurements in other processes. It has to be emphasized that this error includes *all* theoretical uncertainties; there is no additional model dependence.

4.6. Determinations of the strong coupling constant from different processes

A comparison of α_s values obtained in various processes such as deep inelastic lepton–nucleon scattering, $p\bar{p}$ collisions and e^+e^- annihilation constitutes an important test of the universality of QCD. Figure 4.12 shows such a comparison. Only those processes are taken into account which allow for relatively precise determinations of α_s. All measurements of the strong coupling strength have been translated into $\alpha_s(m_Z)$. The results are in good agreement with each other.

The α_s value from τ decays is obtained from the ratio R_τ of the τ hadronic and leptonic decay widths, which can be measured independently from the semileptonic branching fraction and the τ lifetime. Since the two corresponding results $R_\tau^{\text{branching fraction}} = 3.66 \pm 0.05$ and $R_\tau^{\text{lifetime}} = 3.32 \pm 0.12$ [169] differ by 2.6 standard deviations, I have increased the error of the weighted average by a factor of 2, so that the result becomes $R_\tau = 3.61 \pm 0.09$. From this value one can calculate $\alpha_s(m_\tau)$ and extrapolate [170, 30] to m_Z [124, 171, 172]: $\alpha_s = 0.120 \pm 0.009$. For a discussion on the α_s determination from τ decays see section 7.2.1.

The α_s results for ϒ decays, photon structure function and from e^+e^- event topology at ≈ 35 GeV are calculated from the $\Lambda^{(5)}$ values 120 ± 50 MeV, 115 ± 80 MeV and 215 ± 130 MeV of ref. [4]. The strong coupling constant shown in fig. 4.12 for deep inelastic scattering is an unweighted average of two recent analyses [173, 174], which yield $\alpha_s(m_Z) = 0.109 \pm 0.008$ and 0.113 ± 0.005.

The sixth result in the figure is derived from measurements of W + jet production in $p\bar{p}$ collisions by UA2 and UA1 [175]. The α_s values at the W mass are 0.123 ± 0.022 (exp.) ± 0.011 (theor.) (UA2) and 0.127 ± 0.040 (exp.) ± 0.016 (theor.) (UA1), where the theoretical uncertainties are common to both determinations. The value in fig. 4.12 has been calculated from the average of the

UA1 and UA2 results, and is extrapolated to the Z mass.

Measurements of R in e^+e^- annihilation have been combined and analyzed in refs. [22–24]. The value in fig. 4.12 corresponds to data taken at center of mass energies around 35 GeV and is computed as the average value of the three results for $\alpha_s(34\ \text{GeV})$ of 0.17 ± 0.03, 0.17 ± 0.03 and 0.18 ± 0.04 compiled in refs. [22–24] and extrapolated to 91 GeV. Data at $\sqrt{s}$ values between 20 and 65 GeV are consistent with the 35 GeV result.

The meaning of the errors shown in fig. 4.12 is not the same for all α_s values, since often some uncertainties (such as scale and model dependences) are not included. If one ignores this warning and calculates the weighted average of all results, one obtains for the global average $\alpha_s = 0.113 \pm 0.003$ and $\chi^2/N_{\text{Dof}} = 5.9/8$.

The e^+e^- values, in particular from R, are somewhat high, but still consistent with the other results. Future improvements in precision at LEP will reveal if there is a discrepancy or not.

Since the various measurements involve different quark flavors and different energy scales, a comparison of the α_s values is also a test of the flavor independence and the running of α_s.

4.7. Flavor independence of strong interactions

Quantum Chromodynamics predicts the coupling constant α_s to be independent of the quark flavor. Since the quark–gluon and the quark–quark couplings are described by the same constant g_s in the Lagrangian (2.1), a flavor dependence cannot be introduced easily. The only way to allow for a flavor dependent α_s is by having different "QCDs" for different quark flavors and consequently gluons of different "flavor" which do not interact with each other.

For the light quark species, up, down and strange, the QCD prediction of flavor independence is supported by the observation of approximate isospin and SU(3) flavor symmetries. Also the comparison of α_s values measured in charmonium and bottonium decays [176] with those obtained for other processes involving only u, d and s quarks confirms the QCD prediction. However, since these comparisons involve different energy scales and different systematic errors, the precision of such tests is not very high. The relative coupling strengths for charm and bottom quarks can be measured directly in e^+e^- annihilation. The first results obtained at center of mass energies around 30 GeV [177–180] confirm the flavor independence of α_s within large uncertainties.

More precise measurements can be done with the large data samples available at LEP. The following section describes the measurement of the strong coupling constant for bottom quarks by L3 [181].

The flavor composition in hadronic events produced in e^+e^- collisions at the Z^0 pole is different from that at lower center of mass energies. Section 4.7.2 explains how this fact can be used to compare the strong coupling constants for quarks with different electric charge (u, c and d, s, b).

4.7.1. α_s for bottom quarks

The L3 collaboration has measured the strong coupling constant for bottom quarks [181]. At the Z^0 pole the fraction of bottom events in the hadron sample is 22%. The b-quark content can be enhanced by selecting hadronic events with muons or electrons from semileptonic decays of heavy B mesons or hadrons. Cuts of 4 (3) GeV on the momenta of muons (electrons) and of 1.5 (1.0) GeV on the transverse momenta of the leptons with respect to the nearest jet are applied. In a hadron sample of 110 000 events L3 finds 1800 (1100) events with muons (electrons). In the inclusive lepton subsample 87% of the events contain bottom quarks. For both the inclusive lepton and the full hadron samples the 3-jet rates are measured as described in section 4.4.1. One gets for

Table 4.3
Measurements of α_s values for different quark flavors.

Flavor	α_s determ.	Tagging	Experiment	Ref.	α_s ratio
c	$p_\perp^{in}$ distr.	D* decays	TASSO	[177]	c/(udsc) = 1.00 ± 0.28
c	AEEC distr.	D* decays	TASSO	[179]	c/(udsc) = 0.91 ± 0.41
b	AEEC distr.	decay vertices	TASSO	[178]	b/(udscb) = 1.17 ± 0.57
b	jet fraction	semilept. decays	JADE	[180]	b/u = 1.12 ± 0.25
b	jet fraction	semilept. decays	L3	[181]	b/(udsc) = 1.00 ± 0.08

the ratio of 3-jet rates at $y_{cut} = 0.05$, after small corrections for detector, hadronization and bottom mass effects,

$$\frac{f_3^{\mu,e}}{f_3^{had}} = \frac{\sigma_{3\,jets}^{\mu,e}/\sigma_{tot}^{\mu,e}}{\sigma_{3\,jets}^{had}/\sigma_{tot}^{had}} = 1.00 \pm 0.03(stat.) \pm 0.04(syst.)\,. \tag{4.26}$$

This double ratio is sensitive to the ratio of the coupling constants $\alpha_s(b)/\alpha_s(udsc)$. It has the advantage that most systematic uncertainties cancel. The correction factor for acceptance and resolution is 0.97 ± 0.03 for inclusive muon events and 0.93 ± 0.04 for electron events. The fragmentation and mass corrections are $(3 \pm 2)\%$ and $(2 \pm 1)\%$. It has been verified that – within errors – the result is the same for the inclusive electron and muon samples and independent of y_{cut}. With the known bottom content in the two data sets of $(22 \pm 0.5)\%$ and $(87 \pm 3)\%$ one can calculate the ratio of α_s values for b quarks and the lighter species, assuming the first order relation $f_3 \propto \alpha_s$. The result is:

$$\alpha_s^b/\alpha_s^{udsc} = 1.00 \pm 0.05(stat.) \pm 0.06(syst.)\,. \tag{4.27}$$

Here the lighter quarks u, d, s, c are assumed to have the same coupling strengths. The effect of the second order correction on the relation between the 3-jet rate and α_s is negligible. This result is consistent with one and shows the flavor independence of the quark couplings as predicted by QCD. The precision is significantly better than that achieved previously in e^+e^- collisions at $\sqrt{s} \approx 30$ GeV, as is shown in table 4.3.

4.7.2. α_s for "up" and "down" type quarks

At $\sqrt{s} \approx 30$ GeV the cross section is proportional to the square of the charge Q_q^2 (photon exchange). At 91 GeV it is proportional to the sum of the squares of the vector and axial vector coupling constants $V_q^2 + A_q^2$ (Z^0 exchange), see section 2.2.1. Therefore the flavor composition at the Z^0 pole is different from that at lower center of mass energies, as is shown in fig. 2.9b.

The 3-jet fractions determined with the JADE algorithm for $y_{cut} = 0.08$ at 30 GeV and at 91 GeV can be written as

$$f_3^\gamma = 0.73 f_3^{up}(30\,GeV) + 0.27 f_3^{down}(30\,GeV)\,,$$

$$f_3^Z = 0.34 f_3^{up}(91\,GeV) + 0.66 f_3^{down}(91\,GeV)\,. \tag{4.28}$$

Here f_3^{up} stands for the average jet rate of the "up" type quarks u, c with charge $+2/3$. Similarly f_3^{down} denotes the mean value of the jet fractions for "down" type quarks d, s and b of charge $-1/3$.

Table 4.4
3-jet fractions for $y_{cut} = 0.08$ measured near 30 and 91 GeV.

$\sqrt{s}$ (GeV)	Experiment	Ref.	f_3
29	MARK II	[182]	0.229 ± 0.005
34.6	JADE	[150]	0.220 ± 0.004
35.0	TASSO	[183]	0.220 ± 0.005
91	LEP	section 4.4.4	0.183 ± 0.003

The coefficients in eqs. (4.28), the relative fractions of up and down type quarks, are calculated from table 2.2. Kinematical thresholds, higher order corrections and the small contributions of Z^0-graphs at 30 GeV and of γ-exchange diagrams at the Z^0 pole can be neglected.

The second order expression for the 3-jet fraction at $y_{cut} = 0.08$ is given by eq. (4.14) in section 4.4.1. The hadronization correction c_3 is practically flavor independent ($< 2\%$) and varies little with $\sqrt{s}$, as shown in fig. 4.3.

To compare the measurements at the Z^0 resonance and at lower energies one has to assume the running of α_s as predicted by QCD and given in eq. (2.16) in section 2.1.3:

$$\alpha_s(\sqrt{s}) = \frac{\alpha_s(m_Z)}{1 + \beta_0 \alpha_s(m_Z) \ln(s/m_Z^2)}. \tag{4.29}$$

Here the lowest order QCD formula can be applied, since the inclusion of the next order changes the results very little. I use here $\beta_0 = 0.60$ assuming $N_F = 5$. This would not be correct if there were two types of decoupled strong interactions, one for up type quarks, and one for down type quarks. In that case one would have to use $N_F = 2$ and 3, respectively.

The measured 3-jet rates ($y_{cut}=0.08$) at $\sqrt{s} \approx 30$ and 91 GeV are summarized in table 4.4. From a fit to those results, using $f \equiv \mu^2/s = 0.08$, one obtains the ratio of the α_s values for up type and down type quarks at 91 GeV:

$$\alpha_s^{up}/\alpha_s^{down} = 0.94 \pm 0.08. \tag{4.30}$$

The error includes the experimental error of 0.02, a hadronization uncertainty of 0.06 and a renormalization scale uncertainty of 0.05. The latter corresponds to a variation of f in the range 0.001 to 1. The hadronization error has been estimated by assuming an error of the ratio $c_3(35\ \text{GeV})/c_3(91\ \text{GeV})$ of 4%, and an absolute uncertainty, common to both center of mass energies, of $\Delta c_3 = 3\%$. If $N_F = 2$ or 3 is used instead of $N_F = 5$, the above ratio decreases by about 10%.

This result confirms that the strong coupling constant is independent of the weak isospin or the electric charge of quarks.

4.8. Running of α_s

The decrease of the strong coupling constant α_s with increasing energy is a consequence of the gluon self interaction and therefore one of the most important predictions of QCD. While we know from confinement and asymptotic freedom that this is qualitatively true, quantitative tests are difficult for the following reasons:

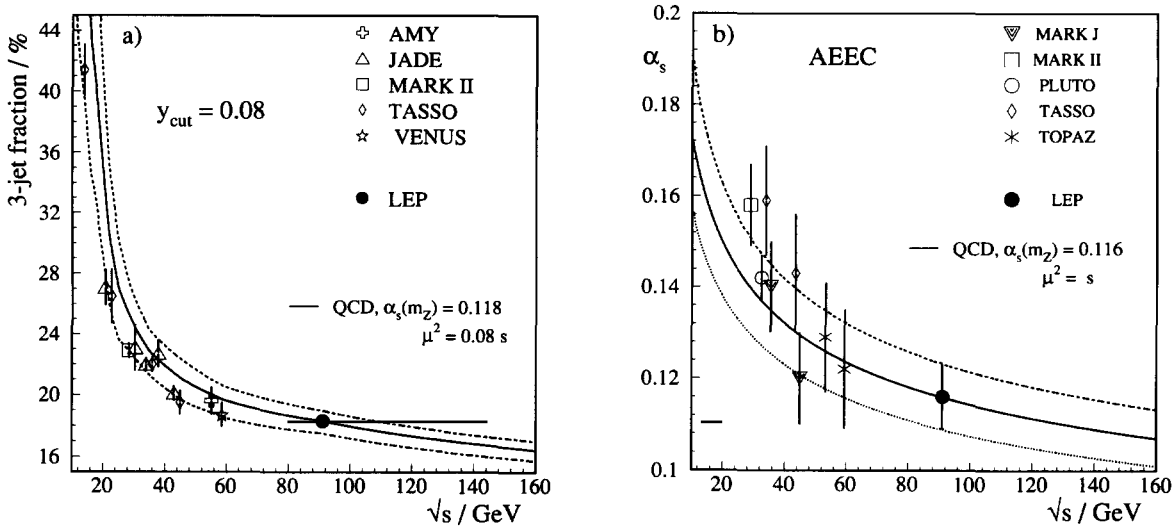

Fig. 4.13. (a) Energy dependence of the 3-jet fraction, (b) energy dependence of α_s from AEEC.

- One needs data for at least two energy points, and both energies should be high enough, so that perturbative QCD can be trusted and non perturbative effects are small or at least energy independent.
- Since the coupling decreases only logarithmically, the points have to be sufficiently far apart. Choosing for example the energies 30 and 90 GeV, one expects the ratio of the corresponding α_s values to be 1.2.
- The measurements have to be done for the same process, since the relative energy scale uncertainties are large when comparing α_s values obtained from different reactions.
- Ideally the measurements should be performed with the same detector to reduce the experimental uncertainties.

The first three conditions are fulfilled when comparing α_s values determined from the structure of hadronic events in e^+e^- annihilation above 20 GeV. The last point is valid to some extent for the results obtained at PETRA which covered the center of mass energy range 12–46 GeV, and for the MARK II measurements at 29 and 91 GeV [182, 153].

Firstly I analyze the 3-jet fractions obtained with the JADE algorithm for $y_{cut} = 0.08$, which have been measured by many experiments at PETRA, PEP, TRISTAN and LEP. It is advantageous to compare the measured jet fractions directly instead of the values of the coupling constant, since hadronization corrections, matrix element calculations and the renormalization scale used to derive α_s from these measurements differ from experiment to experiment.

Figure 4.13a shows the 3-jet fraction measured in e^+e^- annihilation for center of mass energies between 14 and 60 GeV [150, 183, 182, 184, 185] and at 91 GeV [148, 122, 147, 121]. To first order the 3-jet rate is proportional to the strong coupling constant α_s.

The energy dependence is reproduced by the QCD prediction [8], calculated for a value of $\alpha_s = 0.118$, corresponding to the average 3-jet fraction measured at LEP, and $\mu^2/s = y'_{cut} = 0.08$. The QCD predictions contain hadronization effects taken from fig. 4.3. The uncertainties indicated in fig. 4.13 come from the experimental error of the jet rates at 91 GeV and, in particular at low energies, from fragmentation uncertainties.

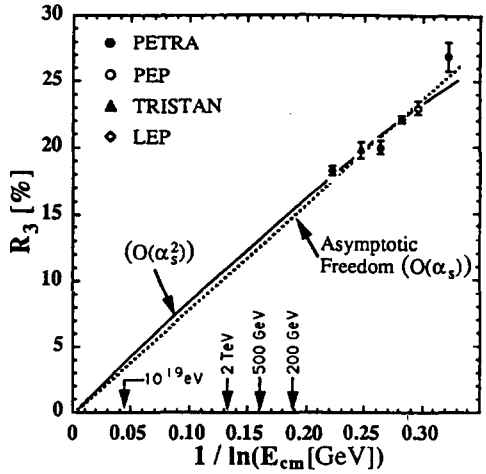

Fig. 4.14. 3-jet fractions, from Bethke [165].

Note that the renormalization scale uncertainty is the same for all the measurements. The conclusion that α_s runs therefore does not depend on a particular choice of μ.

It is interesting to compare the α_s values obtained by the MARK II collaboration, because they are measured with the same detector, taking data once at 29 GeV and once at 91 GeV [182, 153]:

$$\text{jets}: \quad \alpha_s(91\,\text{GeV})/\alpha_s(29\,\text{GeV}) = 0.83 \pm 0.06(\text{stat.}). \tag{4.31}$$

Unfortunately the dominant uncertainty is the statistical error at 91 GeV. The QCD prediction for this ratio is 0.83 (for $\alpha_s(m_Z) = 0.116$) and agrees with the measurements.

The running of α_s can also be demonstrated using values derived from the analysis of the asymmetry of energy–energy correlations [89]. Several groups have determined the strong coupling constant α_s in second order from AEEC [186, 158, 89, 160, 53]. Figure 4.13b shows only results obtained using the string fragmentation model for hadronization corrections and a renormalization scale $f = 1$. Measurements based on the FKSS [44] or GKS [45] matrix element calculations, which were found to be incomplete [11], are not shown. Statistical and systematic errors are combined quadratically. The energy dependence of α_s is reproduced by QCD using the average LEP value [158, 89, 160, 53] of $\alpha_s(m_Z) = 0.116 \pm 0.007$ (for $f = 1$).

Similar results can be obtained for other variables describing the event structure, but the uncertainties are larger and there are less data points available.

Another way to demonstrate the running of α_s is shown in fig. 4.14 [165]. Here the same 3-jet data as shown in fig. 4.13 are plotted as function of $1/\ln\sqrt{s}$, so that to first order one expects a straight line.

The set of experimental results shown in figs. 4.13 and 4.14 demonstrates unambiguously the running of α_s and provides indirect evidence for the gluon self coupling. This is a very important confirmation of QCD.

In order to quantify this statement, I will show that one can determine the coupling strength with a good precision from the *energy dependence* of the 3-jet rate alone. This is possible since α_s determines not only the *normalization* but also the *slope* of the curve in fig. 4.13a, as shown by eq. (2.16). For this determination I group measurements at similar center of mass energies together

Table 4.5
3-jet fractions for $y_{cut} = 0.08$ measured in e^+e^-.

$\sqrt{s}$ (GeV)	Experiment	Ref.	$\langle f_3 \rangle$
14	TASSO	[183]	0.414 ± 0.017
22	JADE,TASSO	[150, 183]	0.270 ± 0.008
29	MARK II	[182]	0.229 ± 0.005
35	JADE,TASSO	[150, 183]	0.220 ± 0.003
44	JADE,TASSO	[150, 183]	0.199 ± 0.004
57	AMY, VENUS	[184, 185]	0.191 ± 0.006
91	LEP	section 4.4.4	0.183 ± 0.003

and calculate the weighted averages*). The results are shown in table 4.5. Then the QCD prediction [8] as function of $\Lambda_{\overline{MS}}$ using $f = 0.08$ and including hadronization (fig. 4.3) is fitted to those data points, leaving the absolute normalization free. The point-to-point hadronization uncertainty is assumed to grow from 2% at 91 GeV to 7% at 22 GeV and 15% at 14 GeV. The result is

$$\alpha_s^{\text{slope}} = 0.098^{+0.016}_{-0.013}, \tag{4.32}$$

where the error includes experimental and theoretical uncertainties. The latter ones contain fragmentation errors and a scale uncertainty, estimated from a variation of f between 0.001 and 1. The above value is remarkably precise and consistent with the value obtained from the absolute jet fractions at 91 GeV,

$$\alpha_s^{\text{normalization}} = 0.118^{+0.010}_{-0.006}. \tag{4.33}$$

Here the error is computed in a similar way as for α_s^{slope}.

Using information from both the slope and from the absolute normalization one can fit the number of flavors N_F. The result

$$N_F = 7.1^{+1.9}_{-1.6} \tag{4.34}$$

is consistent with the expectation of $N_F = 5$. The strong coupling constant is treated as a free parameter in this fit. This calculation has been done using the analytical formulas of ref. [46], where the N_F dependence is explicitly given. The errors have been obtained with the hadronization uncertainties as given above and an absolute fragmentation uncertainty of 3%, and by a variation of f between 0.001 and 1.

5. Test of QCD matrix elements

With the only free parameter in perturbative QCD, α_s, known, the QCD matrix element calculations can be tested by comparing the measured jet distributions in multi-jet events to the theoretical predictions. A few comparisons are shown in the previous section, for example the 3-jet fraction

*) The published VENUS data are not corrected for detector acceptance and resolution and photon radiation. The 3-jet rate in ref. [185] has been decreased by 5% to take these effects into account.

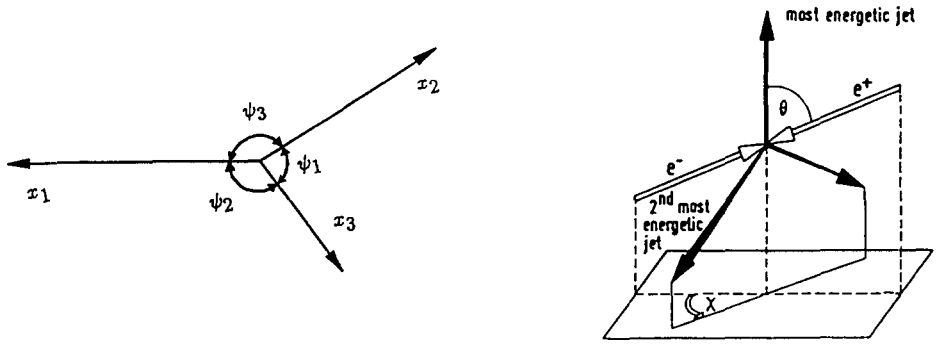

Fig. 5.1. Scaled parton energies and angles for 3-jet events.

as a function of the jet resolution parameter in fig. 4.5. Here a more systematic study of 3-jet and 4-jet events is presented.

Events with three jets can be used to distinguish between QCD with spin-1 gluons and an alternative model with scalar gluons. The triple gluon vertex contributes to events of type $e^+e^- \to q\bar{q}gg$. Thus 4-jet events can be used to distinguish between QCD and an abelian model without boson self coupling.

In the case of 3-jet events the QCD calculations are available in next to leading order, while the distributions for 4-jet final states have been calculated only on the Born level so far.

5.1. 3-jet events

For unpolarized beams, an event of type $e^+e^- \to 3$ jets can be described by four independent kinematical variables (apart from the jet masses). They can be chosen as x_1 = energy of the most energetic jet normalized to the beam energy, x_2 = energy of the second most energetic jet normalized to the beam energy, θ = polar angle of the first jet with respect to the e^- direction, χ = angle between the jet plane and a plane spanned by the first jet and the beam. Here no distinction between quark, antiquark and gluon jets is made. I refer to the most energetic jet as the "first jet", i.e.

$$x_1 \geq x_2 \geq x_3, \quad \text{with} \quad x_1 + x_2 + x_3 = 2, \tag{5.1}$$

assuming massless partons. Figure 5.1 (from ref. [187]) illustrates those definitions.

The differential cross section for the process $e^+e^- \to 3$ jets can be written in the general form

$$\mathrm{d}\sigma/\mathrm{d}x_1\,\mathrm{d}x_2\,\mathrm{d}\cos\theta\,\mathrm{d}\chi = \sum_{i=1}^{4} f^i(\cos\theta,\chi)\,\mathrm{d}\sigma^i/\mathrm{d}x_1\mathrm{d}x_2, \tag{5.2}$$

where the sum extends over four different Z^0/γ spin states and interference terms i [187].

While the functions f^i are determined by the initial state (e^+e^-) and the exchanged boson (Z^0), the helicity cross sections $\mathrm{d}\sigma^i/\mathrm{d}x_1\mathrm{d}x_2$ are sensitive to the final state strong interactions ($q\bar{q}g$) and depend on the gluon spin (0 or 1). In lowest order, their form does not depend on the strong coupling constant, which appears as an overall factor in eq. (5.2). The helicity cross sections have been evaluated first for massless partons and photon exchange to $O(\alpha_s)$ in ref. [188] for vector

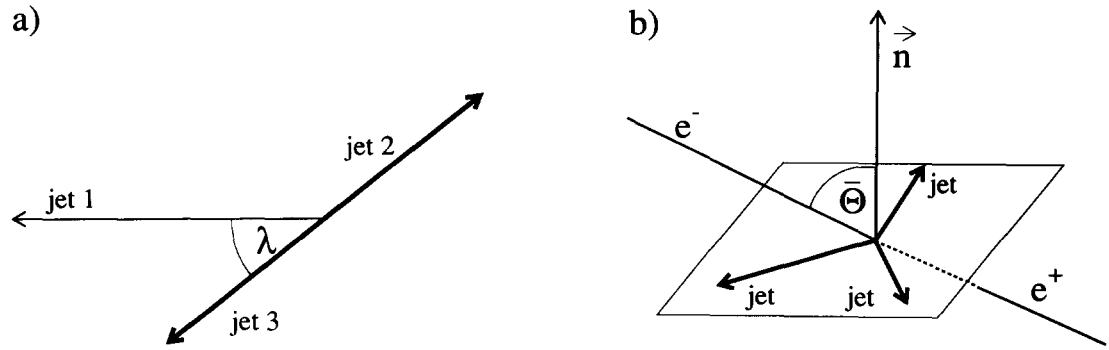

Fig. 5.2. (a) Ellis–Karliner angle λ, (b) polar angle of the normal to the 3-jet plane $\bar{\theta}$.

gluons (QCD) and in ref. [62] for scalar gluons. The calculations have been refined by including mass effects [189], Z^0 exchange [187, 190], and $O(\alpha_s^2)$ corrections [49] (for the spin-1 case).

In the vector gluon case the helicity cross sections for $e^+e^- \to \gamma \to q\bar{q}g$ and for $e^+e^- \to Z^0 \to q\bar{q}g$ are identical. For spin-0 gluons the helicity cross section terms proportional to V_q^2 and A_q^2 are different from each other. Here V_q and A_q denote the vector and axial vector couplings of the quark q to the Z^0 boson, respectively. Thus in the scalar gluon case the 3-jet distributions for Z^0 exchange differ from those for γ exchange.

The coupling constant α_s for QCD and $\tilde{\alpha}_s$ for the scalar gluon model, which appear as overall normalization factors in (5.2), are different. Furthermore, the matrix element calculations are performed to first order in $\tilde{\alpha}_s$ in the scalar and to second order in α_s for vector gluons. To avoid the corresponding normalization problems all comparisons presented here are based only on the *shape* of the distributions.

Integrating (5.2) over the angular variables and one of the energy fractions gives the cross section dependence on the variables x_i. The distributions in x_1, and in particular in x_2 and x_3, are quite different for vector and scalar gluons and thus allow to discriminate between these models. The difference is mainly due to the poles at $x_2 = 1$ and $x_3 = 0$, which exist in QCD, but not in the scalar gluon model. I will illustrate this for the infrared divergence $x_3 \to 0$: to first order in α_s the γ, Z^0 vector coupling parts of the QCD and scalar gluon matrix elements are given by

$$d\sigma^{QCD}/dx_q\, dx_{\bar{q}} \sim (x_q^2 + x_{\bar{q}}^2)/(1-x_q)(1-x_{\bar{q}}), \tag{5.3}$$

$$d\sigma^{scalar}/dx_q\, dx_{\bar{q}} \sim x_g^2/(1-x_q)(1-x_{\bar{q}}). \tag{5.4}$$

Here x_q, $x_{\bar{q}}$ and $x_g = 2 - x_q - x_{\bar{q}}$ denote the scaled momenta of the (massless) quark, antiquark and gluon, respectively. For $x_g \to 0$, and consequently $x_q \to 1$, $x_{\bar{q}} \to 1$, the vector gluon cross section becomes large ($\to \infty$), while it remains finite in the scalar case.

Also the Ellis–Karliner angle λ between the third and first jet, defined in the center of mass system of jets 2 and 3 (see fig. 5.2a), allows a clear distinction between spin-1 and spin-0 gluons [191]. For massless partons:

$$|\cos\lambda| = (x_2 - x_3)/x_1. \tag{5.5}$$

The differential angular cross section can be calculated from (5.2) by integrating over a certain kinematic range of the variables x_1 and x_2. It can be defined for example by the thrust value T.

For three massless partons $T = 1 - x_1$. Then

$$d\sigma/d\cos\theta\, d\chi = \sum_i f^i(\cos\theta, \chi)\sigma^i(T). \tag{5.6}$$

The angle $\bar{\theta}$ of the normal to the 3-jet plane with respect to the beam direction (fig. 5.2b) is related to θ and χ via

$$\cos\bar{\theta} = \sin\theta \sin\chi. \tag{5.7}$$

With the explicit expressions for f_i one obtains for the $\bar{\theta}$ distribution

$$d\sigma/d\cos\bar{\theta} \propto 1 + \bar{\alpha}(T)\cos^2\bar{\theta}. \tag{5.8}$$

In first order QCD the coefficient $\bar{\alpha} = -1/3$ is independent of the thrust value. Second order corrections are found to be very small [49]. For spin-0 gluons $\bar{\alpha}$ rises with decreasing thrust values and is always bigger than the QCD prediction.

5.1.1. Jet energy distributions

The distributions of jet energies and of the Ellis–Karliner angle have been measured by L3 [51] and OPAL [192]. The two analyses, which are based on about 100 000 hadronic events, are quite similar. Here I describe briefly the OPAL method.

Both track and calorimetric information are used to measure hadron events in a polar angle range $|\cos\theta_{\text{thrust}}| < 0.9$. Jets are reconstructed using the JADE algorithm [150] as introduced in section 4.4.1 with a resolution parameter $y_{\text{cut}} = 0.01$ ($y_{\text{cut}} \approx 1 - x_1$). With this small value a phase-space region is selected which is most sensitive to the gluon spin. The x_i are determined from the jet directions, which can be measured more precisely than jet energies:

$$x_i = 2\sin\psi_i/(\sin\psi_1 + \sin\psi_2 + \sin\psi_3), \tag{5.9}$$

where ψ_i is the angle between the two jets different from jet i, see fig. 5.1. The formula (5.9) is strictly valid only for massless partons. The measured x_2 and $\cos\lambda$ distributions are corrected for detector effects, photon radiation and hadronization and decays.

Figure 5.3 shows the distributions of the scaled energy of jet 2 and of the Ellis–Karliner angle as measured by L3 [51] and OPAL [192], respectively. In the L3 analysis jets are reconstructed with the JADE algorithm. All events which have three jets for $y_{\text{cut}} = 0.02$ are selected. The systematic errors are typically between 5% and 10% per bin. The measurements are compared with the QCD predictions [41,43] and to the scalar gluon model distribution [187]. In fig. 5.3b the results of both the parton shower and matrix element calculations are shown. The solid line in fig. 5.3a is obtained from the second order QCD matrix element. The theoretical curves are normalized to the number of data events. In all cases good agreement is found between the QCD predictions and the measurements, while the scalar model clearly fails to describe the data. Also other event shape variables such as thrust can distinguish between the different models [8].

5.1.2. Orientation of the 3-jet plane

The orientation of 3-jet events has been studied at the Z^0 pole by DELPHI [193] and L3 [51]. Here I will present the DELPHI measurement of the polar angle distribution of the normal to the three jet plane as a function of the thrust value. The analysis is based on 76 000 hadronic events in a polar angle range $|\cos\theta_{\text{thrust}}| < 0.75$. Only charged tracks are used. The measured $\cos\bar{\theta}$

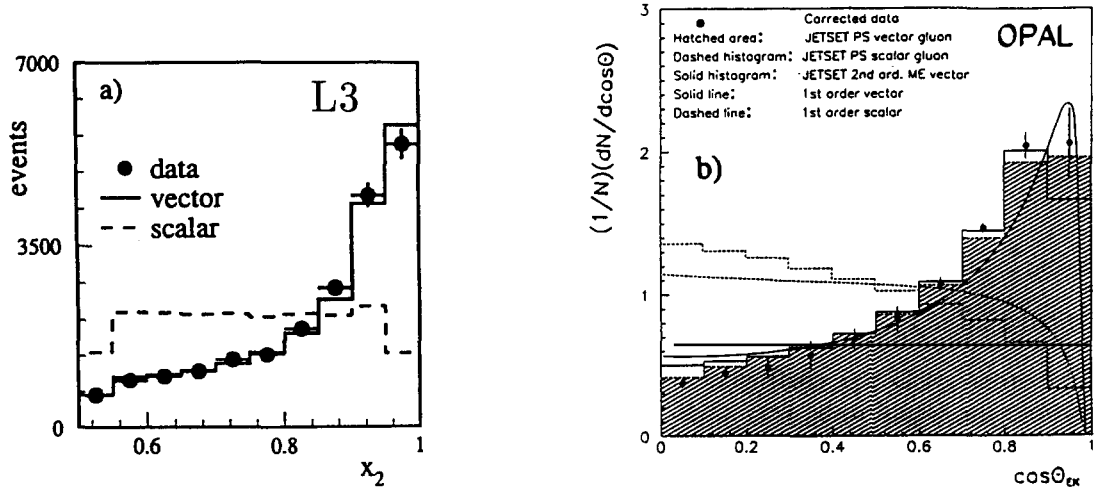

Fig. 5.3. (a) Distribution of energy fraction x_2 measured by L3 [51], (b) Ellis–Karliner angle distribution measured by OPAL [192].

distribution is corrected for detector acceptance and resolution, for initial state photon radiation and for fragmentation effects. Hadronic events with $T < 0.9$ are subdivided into four bins according to their thrust value T. For each of the four resulting data samples a function of the form (5.8) is fitted to the $\cos\bar{\theta}$ distribution and the parameter $\bar{\alpha}$ is determined. The result is shown in fig. 5.4. The distribution is compared with the QCD prediction of $-1/3$ and the scalar model curve [49].

Good agreement is found between the QCD predictions and the measurements, while the scalar gluon model fails to describe the data. However, the discriminating power is substantially smaller than for the jet energy distributions discussed in the previous section. The L3 collaboration has obtained similar results and arrives at the same conclusion.

The orientation of 3-jet events has been studied before at $\sqrt{s} \approx 30$ GeV using about 2000 events [194]. QCD to first order reproduces the measured distributions.

The spin-0 model has been ruled out already from analyses of other reactions [195], and also

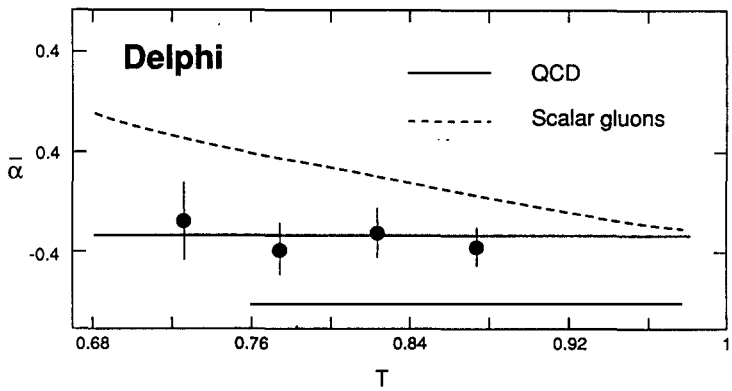

Fig. 5.4. Distribution of $\bar{\alpha}$ measured by DELPHI [193].

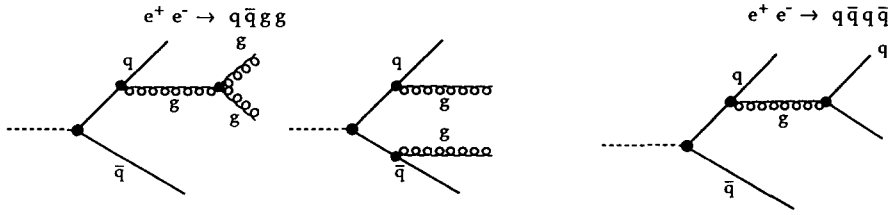

Fig. 5.5. Feynman graphs for 4-jet production.

from e^+e^- data at lower energies (from jet energy distributions only) [33]. However, at LEP the differences between the two alternatives are much bigger, and the QCD predictions (now available to second order) can be tested with a higher precision.

5.2. *4-jet events*

QCD predicts two classes of 4-jet events which correspond to the two processes

$$Z^0 \to q\bar{q}gg, \tag{5.10}$$

$$Z^0 \to q\bar{q}q\bar{q}, \tag{5.11}$$

at the parton level. The corresponding generic Feynman diagrams are shown in fig. 5.5.

The first graph for $q\bar{q}gg$ events contains a "three-gluon vertex", a consequence of the nonabelian nature of QCD.

An alternative model without self coupling of the spin-1 gluons can be constructed with 3 color degrees of freedom for the quarks [196]. Here only the double bremsstrahlung diagrams contribute to the process $e^+e^- \to q\bar{q}gg$.

As in the 3-jet analysis all comparisons between data and theoretical models are based only on the *shape* of the distributions, in order to avoid normalization problems due to the different coupling constants.

5.2.1. *Distinguishing QCD from the abelian model*

Different variables have been proposed that are sensitive to the differences between QCD and the abelian model [197–203]. Most of them are based on angular correlations between the four energy ordered jets. The most energetic jets 1 and 2 are likely to correspond to the "primary" quarks. The main difference between QCD and the abelian model in the distribution of those variables stems from the difference in the contribution of $q\bar{q}q\bar{q}$ final states to the 4-jet sample. The fraction of four-quark final states is about 5% in QCD, but 30% in the other model [202].

The angular variables have been studied by L3 [204] and OPAL [205] in order to discriminate between QCD and the alternative abelian model.

The L3 analysis is based on about 4000 4-jet events selected with a resolution parameter $y_{cut} = 0.02$ for the JADE clustering scheme.

The distributions for the following observables have been measured and corrected for detector effects and photon radiation:

– The variable proposed by Körner, Schierholz and Willrodt [197], Φ_{KSW}, is defined for events, for which there are two jets in both hemispheres defined by the thrust axis. Φ_{KSW} is the angle between

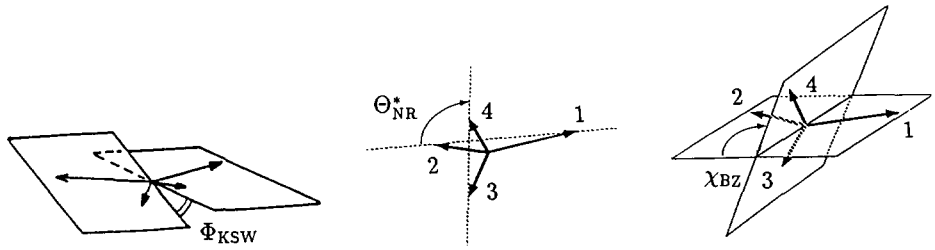

Fig. 5.6. Definition of angular variables sensitive to the three-gluon vertex.

the oriented normals to the plane containing the jets in one hemisphere and to the plane defined by the other two jets. Gluon alignment in the splitting process $g \to gg$ favors $\Phi_{KSW} \approx \pi$, so that the two softest particles point to the same side, whereas $g \to q\bar{q}$ prefers the planes to be orthogonal.
- The Nachtmann–Reiter angle [198], Θ^*_{NR}, is the angle between the momentum vector differences of jets 1, 2 and jets 3, 4. Due to the different helicity structures, $\Theta^*_{NR} \approx 0$ is favored by the process $g \to gg$ and $\Theta^*_{NR} \approx \pi/2$ is favored by $g \to q\bar{q}$.
- Bengtsson and Zerwas [199] define χ_{BZ} as the angle between the plane containing jets 1, 2 and the plane containing jets 3, 4. Linear polarization of the gluon in $e^+e^- \to q\bar{q}g$ results in different distributions of χ_{BZ} for $g \to gg$ and $g \to q\bar{q}$.

These definitions are illustrated in fig. 5.6 (from ref. [202]). Since here only the energy ordered jets are used to calculate the above angles, the differences between QCD and the abelian model for the $q\bar{q}gg$ final states are considerably smaller than in the case of identified quark and gluon jets.

All three measured distributions can be reproduced by the corresponding QCD predictions. The angle Φ_{KSW} turns out to be less sensitive than the other two observables for the distinction of QCD and the abelian model. The corrected and normalized distribution of the Nachtmann–Reiter angle χ_{NR} is shown in fig. 5.7a. The measurements are compared with the predictions of QCD and the abelian model. To estimate the theoretical uncertainties (hatched bands in the figure) the predicted angular distributions are determined once from the matrix element calculations and once using the parton shower generator JETSET. The measurements are reproduced by QCD, while the predictions of the abelian model are clearly incompatible with the data.

Similar conclusions can be drawn from the measured distribution of the Bengtsson–Zerwas angle χ_{BZ}, as is shown in fig. 5.7b for the OPAL data [205].

From both the L3 and OPAL analyses the abelian model can be ruled out. OPAL has set an upper limit for the fraction of four-quark final states of 9.1% at the 95% confidence level. This result is consistent with the QCD prediction of 4.7%, but not compatible with the fraction of 31.4% predicted by the abelian model. Similar studies have been performed for smaller event samples at $\sqrt{s} \approx 60$ GeV [206].

The 3-gluon coupling influences also event shape variables and jet production [163]. The measured dependence of the 3-jet fraction as function of the jet resolution parameter is not compatible with the abelian model [165].

Also the measured jet production rate in hadron collisions can be considered as evidence for gluon–gluon scattering [207, 208].

5.2.2. *Measuring color factors*

ALEPH [209] and DELPHI [200] have studied 4-jet events in more detail and measured the color factors appearing in the 4-jet differential cross section, which can be written in the following

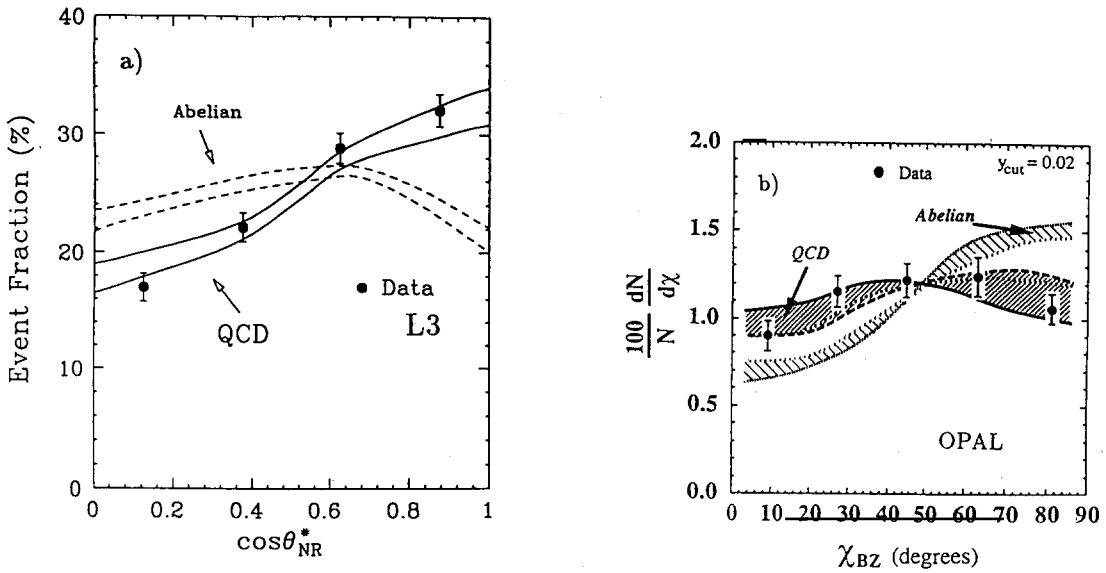

Fig. 5.7. (a) Nachtmann–Reiter angle measured by L3 [204], (b) Bengtsson–Zerwas angle as measured by OPAL [205].

way [43]:

$$\sigma_{4\text{-jet}} \sim C_F\sigma_A + (C_F - \tfrac{1}{2}C_A)\sigma_B + C_A\sigma_C + T_F N_F\sigma_D + (C_F - \tfrac{1}{2}C_A)\sigma_E. \qquad (5.12)$$

The formulas for the cross sections σ_i are given in ref. [43]. The first two terms in eq. (5.12) correspond to double gluon bremsstrahlung graphs, the third term involves all contributions to $q\bar{q}gg$ events containing the triple gluon vertex (including interference terms with double bremsstrahlung contributions), and the last two terms describe 4-quark final states. The contribution of the term $(C_F - \frac{1}{2}C_A)\sigma_E$ is very small. The number of flavors N_F is set to five in the analyses described here and also in the previous section*).

The color factor C_F is a measure of the quark–gluon coupling strength, C_A is proportional to the $g \to gg$ coupling and T_F defines the strength of the $g \to q\bar{q}$ coupling, see section 2.1.2. In alternative theories as for example the QED like abelian model the color factors are different while the cross sections σ_i are the same as in Quantum Chromodynamics. The color factors for the two theoretical models are compared in table 5.1.

Since the absolute normalization of the 4-jet cross sections is not well known, one can only compare the shape of the measured and predicted cross sections and determine the ratio of color factors C_A/C_F and T_F/C_F.

ALEPH determines the color factor ratios from a maximum likelihood fit to the measured differential cross section. A 4-jet event can be described by five independent variables (apart from the jet masses). The ALEPH analysis uses the scaled invariant masses squared, y_{ij}, of the jets i and j. About 4000 4-jet events are selected with a JADE jet resolution parameter $y_{cut} = 0.03$ out of 70 000 hadronic Z^0 decays.

*) This is correct only if the $q\bar{q}$ system has an invariant mass well above the bottom mass, since the matrix element calculations assume massless partons. In the LEP analysis the effective number of flavors is probably slightly below 5, but the corresponding change of the cross section is much smaller than the systematic errors.

Table 5.1
Color factors in QCD and abelian model.

	C_F	C_A	T_F
QCD	4/3	3	1/2
abelian	1	0	3

The DELPHI analysis is based on an event sample of similar size. Here the two-dimensional distribution in the variables $|\cos\Theta^*_{NR}|$ and α_{34} is measured and fitted, where α_{34} denotes the angle in between the two least energetic jets 3 and 4.

The results of both the ALEPH and DELPHI analyses are shown as contours (at the 68% confidence level) in the C_A/C_F versus T_F/C_F plane in fig. 5.8 [209,200]. Also shown are predictions of the abelian model and of SU(N) type gauge theories, in particular QCD with $N = 3$.

ALEPH and DELPHI obtain the color factor ratios

$$\text{ALEPH}: \quad C_A/C_F = 2.20 \pm 0.40, \quad T_F/C_F = 0.65 \pm 0.45, \tag{5.13}$$

$$\text{DELPHI}: \quad C_A/C_F = 1.87 \pm 0.41, \quad T_F/C_F = 0.20 \pm 0.18. \tag{5.14}$$

Table 5.2 compares the combined ALEPH and DELPHI measurements of the color factors with the predictions for the two models of strong interactions. The strength of the triple gluon vertex is measured to be non-zero with a significance of more than five standard deviations*). The abelian model can be ruled out from the measured ratios C_A/C_F and T_F/C_F. QCD reproduces the data very nicely. A distinction between SU(2), SU(3) and SU(4) is not possible in this analysis.

*) In the ALEPH and DELPHI analyses higher order corrections to the *shape* of the 4-jet distributions are assumed to be small; this is motivated by the smallness of the second order corrections to the form of the 3-jet distributions. See also ref. [203].

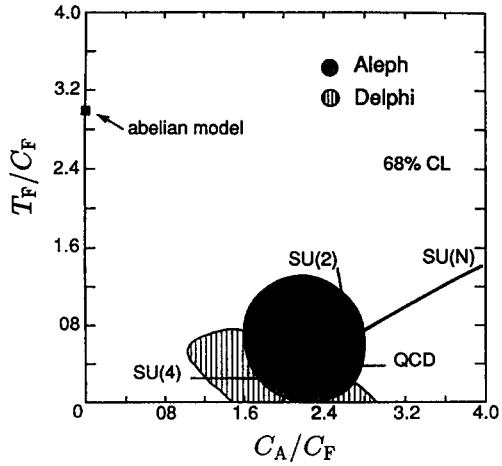

Fig. 5.8. QCD color factors as measured by ALEPH and DELPHI.

Table 5.2
Color factor ratios.

	C_A/C_F $g \to gg$	T_F/C_F $g \to q\bar{q}$
LEP	2.0 ± 0.3	0.3 ± 0.2
QCD	2.25	0.375
abelian	0	3

LEP has provided clear evidence for the existence of the triple gluon vertex and has found the coupling strength to be in quantitative agreement with the QCD predictions. Thus one of the fundamental properties of the gauge theory of strong interactions has been tested.

Also in the electroweak Standard Model with an $SU(2) \times U(1)$ gauge structure boson self coupling is expected to exist. However, this theoretical prediction can not yet be tested directly since the W bosons are so heavy*). Only when LEP will take data at center of mass energies above the W pair production threshold, in a few years from now, can the self interactions of the bosons γ, W and Z be studied experimentally.

6. "Soft" hadron physics

In the preceding sections measurements and QCD predictions have been compared at the *jet level*, corresponding to "hard" quarks and gluons.

In this section hadronic events are investigated at the *hadron level* and measurements of particle spectra, string effect, local particle density fluctuations etc. are presented. For many "soft" phenomena QCD predictions exist, in form of parton shower Monte Carlo generators and analytical (next to) leading log calculations. However, in studies at the hadron level the importance of fragmentation and particle decays is significantly increased with respect to the jet-level analyses. Consequently it is difficult to test the perturbatively calculated QCD predictions and the hadronization schemes separately.

In the previous sections tests of the fundamental properties of QCD have been described. Here the goal is not so much a test of the QCD Lagrangian, but rather to explore to what extent QCD calculations can successfully be applied to soft phenomena.

Firstly I will outline briefly the qualitative results of the QCD calculations for particle spectra, string effect etc. Then I will describe the various measurements done at LEP and compare the results with the QCD predictions.

6.1. Gluon interference

Interference of gluons leads to the following two phenomena:

- *Intra-jet effects.* The (next to) leading log QCD calculations [57, 9] take into account interference effects between soft gluons, as prescribed by quantum mechanics. In this context the expression "soft gluon coherence" is frequently used. One finds that *destructive* interference occurs if the emission

*) First evidence for the the $W^{\pm}$–γ coupling comes from the observation of $W \to \ell\nu\gamma$ decays [210].

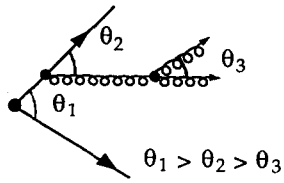

Fig. 6.1. Angular ordering.

angles in subsequent parton branchings increase. This means that effectively the subsequent angles decrease, as shown schematically in fig. 6.1 [9]. This phenomenon is generally referred to as "angular ordering" and used for example in parton shower generators to take into account interference effects.

Consequently the available phase space for soft gluons inside a jet is decreased. This leads to reduced parton multiplicities and a suppression of partons with low momentum.

- *Inter-jet effects.* Analytical QCD calculations predict for 3-jet events destructive inter-jet interference effects in the region between the q and the $\bar{q}$ jets [211, 9]. Thus less particles are produced in between the quark and antiquark jets in comparison to the other two inter-jet regions. This is known as the "string effect", see below.

For the test of the parton level predictions a model for hadronization and decays is needed. In case of Monte Carlo generators, string or cluster fragmentation is used together with empirical decay tables. In the context of analytical calculations the hypothesis of "local parton hadron duality" (LPHD) [212, 213] is invoked. It suggests that the calculated parton distributions can be compared directly with the measurements for (long lived) hadrons.

6.2. Charged particle multiplicity

Five experiments have measured the charged particle multiplicity distribution at the Z^0 pole and compared their results with different models [214–216, 91, 217]. The parton shower Monte Carlo program JETSET can reproduce the data well. This is also true for certain phenomenological models, for example the log-normal probability function [218] and, to a lesser extent, the negative binomial distribution, as shown in fig. 6.2 for the ALEPH analysis [214]. A comparison with lower energy e^+e^- data supports the KNO scaling hypothesis [219], that the distribution of $n/\langle n\rangle$ is independent of the center of mass energy.

More detailed studies have been performed by DELPHI and OPAL [215, 220, 217]. Multiplicity distributions have been measured separately for the whole event, for a single hemisphere defined by the thrust axis and for events with different jet multiplicities. Also the dependence of the charged multiplicities on rapidity and transverse momenta has been analyzed. Figure 6.3 shows as an example the comparison between multiplicity distributions measured by DELPHI [215] for a single hemisphere and the JETSET parton shower program for different rapidity ranges. Here rapidity is defined with respect to the thrust axis as defined in eq. (3.2). In all cases good agreement between data and the JETSET Monte Carlo has been found. Multiplicity distributions obtained from the program HERWIG have been compared with measurements only by L3 and OPAL. HERWIG describes the data slightly less well.

Analytical QCD calculations make predictions for the mean charged multiplicity

$$n_{\mathrm{ch}} = \langle n\rangle \tag{6.1}$$

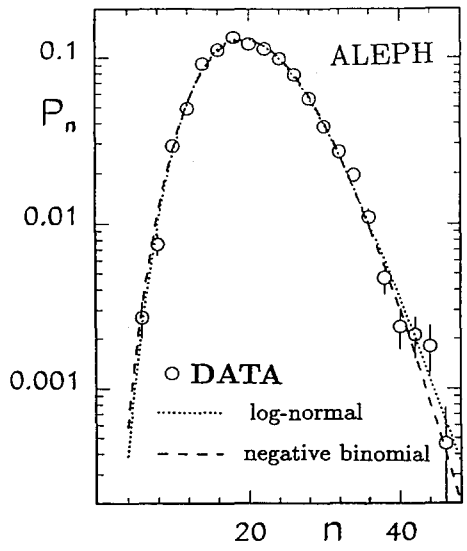

Fig. 6.2. Charged particle multiplicity distribution, from ALEPH [214].

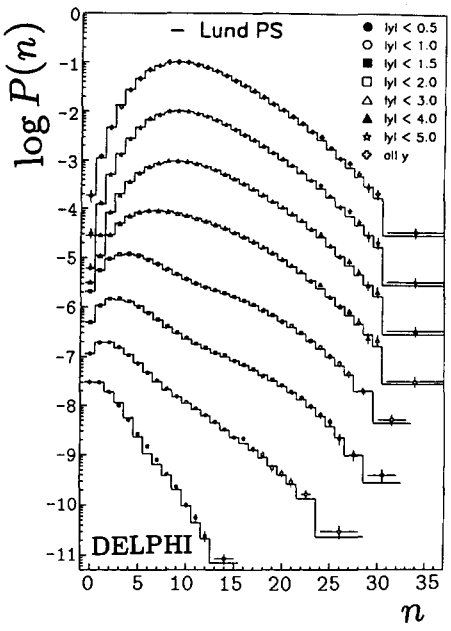

Fig. 6.3. Multiplicity distributions for a single hemisphere, from DELPHI [215].

[221,222] and the second binomial moment

$$R_2 = \langle n(n-1)\rangle / \langle n\rangle^2 \tag{6.2}$$

[223–225] as a function of center of mass energy.

The values of those two quantities as measured at the Z^0 pole are summarized in fig. 6.4 [214–216,91,217]. All the primary produced particles or those produced in the decay of particles with an average lifetime smaller than 3×10^{-10} s are considered. This means that the particles produced in the decays $K_s^0 \to \pi^+\pi^-$ and $\Lambda \to p\pi$ are included. The weighted averages of

$$n_{ch} = 20.9 \pm 0.2, \tag{6.3}$$

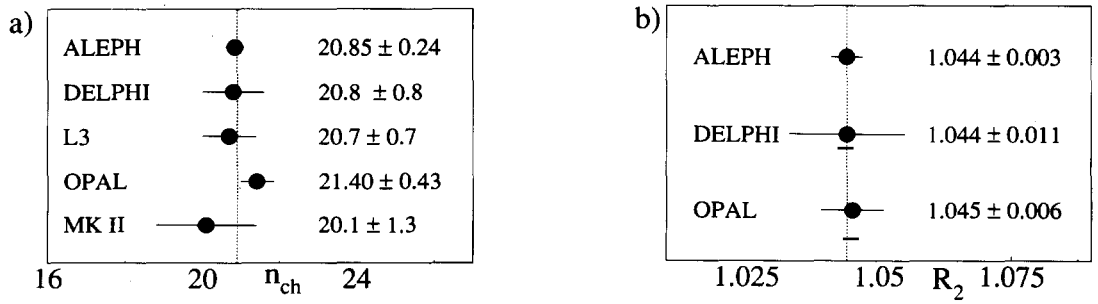

Fig. 6.4. (a) Mean charged multiplicity, (b) second binomial moment.

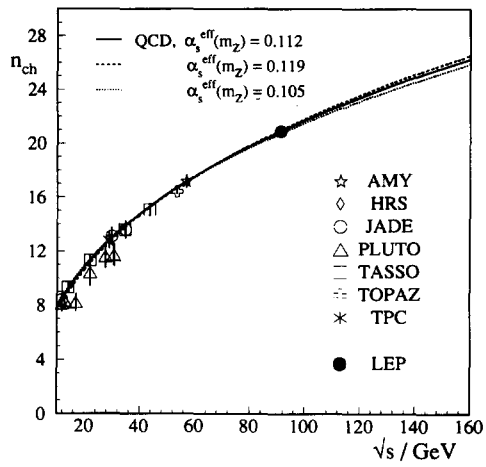

Fig. 6.5. Charged multiplicity as function of center of mass energy.

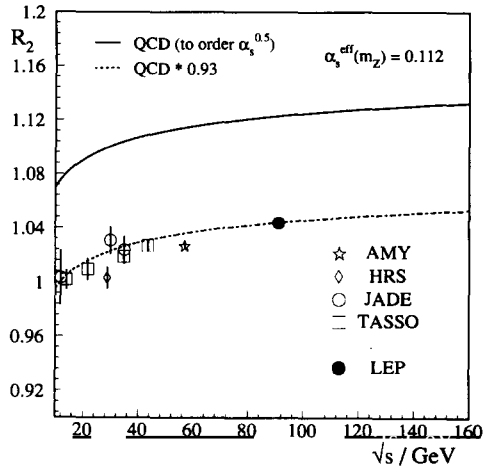

Fig. 6.6. Second binomial moment of charged multiplicity distribution.

$$R_2 = 1.044 \pm 0.003 \tag{6.4}$$

are in agreement with the predictions made by the JETSET and HERWIG generators.

Figure 6.5 shows the increase of n_{ch} with center of mass energy between $\sqrt{s} = 12$ and 91 GeV [226–232]*). The energy dependence of n_{ch} has been calculated to next-to-leading order. QCD (plus LPHD) predicts a function of the form [222]

$$n_{ch} = a[\alpha_s^{eff}(s)]^b \exp[c/\sqrt{\alpha_s^{eff}(s)}]\,. \tag{6.5}$$

Here α_s^{eff} is an effective strong coupling constant which is expected to be close to the $\overline{MS}$ value if the $O(\sqrt{\alpha_s})$ corrections neglected in (6.5) are small. The s dependence of α_s^{eff} is described by eq. (2.19) in section 2.1.3. The parameters b and c are (with $N_F = 5$):

$$b = \tfrac{1}{4} + (5/54\pi\beta_0)N_F = 0.492\,, \quad c = \sqrt{6}/\sqrt{\pi}\,\beta_0 = 2.27\,, \tag{6.6}$$

where β_0 is defined in eq. (2.14). The normalization factor a cannot be calculated. The QCD fit shown in fig. 6.5 is obtained by assuming that the systematic uncertainties of PETRA data at different $\sqrt{s}$ values measured by the same detector can be split into a common and a point-to-point error of the same size. The TOPAZ data, for which a systematic error is not published, are not used in the fit. The result for the two free parameters is

$$\alpha_s^{eff}(m_Z) = 0.112 \pm 0.007 \tag{6.7}$$

and $a = 0.07 \pm 0.01$. Figure 6.5 shows that the resulting curve describes the measurements well. The dotted and dashed lines correspond to the errors on α_s^{eff} as given in (6.7). The χ^2 value is 10.7 for ten degrees of freedom. Note that within errors α_s^{eff} agrees with the value of $\alpha_s = 0.119$ of section 4, indicating that higher order corrections and non perturbative effects are small.

*) The PLUTO results have been read from fig. 1 in ref. [229].

Without angular ordering the coefficient c would be bigger by a factor $\sqrt{2}$. Using this value in a fit leads to α_s values which are unacceptably low (0.07).

It has to be stressed that the comparison between data and QCD calculations, which assume massless quarks, make sense only if the multiplicities for heavy quarks (in particular bottom) are similar to those of light quarks. This is important because the flavor composition changes with center of mass energy, see section 2.2.1. At 29 GeV, where bottom events contribute about 10%, the average multiplicity for $b\bar{b}$ events is found to be about 20% higher than for the events with light primary quarks [231]. At LEP energies (b fraction about 20%) the JETSET program predicts that in bottom events the number of charged particles is 10% higher than for the whole hadron sample. Therefore the bottom effect is about 2%, both at small and high center of mass energies, and does not cause a problem for the analysis presented above.

The measured dependence of the second binomial moment R_2 on the center of mass energy is shown in fig. 6.6 [226–228, 230]. For the ratio R_2 next-to-leading order QCD calculations make an absolute prediction [223]:

$$R_2 = 1 + A + B\sqrt{\alpha_s^{\text{eff}}(s)} + \cdots \tag{6.8}$$

The parameters A and B are (with $N_F = 5$):

$$A = \tfrac{3}{8} = 0.375, \quad B = (-891 + 8N_F)(5/1296\sqrt{6\pi}) = -0.7562. \tag{6.9}$$

A fit with $\alpha_s^{\text{eff}}(m_Z)$ as a free parameter does not lead to an acceptable description of the measurements. Only if the QCD prediction is scaled by a factor of 0.93, the measured moments can be reproduced, as shown in fig. 6.6. Here the value $\alpha_s^{\text{eff}}(m_Z)$ in (6.7) is used for the QCD graphs. In ref. [224] also the coefficient for the α_s term in the expansion (6.8) has been calculated to be $C = -0.25$*). It reduces the discrepancy between measurements and $O(\sqrt{\alpha_s})$ calculation by a about 40%. When resumming higher order contributions to the multiplicity distribution the calculated second moment is still systematically above the experimental results [225]. The dispersion

$$D = \sqrt{\langle n^2\rangle - \langle n\rangle^2} \tag{6.10}$$

is related to R_2 via

$$D = \langle n\rangle\sqrt{R_2 - 1 + 1/\langle n\rangle}. \tag{6.11}$$

An overestimate of the second binomial moment by 8% ($= 1/0.93 - 1$) is equivalent to an excess of 40% in the dispersion D at 91 GeV. This discrepancy can be either due to uncalculated higher order corrections to R_2, which are presumably of the order $O(\alpha_s) = 0.1$ [233], or non perturbative effects, or due to particle decays. Using the JETSET generator the magnitude and sign of the latter effect can be estimated: particle decays change the second binomial moment by $\Delta R_2 \approx +0.02$ and therefore cannot explain the discrepancy.

One can summarize the comparisons presented in this section as follows: the measured center of mass energy dependence of the mean charged multiplicity can be reproduced well by analytical next-to-leading order calculations. The absolute size of the second binomial moments is overestimated by 8%. The small $\sqrt{s}$ dependence is described qualitatively by the QCD formula. This is a first partial success of the analytical QCD calculations plus LPHD hypothesis.

*) This calculation has not been confirmed yet and is not used in the later publication given in ref. [223].

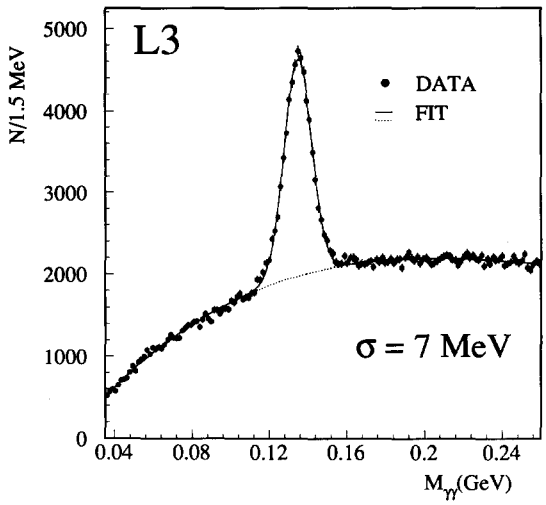

Fig. 6.7. $\gamma\gamma$ invariant mass distribution measured by L3 [216].

The parton shower program JETSET (including string fragmentation and decays) reproduces all measurements of n_{ch} and R_2. The Monte Carlo results are practically unchanged if soft gluon coherence effects are switched off.

6.3. *Particle identification (light flavors)*

Before discussing particle spectra for different hadrons I will briefly describe how light hadrons (those made out of u, d and s quarks) are identified in hadronic Z^0 events.

Figure 6.7 shows the $\gamma\gamma$ invariant mass distribution as measured by L3 [216]. One finds a clear π^0 signal at 135 MeV. It has a width of about 7 MeV and contains 31 000 π^0 mesons. This analysis is based on isolated photons measured in the electromagnetic calorimeter. The π^0 detection efficiency varies between 2% and 6% depending on the meson momentum.

Short lived neutral kaons have been identified by OPAL [234] and DELPHI [235]: K_s^0 mesons (m = 498 MeV, $c\tau$ = 2.7 cm) are reconstructed from pairs of oppositely charged particles (assumed to be pions) originating from a secondary vertex. The resulting invariant mass spectrum is shown in fig. 6.8a for the OPAL analysis [234]. This analysis is based on the information from the central tracking chambers. The peak contains 14 000 kaons and has a width of 6.5 MeV. The reconstruction efficiency varies between 5% and 27%, depending on the K_s^0 momentum.

The production of charged kaons with momenta between 1 and 2 GeV has been measured by DELPHI using the barrel RICH (Ring Image CHerenkov counter) [235]. The yield is found to agree with that of neutral kaons.

DELPHI has also identified $K^{*\pm}$ mesons (892 MeV) [235] via the decay chain $K^{*\pm} \rightarrow K_s^0 + \pi^\pm \rightarrow \pi^+\pi^- + \pi^\pm$.

Also Λ baryons (m = 1116 MeV, $c\tau$ = 7.9 cm) have been reconstructed by DELPHI [235]. Hadrons are measured in the central tracking detectors. Pairs of oppositely charged particles originating from a secondary vertex are selected. One of the particles is assumed to be a proton, the other a pion. Ξ baryons have been identified via their decays $\Xi^- \rightarrow \Lambda\pi^-$ and $\Xi^+ \rightarrow \bar{\Lambda}\pi^+$ [235].

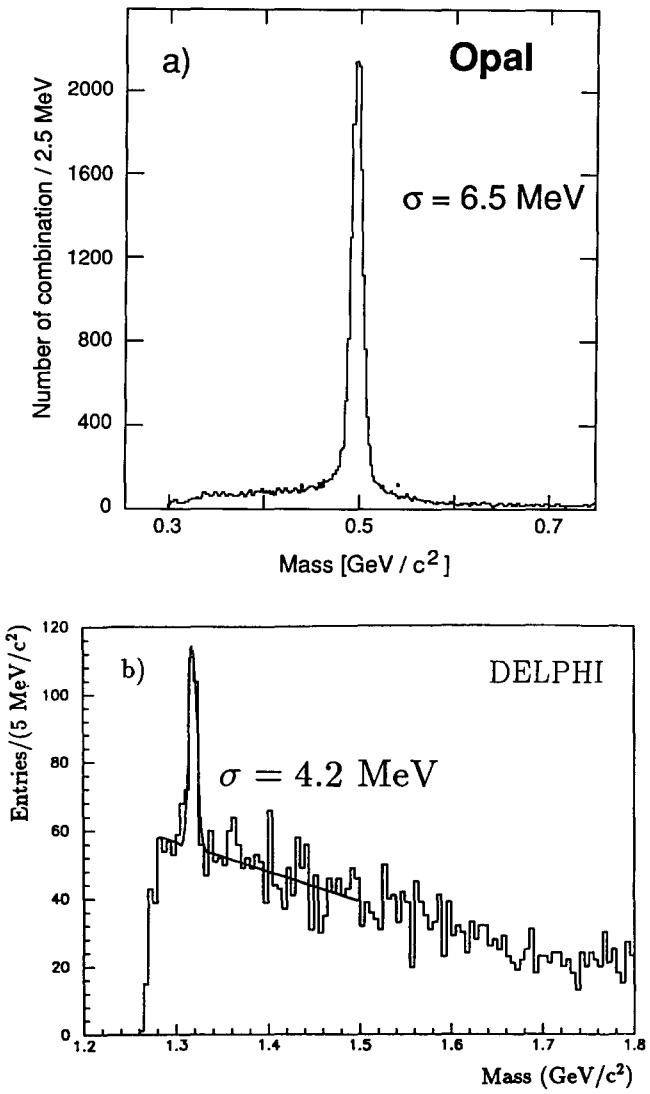

Fig. 6.8. (a) $\pi^+\pi^-$ invariant mass distribution measured by OPAL [234], (b) $\Lambda\pi$ invariant mass distribution measured by DELPHI [235].

The invariant mass spectrum for the right $\Lambda\pi$ combinations ($\Lambda\pi^-, \bar{\Lambda}\pi^+$) is shown in fig. 6.8b. The width of the Ξ peak is about 4 MeV.

The average number of mesons and baryons per hadronic Z^0 decay is shown in table 6.1. The numbers are the sums of particle and antiparticle yields. In case of the neutral kaons both K_s^0 and K_ℓ^0 are included.

The particle yields normalized to the average charged multiplicity are in agreement with the measurements at lower center of mass energies [64].

Table 6.1
Particle yields in hadronic Z^0 decays.

Hadron	$\langle n \rangle$	Ref.
π^0	9.8 ± 0.7	[216]
K^0, $\bar{K}^0$,	2.12 ± 0.06	[235, 234]
$K^{*\pm}$	1.33 ± 0.26	[235]
Λ, $\bar{\Lambda}$	0.36 ± 0.07	[235]
$\Xi^{\pm}$	0.020 ± 0.005	[235]

6.4. Particle spectra

An interesting prediction of perturbative QCD concerning the inclusive momentum spectra is the reduction of the number of soft gluons due to destructive interference. This behavior can be studied best in terms of the variable $\xi_p = \ln(1/x_p)$, where x_p denotes the ratio of particle momentum p to the beam energy $\sqrt{s}/2$. The QCD calculations predict a ξ_p distribution with a maximum, ξ_p^*, at ≈ 3.8 for $\sqrt{s} = 91$ GeV, which corresponds to $x_p \approx 0.02$ and $p \approx 1$ GeV [213, 221, 236]. The value of ξ_p^* is predicted to move to higher values with increasing center of mass energy. For massive particles the spectrum is modified such that the peak position is shifted to lower values.

The result of QCD calculations in "modified leading log approximation" (MLLA) [213, 9] can be written in the form:

$$\sigma_{\text{had}}^{-1} \, \mathrm{d}\sigma/\mathrm{d}\xi_p = N(\sqrt{s}) f(\sqrt{s}, \Lambda_{\text{eff}}, Q_0; \xi_p) . \tag{6.12}$$

Here Λ_{eff} is an effective scale parameter, which is independent of center of mass energy and particle type. An increase in Λ_{eff} corresponds to a decrease in the position of the maximum, ξ_p^*. Q_0 is an effective cut-off parameter in the quark–gluon cascade and increases with particle mass. However, the exact relation between Q_0 and mass is not known. For light hadrons, such as pions, one can set $Q_0 = \Lambda_{\text{eff}}$ ("limiting spectrum"). The (unpredicted) normalization factor N, which describes the hadronization, is a function of the center of mass energy $\sqrt{s}$ and the particle type.

At the Z^0 resonance spectra have been measured for neutral pions [216], Λ baryons [235], neutral kaons [235, 234] and also for all long lived charged particles [237, 235, 216, 234]. Charged particles include, in addition to pions (80%), heavier hadrons, mainly kaons (10%) and protons (5%). The "average mass" of charged particles is 220 MeV.

Figure 6.9 shows the measured ξ_p distributions for neutral pions [216], neutral kaons [234] and charged particles [238]. One sees clearly the "humpbacked" shape of the distribution and a shift of the peak position to lower values with increasing particle mass. Also the spectra predicted by QCD (MLLA) are shown, which describe the measured distributions fairly well, in particular in the region of the maximum, for which the calculations are valid. The QCD curves are obtained in the following way [239]: for all particles a value of $\Lambda_{\text{eff}} = 150$ MeV (corresponding to $\alpha_s^{\text{eff}} = 0.111$) is used, for which all particle spectra can be described. In case of the neutral pions the limiting spectrum ($Q_0 = \Lambda_{\text{eff}}$) is calculated, with an additional phase space factor $(p/E)^3$ [239]. For the kaons the ξ_p distribution is computed using $Q_0 = 300$ MeV, as determined from a comparison to the measured spectrum. In addition an estimate of the proton spectrum is shown, assuming an average number of protons per hadron event of about one [41]. Making use of isospin symmetry the QCD spectra for charged pions and kaons can be obtained from the calculated distributions

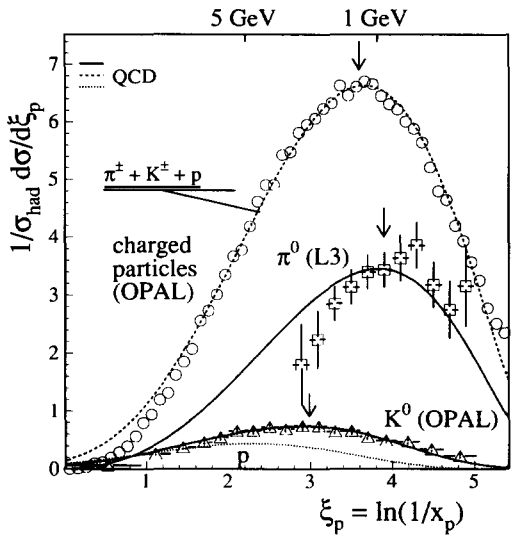

Fig. 6.9. ξ_p distributions for π^0, K^0 and charged particles.

for π^0 and K^0. Adding up the $\pi^{\pm}$, $K^{\pm}$ and p spectra gives the QCD prediction for the charged particles, shown by a dashed line in fig. 6.9.

Table 6.2 shows the measured peak positions as a function of the particle mass*). The result is in qualitative agreement with the QCD predictions. If one uses the limiting spectrum the measurements can be reproduced fairly well by setting Λ_{eff} equal to the particle mass given in table 6.2.

Particle decays have a large influence on the x_p and ξ_p distributions. One expects roughly a shift of $\ln 2 = 0.69$ in the peak position due to two-body decays. This corresponds to a decrease of α_s^{eff} by about 0.015. Therefore the absolute size of α_s^{eff} and the good agreement with α_s from section 4 should not be over-interpreted. Monte Carlo studies show that the peak position is indeed shifted substantially when replacing hadrons produced directly in the fragmentation process by their decay products. However, the form of the spectrum changes little and can in both cases be described by the MLLA formula (6.12) [237].

*) Note that the ξ^* values for K^0 as measured by OPAL (2.91 ± 0.04) and DELPHI (2.62 ± 0.11) are not in good agreement.

Table 6.2
Peak position in ξ_p distribution.

Hadron	m (MeV)	ξ_p^*	Ref.
π^0	135	4.11 ± 0.18	[216]
charged	220	3.63 ± 0.02	[237, 235, 216, 238]
K^0	498	2.88 ± 0.04	[235, 234]
Λ	1116	2.82 ± 0.25	[235]

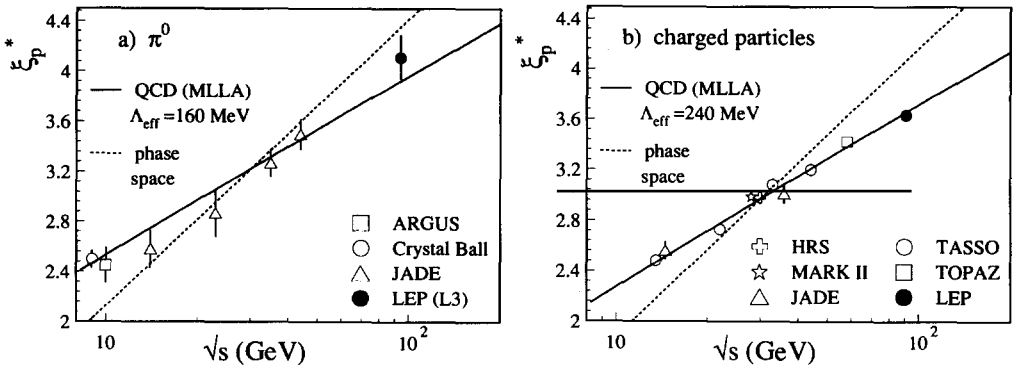

Fig. 6.10: Position of the maximum in the ξ_p distributions for (a) neutral pions, (b) charged particles.

The ALEPH collaboration [237] has also analyzed inclusive charged particle spectra in a restricted cone around the jet axis and measured the charged particle energy multiplicity correlation defined in ref. [240]. While the QCD calculations reproduce the measured spectra qualitatively, they can not describe their cone size dependence.

The OPAL collaboration has compared the measured ξ_p distribution with the predictions of parton shower models with and without coherence effects [238]. Both calculations describe the data well, the differences are found to be small. It is even possible to reproduce the data at $\sqrt{s} = 91$ GeV with an incoherent parton shower plus independent jet fragmentation [241]. This analysis shows, that the suppression of low energy particles is not only due to soft gluon interference, but also to phase space effects.

In order to distinguish between the two effects one can study the evolution of the position of the maximum with $\sqrt{s}$. Figure 6.10 shows the dependence of ξ_p^* for neutral pions and charged particles on the center of mass energy [242–245, 228, 246–248]. The maximum is determined from a fit to the measured spectra using the MLLA calculations. The errors include statistical uncertainties as well as systematic effects estimated from a variation of the fit range. The lines are the QCD predictions using values for Λ_{eff} determined from a fit to all points in figs. 6.10a and 6.10b. For better readability of this graph, different points at the same center of mass energy were slightly shifted horizontally. In case of the π^0's data around 10 GeV are also included.

Over the wide range from 9 to 91 GeV good agreement between data and QCD calculations is found, while the $\sqrt{s}$ dependence expected for phase space ($\xi_p = \ln\sqrt{s} + \text{const.}$) is clearly incompatible with the measurements.

Both ALEPH and OPAL have also studied the center of mass energy dependence of ξ_p^* for parton shower models with and without gluon interference effects [237, 238]. The version of the JETSET program with coherent parton branchings describes the data as well as the MLLA curve. In the incoherent case the agreement is acceptable only if string fragmentation is used. This indicates that parton level interference effects can be effectively parametrized by the string model.

The intrajet coherence studies presented in sections 6.2 to 6.4 can be summarized in the following way:

Analytical (next to) leading log QCD calculations together with the simple LPHD assumption allow a quantitative description of particle spectra, and in particular of the center of mass evolution of spectra and of average charged multiplicities. However, the analytical calculations fail to reproduce the width of the multiplicity distribution. The parton shower programs JETSET and HERWIG,

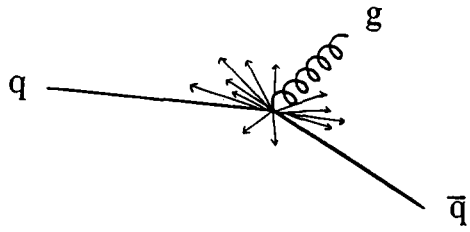

Fig. 6.11. String effect.

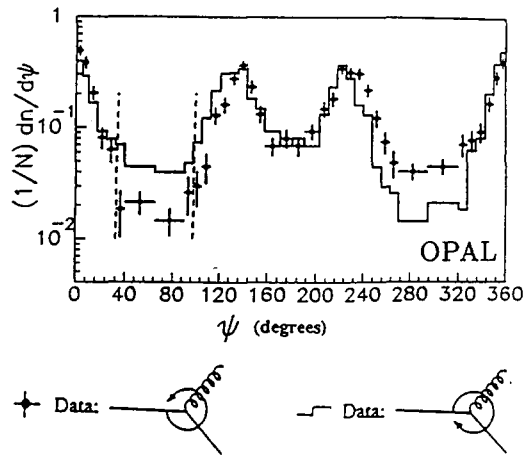

Fig. 6.12. String effect measured by OPAL [253].

which include coherence effects, reproduce all measured distributions.

These results provide strong evidence for the gluon coherence effects inside jets as predicted by QCD.

6.5. *String effect*

After the studies of *intra*-jet coherence effects described in the last two sections now *inter*-jet phenomena are to be analyzed.

About ten years ago the JADE collaboration found that in events of type $e^+e^- \rightarrow$ 3 jets at $\sqrt{s} \approx 30$ GeV less particles are produced in between the q and $\bar{q}$ jets in comparison to the other two inter-jet regions [34], see fig. 6.11. This observation was confirmed by other e^+e^- experiments [249].

The name "string effect" was given to this phenomenon. This name does not distinguish between the observation and a possible interpretation.

This asymmetry in the particle flow in the 3-jet plane can be explained in different ways:

(a) String fragmentation model, which predicted the effect [250]. In 3-jet events a string is stretched from the quark via the gluon to the antiquark. Most particles are therefore produced in between the quark and the gluon and in between the antiquark and the gluon, and only a few hadrons are created between the quark and antiquark.

(b) Analytical QCD calculations including coherence. One finds destructive inter-jet interference effects in the region between the q and the $\bar{q}$ jets [251, 9].

(c) Differences in the parton shower evolution and/or fragmentation of the primary quarks and hard gluons.

While both models (a) and (b) describe qualitatively the observed effect, they make different predictions for certain observables [211, 12, 252]. However, the corresponding measurements are difficult and have not been done yet.

The string effect *cannot* be explained by models based on an incoherent parton shower plus "independent jet fragmentation" [11, and references therein]. For this reason those hadronization schemes are hardly used any more.

Both DELPHI and OPAL have established, using different methods, the string effect at 91 GeV [85,253].

The DELPHI collaboration [85] has used a method similar to the one applied by JADE [34]. The three jets are energy ordered. The least energetic jet has a probability of more than 50% for being the "gluon jet". Both parton shower models as well as the matrix element generator plus string fragmentation can reproduce the measured particle flow in the event plane, and in particular the asymmetry in the dips between jets 1, 2 and 3, 1. The matrix element generator together with an "independent fragmentation model" cannot describe the data.

The OPAL collaboration [253,254] has selected 3-jet events with at least one lepton. Most likely these are bottom or charm events. The lepton is required to be close to the second or third most energetic jet. The "leptonless" jet out of the two least energetic jets is likely to be the gluon jet. In order to avoid kinematic biases only symmetric configurations are analyzed, for which the angle between the q and g jets is nearly the same as that between the q and $\bar{q}$ jets. For angles of $130 \pm 10°$ the purity of the "gluon jet" is about 70%.

Figure 6.12 shows the measured particle flow in the event plane [253]. One curve (points) shows the particle flow starting at the high energy quark and ending at the gluon jet; the histogram is obtained by proceeding in the opposite sense. It can be seen clearly that there is a depletion of particles in between the most energetic quark jet and the second quark jet, compared to the region between the first quark and the gluon. This demonstration of the string effect for heavy quark events does not involve any Monte Carlo comparisons and is therefore model independent.

The ratio of integrated particle flows in the quark–gluon and quark–antiquark inter-jet regions is measured to be

$$r = N_{q\bar{g}}/N_{q\bar{q}} = 1.62 \pm 0.07(\text{stat.}). \tag{6.13}$$

The corresponding prediction of the JETSET PS program with string fragmentation is $r = 1.54 \pm 0.02$, in agreement with the experimental result. The program COJETS, which is based on an incoherent parton shower evolution and independent jet fragmentation, predicts $r = 1.02 \pm 0.01$. The result (6.13) is not corrected for the fact that the gluon and quark jet purities are only about 70% and 85%. A correction would increase the ratio to $r \approx 2$. The QCD prediction for the particle flow ratio in the middle between jets in symmetric 3-jet configurations (all jets have the same energy) is $r = 22/7$ [9], in qualitative agreement with the experimental results.

In summary one can say that the "string effect" is well established, but a distinction between different possible interpretations is not yet possible.

6.6. *Energy-multiplicity–multiplicity correlations*

To study inter-jet coherence effects further, an energy-multiplicity–multiplicity correlation function $C(\phi)$ has been introduced in ref. [255]. It is a measure of interference effects for two particles at similar polar angles with respect to the jet axis and separated by an azimuthal angle ϕ. It is constructed from all (charged) particles in hadronic events in the following way:

$$C(\phi) = C_{\text{EMM}}(\eta_{\min}, \eta_{\max}, \phi) C_{\text{E}} / |C_{\text{EM}}(\eta_{\min}, \eta_{\max})|^2. \tag{6.14}$$

The energy-multiplicity–multiplicity correlation C_{EMM} is calculated from all sets of three particles i, j, k in an event:

$$C_{\text{EMM}}(\eta_{\min}, \eta_{\max}, \phi) = \frac{1}{\Delta_{\text{bin}} N} \sum_{\text{events}} \sum_{\eta_{\min} \le \eta_{j,k} \le \eta_{\max}} E_i \delta_{\text{bin}}(\phi_{\text{bin}} - |\phi_j - \phi_k|). \tag{6.15}$$

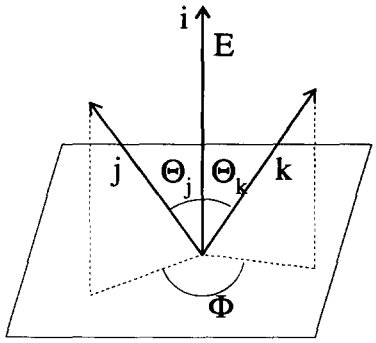

Fig. 6.13. Energy-multiplicity–multiplicity correlation: definition of angles.

$\delta_{\text{bin}}(\phi_{\text{bin}} - \phi)$ is 1 for angles ϕ inside the bin around ϕ_{bin} and 0 otherwise. N is the total number of events and Δ_{bin} denotes the bin width. Only those configurations are considered for which the particles j and k have polar angles θ_j, θ_k with respect to particle i such that the corresponding pseudorapidities $\eta = -\ln\tan\theta/2$ are in an interval defined by $\eta_{\min}, \eta_{\max}$. An entry is made in a histogram at the angle $\phi = |\phi_j - \phi_k|$ with weight E_i. ϕ_j, ϕ_k are the azimuthal angles with respect to the direction of particle i. In configurations with a large weight the particle i is close to a jet axis. The definitions of the angles are illustrated in fig. 6.13.

The normalization factors in eq. (6.14) are

$$C_{\text{EM}}(\eta_{\min}, \eta_{\max}) = \frac{1}{N} \sum_{\text{events}} \sum_{\eta_{\min} \le \eta_{j,k} \le \eta_{\max}} E_i, \tag{6.16}$$

$$C_{\text{E}} = \frac{1}{N} \sum_{\text{events}} \sum_{i} E_i. \tag{6.17}$$

Gluon interference effects lead to a suppression of particles at large ϕ and to a value of the energy-multiplicity–multiplicity correlation function below one [255]. The correlation function has been measured by ALEPH and DELPHI [237, 256] for charged particles. Agreement between data and Monte Carlo calculations based on coherent parton showers and/or string fragmentation is observed, as is shown in fig. 6.14 for the DELPHI measurements. Here the pseudorapidity boundaries $\eta_{\min} = 1$ and $\eta_{\max} = 2$ are used which correspond to the polar angle range $15° \le \theta \le 40°$. The correlation function obtained from the generator COJETS [82] (incoherent parton shower plus independent jet fragmentation) cannot reproduce the data. However, particle decays have a large influence on energy-multiplicity–multiplicity correlations [257], so that the interpretation of the measurements is difficult. Here more studies are needed.

6.7. *Quark jets versus gluon jets*

Gluons carry a larger color charge ($C_{\text{A}} = 3$) than quarks ($C_{\text{F}} = 4/3$). This leads to the qualitative QCD prediction that gluon jets are broader and contain softer particles than quark jets of the same

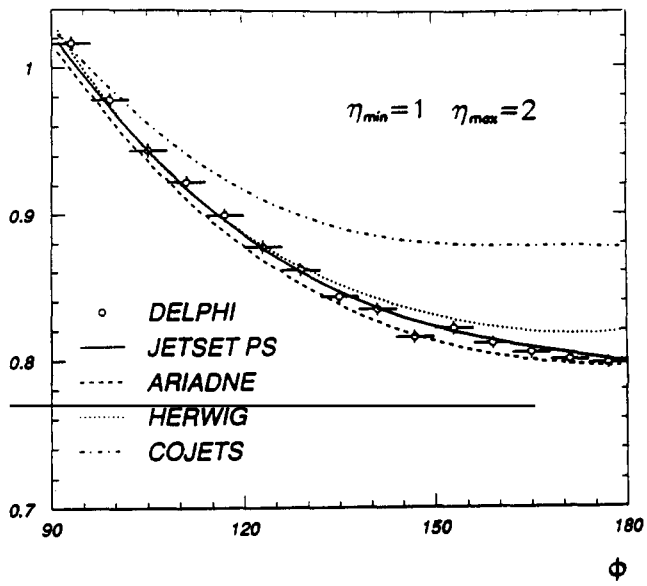

Fig. 6.14. Energy-multiplicity–multiplicity correlation measured by DELPHI [256].

energy [258]. A QCD calculation predicts for the ratio r_{qg} of gluon and quark jet multiplicities [259]:

$$r_{qg} = \langle n_{gluon}\rangle/\langle n_{quark}\rangle = \tfrac{9}{4}[1 + \alpha\sqrt{\alpha_s^{eff}} + \beta\alpha_s]. \tag{6.18}$$

The parameters α and β are (with $N_F = 5$):

$$\alpha = -(27 + N_F)/27\sqrt{6\pi} = -0.273, \tag{6.19}$$

$$\beta = -(27 + N_F)(675 - 86N_F)/34992\pi = -0.0713. \tag{6.20}$$

With $\alpha_s^{eff} = \alpha_s = 0.119$ one obtains the prediction

$$r_{qg}(91\text{ GeV}) = \tfrac{9}{4} \times (1 - 0.10) = 2.0. \tag{6.21}$$

The calculated corrections modify the lowest order prediction of 9/4 by only 10%. It has to be stressed that this calculation is valid only for "isolated" quarks and gluons and does not necessarily apply to $q\bar{q}g$ configurations.

Several studies of the differences between quark and gluon jets in e^+e^- collisions have been carried out at lower center of mass energies [260]. Often the quark and gluon jets to be compared have different energies or belong to different event types (2-jet, 3-jet), so that the interpretation of those measurements is ambiguous.

OPAL has applied the quark tagging method as described in section 6.5 to study the difference between quark and gluon jets [254]. This is done in a model independent way by comparing gluon jets in events with identified quarks to a mixture of quark and gluon jets in a sample of 3-jet events containing all flavors. The observed differences are rather small and can be summarized as follows:

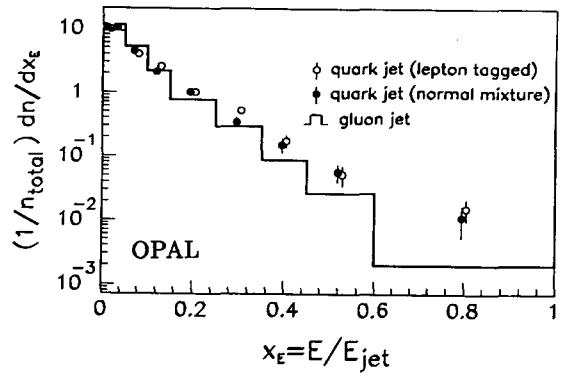

Fig. 6.15. Hadron energy spectra in quark and gluon jets measured by OPAL [254].

- gluon jets are broader than quark jets,
- hadrons in the *core* of gluon jets ($\pm 15°$ around jet axis) are softer than in quark jets,
- charged multiplicities are quite similar in quark and gluon jets:

$$r_{qg} = 1.02 \pm 0.04(\text{stat.})^{+0.06}_{-0.00}(\text{syst.})\,. \tag{6.22}$$

Here all charged particles within $\pm 34°$ around the jet axis are considered.
The hadron spectra in quark and gluon jets are compared in fig. 6.15 [254].

The charged multiplicities of quark and gluon jets have also been studied by DELPHI using a different method [220]: a sample of about 600 symmetric 3-jet events, in which all jets have nearly the same energy, is selected. If one orders the jets according to their multiplicities, $n_1 \geq n_2 \geq n_3$, the ratio $\langle n_1 \rangle / (\langle n_2 \rangle + \langle n_3 \rangle)$ is sensitive to the ratio of the average quark jet and gluon jet multiplicities. The measured value of $r_{qg} = 1.23 \pm 0.21$ is consistent with unity.

The JETSET Monte Carlo prediction (for charged multiplicities as defined in the OPAL analysis) is $r_{qg} = 1.11 \pm 0.01$ [254], in agreement with the experimental result. However, the experimental results are inconsistent with the $O(\alpha_s)$ QCD prediction of 2.0. It is not clear whether this is due to higher order effects, fragmentation corrections, phase space effects and particle decays, or, if the calculations are not applicable to 3-jet events at $\sqrt{s} = 91$ GeV. A possible cause is the fact that soft hadrons cannot be uniquely assigned to a given jet, thus diminishing possible differences between quark and gluon jets.

6.8. *Intermittency*

The word "intermittency" is used to denote local particle density fluctuations, as seen first in cosmic ray events, hadron–hadron collisions etc. [261,262, and references therein]. The interest in studies of intermittency effects lies in the fact that Monte Carlo models *cannot* describe most of these measurements. It is therefore important to study intermittency also in e^+e^- events and to compare the results with the QCD models. This has been done for data taken at $\sqrt{s} \approx 30$ GeV with contradictory results: while the TASSO collaboration finds data and Monte Carlo predictions to be in disagreement [263] *), a recent CELLO study comes to the opposite conclusion [264]. The LEP results presented here support the CELLO analysis.

*) However, the significance of the discrepancy is not very clear, since the sensitivity to the Monte Carlo parameters has not been studied.

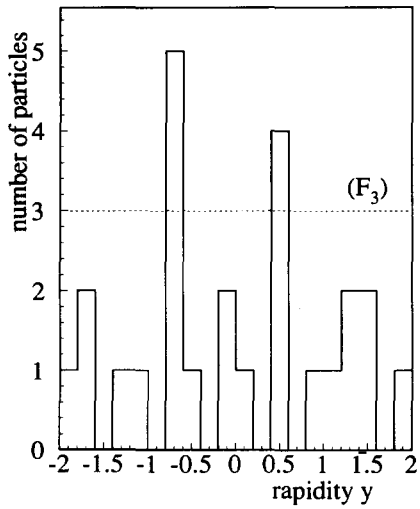

Fig. 6.16. Intermittency: example for rapidity distribution for one event.

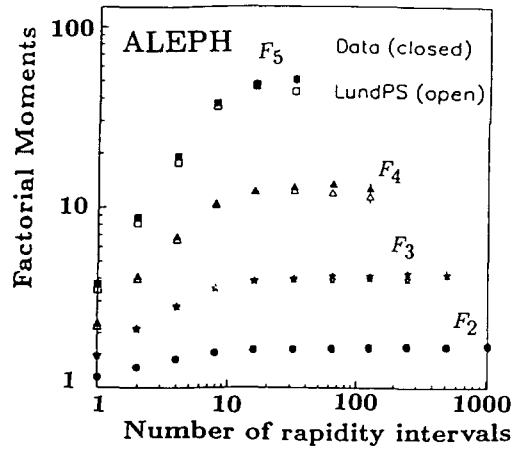

Fig. 6.17. Factorial moments measured by ALEPH [266].

Intermittency is measured via factorial moments [265], which can be defined for one or more dimensions. Here the one-dimensional case is briefly described. To measure factorial moments one has to choose a phase space variable with a distribution which is approximately flat. Often one uses rapidity y,

$$y = \tfrac{1}{2}\ln[(E + p_\parallel)/(E - p_\parallel)],$$

which is calculated for each particle in an event. E and $p_\parallel$ denote the energy and the longitudinal momentum component with respect to the thrust axis. The rapidity interval Y which is considered in the analysis is then subdivided into M subintervals of size $\delta y = Y/M$. For each event one can count the number of particles n_m per bin and the total number of particles $N = \sum n_m$. The factorial moments of rank i are then defined as an average over many events in the following way:

$$F_i(\delta y) = \frac{M^{i-1}}{\langle N\rangle^i}\left\langle \sum_{m=1}^{M} n_m(n_m-1)\cdots(n_m-i+1)\right\rangle . \tag{6.23}$$

Note that only subintervals with at least i particles contribute to the factorial moments of rank i, as is illustrated in fig. 6.16 for the third moment. The analysis must then be repeated for decreasing subinterval sizes δy (increasing resolution). The result may belong to one of the two classes [265]: (a) no correlation between particles: F_i = const., (b) self similar cascades: power law $F_i \sim (\delta y)^{-f_i} \sim M^{f_i}$.

Self similar cascades are indeed expected in $e^+e^- \rightarrow$ hadrons events, in which quark–gluon cascades appear quite naturally. This can be illustrated in the following way: in a given event three jets may appear as three "peaks" in the rapidity distribution. When increasing the resolution (decreasing δy) a peak might be resolved into three local maxima, since the primary quark forming that peak might have radiated a gluon which has split into a $q\bar{q}$ pair. This means that the structure of the distribution (three peaks) remains the same when changing resolution. Of course this can be at most a qualitative picture. In addition, other effects like hard gluon radiation, fragmentation,

Bose–Einstein correlations and particle decays (resonances, $\pi^0 \to e^+e^-\gamma$) can contribute to the rise of factorial moments with M.

ALEPH, DELPHI and OPAL have measured factorial moments for large data samples [266–268]. The ALEPH results for the factorial moments F_2–F_5 as a function of the number of subdivisions of the rapidity interval are shown in fig. 6.17 [266].

At small M the measured factorial moments increase with M. This implies the presence of local particle density fluctuations. The data can be reproduced by the JETSET parton shower Monte Carlo generator, therefore it can be explained by known physics. The main contribution to the rise of the moments in fig. 6.17 stems from hard gluon emission. Similar agreement between measured and predicted factorial moments has been obtained for different variables and also for analyses in more than one dimension.

For reactions other than e^+e^- the corresponding models do not reproduce the measurements [261]. A possible explanation is that those models are not yet as developed as the sophisticated generators used to simulate e^+e^- collisions.

6.9. *Bose–Einstein correlations*

Identical bosons obey Bose–Einstein statistics and prefer to occupy the same quantum state. This phenomenon has been studied at LEP for like sign charged pions by ALEPH [269], DELPHI [270] and OPAL [271]. Bose–Einstein correlations are described by the correlation function

$$C(p_1,p_2) = \rho(p_1,p_2)/\rho(p_1)\rho(p_2)\,.$$

Here $\rho(p_1,p_2)$ is the joint two-pion probability density and $\rho(p_i)$ denote the single pion probabilities. p_i are the particle four-momenta. Assuming a pion source with a Gaussian shape in the rest frame of the pion pair, one obtains a correlation function of the form

$$C(Q) = 1 + \lambda \exp(-Q^2R^2)\,, \tag{6.24}$$

where $Q^2 = (p_1 - p_2)^2 = m^2(\pi\pi) - 4m_\pi^2$ and R is the source size. The parameter λ, which assumes values between 0 and 1, is a measure of the strength of the effect.

The principal experimental difficulty is the choice of a reference sample not affected by Bose–Einstein correlations in order to measure the product $\rho(p_1)\rho(p_2)$. One such reference sample consists of oppositely charged pions. A second method is based on event mixing. Finally, Monte Carlo calculations not incorporating Bose–Einstein effects can be used.

Figure 6.18 shows the ratio of like sign and oppositely charged pions as a function of Q as measured by OPAL [271]. The data shown have been divided by the corresponding Monte Carlo correlation function (without Bose–Einstein effects) to correct for resonance decays. In addition, a correction for final state Coulomb interactions has been applied.

The averaged results on correlation strength λ and source size R at LEP are [272]:

$$\lambda = 0.5 \pm 0.2\,, \quad R = 0.8 \pm 0.1\ \text{fm}\,. \tag{6.25}$$

These values are *not* corrected for non pion contamination, which would increase the value of λ by about 20% [272].

The parameters measured at LEP are not different from those measured in e^+e^- annihilation at lower center of mass energies. A source size of about 1 fm which describes the size of the hadronization region is measured. Similar values are found in hadron–hadron and lepton–hadron collisions [272].

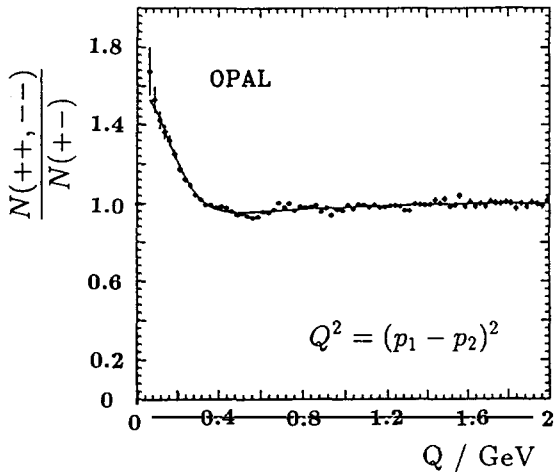

Fig. 6.18. Bose–Einstein correlations measured by OPAL [271].

While the source size and the correlation strength cannot (yet) be calculated within QCD, the experimental result $R \approx 1/\Lambda_{\overline{\text{MS}}} \approx 1$ fm qualitatively confirms our hadronization models.

7. Future QCD tests at LEP/SLC

7.1. $e^+e^- \to$ hadrons

LEP will continue to run at the Z^0 peak in the years 1992 and 1993. In later years the beam energy will be increased beyond the W mass. Possibly, data will be taken with polarized beams. SLC plans Z^0 runs with longitudinal polarization already for the year 1992. With increased statistics, higher center of mass energies or polarization more QCD tests will become possible. The physics potential for each of these three cases is analyzed briefly in the following sections.

7.1.1. Increased statistics (a few million Z^0 events)

The statistical and systematic errors of $R_Z = \Gamma_{had}/\Gamma_{lep}$ will decrease. The uncertainty in R_Z is currently and also in the future dominated by the error on Γ_{lep}. With 250 000 lepton events per LEP detector the statistical error will be 0.2%. The systematic uncertainties in acceptance correction and background subtraction can probably be reduced to less than 0.5% per experiment [132]. Averaging over all LEP experiments an error of $\Delta R_Z/R_Z \approx 0.2\%$ could be achievable. This translates into an error of the strong coupling constant as measured from R_Z of $\Delta\alpha_s \approx 0.005$.

More detailed studies of "soft" phenomena will be performed. In particular the study of particle yields, especially for "rare" hadrons, and correlations will profit from a large increase in the event samples [273]. The search for "anomalous" events, in particular those with exceptionally large factorial moments, will continue.

Interesting comparisons will become possible between events of type $q\bar{q}g$ and $q\bar{q}\gamma$, since both gluons and photons are vector bosons, and since the 3-"jet" matrix elements are the same in both cases to lowest order. Due to the smallness of α, $q\bar{q}\gamma$ final states are rare. Only a few events out

of thousand hadronic events contain an isolated final state photon with an energy above 10 GeV [105, 106]. The first studies of these events have already been done by the OPAL collaboration [106]. Final state photons also provide a sharp tool to study the parton shower development, see section 3.6.

Very important will be the study of multi-jet events using flavor tagging, which works best for bottom events. The bottom jets can be identified via their semileptonic decays into leptons, see section 4.7.1. Since only a few percent of all hadron events can be used, a large number of Z^0 events is needed. Several methods to distinguish quark and gluon jets have been suggested [274–279], which do not rely on bottom tagging. So far they have not been used in connection with hadronic Z^0 events. If quark and gluon jets can be distinguished, the following studies can be done (or improved): (a) comparing quark and gluon jets and the particle flow in between (section 6), (b) repeating all matrix element tests as described in section 5 with identified quark, antiquark and gluon jets. In particular point (b) is very important. The tests become more significant, since the differences between QCD and alternative theories of the strong interactions, such as the abelian model, are enhanced by a factor of about two [280, 202, 203, 281].

Crucial for an increase in the accuracy of α_s measurements and QCD tests are improvements in the calculations of the perturbative series expansion. Important applications are 3-jet like variables, which can be used to determine the strong coupling constant, and the 4-jet cross section, which today is known only at the Born level.

7.1.2. Higher beam energy (160 GeV)

Here an interesting measurement would be that of the ratio

$$f \equiv \alpha_s(160\ \text{GeV})/\alpha_s(91\ \text{GeV}), \tag{7.1}$$

to test the running of the strong coupling constant. However, the expected effect is small, $f = 0.92$. One of the major difficulties, unknown at the Z^0 pole, is "hard" initial state photon radiation. For more than half of the events at least one photon will be radiated such that the invariant mass of the final state hadrons is close to the Z^0 mass, see fig. 2.10 in section 2.2.1. Due to the small cross section of about 0.16 nb [39] for the process $e^+e^- \to$ hadrons a luminosity of about 500 pb^{-1} is necessary to measure f from the 3-jet rates with a statistical error of about 2% in one experiment.

It has been proposed to study angular ordering using multi-jet events at high center of mass energies, however it will be very difficult to achieve significant results [282, 273].

7.1.3. Polarization

Both transverse and longitudinal polarization modify the orientation of 3-jet events [187], which should therefore be measured if beam polarization becomes available.

In case of transversely polarized beams the measurement of the asymmetry in the azimuthal distribution $A_\perp$ of hadronic events as defined by $d\sigma/d\phi \sim 1 + A_\perp \sin(2\phi)$ allows a determination of α_s with a precision of 10–15% [283]. While the accuracy is not as high as for the other α_s measurements, the method is different and provides another test of QCD.

7.2. QCD tests using other processes

While all QCD tests presented so far are based on the process $e^+e^- \to$ hadrons, other interesting tests will become possible with increased statistics and higher center of mass energies.

7.2.1. τ decays

The QCD correction to the ratio

$$R_\tau \equiv \frac{\Gamma(\tau \to \text{hadrons})}{\Gamma(\tau \to \text{e})} = \frac{1 - B_\text{e} - B_\mu}{B_\text{e}} \approx 3.5 \tag{7.2}$$

is related to the QCD correction for the corresponding quantity R_Z for Z decays as introduced in section 4.3. The perturbative part is therefore known to $O(\alpha_s^3)$, and non perturbative effects are found to be as small as 1% in R_τ [124,171,172]. The quantity R_τ can be measured via the semileptonic branching ratios and also from the lifetime of the τ lepton. The results [169],

$$R_\tau^{\text{branching fraction}} = 3.66 \pm 0.05\,, \quad R_\tau^{\text{lifetime}} = 3.32 \pm 0.12\,,$$

differ by 2.6 standard deviations. For a few million Z^0 events the average of the semileptonic branching ratios B_e and B_μ and tau lifetimes measured by the four LEP experiments will hopefully resolve this discrepancy. A precision $\Delta B/B \approx 1\%$ can probably be reached, which translates into $\Delta R_\tau \approx 0.04$ and an experimental uncertainty of $\Delta\alpha_s(m_Z) \approx 0.003$.

Note that for a given relative uncertainty of R the precision on $\alpha_s(m_Z)$ reachable from R_τ is significantly higher than the accuracy obtainable from R_Z. This is due to the fact that ΔR_τ measures $\alpha_s(m_\tau)$: since this value is much larger (about 0.33) than α_s at the Z^0 mass, the QCD correction can be measured with a comparatively small relative error. Furthermore, the relative uncertainty in α_s shrinks significantly when extrapolating [170, 30] it from $m_\tau = 1.8$ GeV to $m_Z = 91.2$ GeV. The uncertainty due to the extrapolation itself is currently being studied [284].

The authors of ref. [172] estimate the theoretical uncertainties of $\alpha_s(m_Z)$ determined from R_τ to be as small as 0.2%. However, since $\alpha_s(m_\tau)$ is very large, the convergence of the perturbative expansion is much slower than at the Z^0 mass. In ref. [285] the effective expansion parameter is shown to be $4\pi e\beta_1\alpha_s$, which is as large as 0.7 for $\alpha_s(m_\tau) = 0.33$. The perturbative QCD correction to third order in α_s is [124, 171, 172]

$$\delta_{\text{QCD}}^\tau = \alpha_s(m_\tau)/\pi + 5.20[\alpha_s(m_\tau)/\pi]^2 + 26.4[\alpha_s(m_\tau)/\pi]^3\,, \tag{7.3}$$

for $\mu = m_\tau$. If one varies the renormalization scale between the τ mass and 1 GeV, the value for $\alpha_s(m_\tau)$ changes according to eq. (4.4) by about -0.05. This translates into an uncertainty of -0.006 in $\alpha_s(m_Z)$. Therefore uncalculated higher order corrections might be larger than assumed in ref. [172].

Obviously, measurements of semileptonic τ properties are not restricted to LEP; in particular τ-charm factories might do better.

7.2.2. W decays

At LEP200 W bosons will be pair-produced via the process

$$\text{e}^+\text{e}^- \to \text{W}^+\text{W}^-\,.$$

In principle one can use the quantity R_W, defined in analogy to R_Z and R_τ, to determine α_s. However, with the small number of expected events (10 000 per experiment) and non-negligible systematic uncertainties, a very precise determination of the strong coupling constant will not be possible.

7.2.3. Two-photon physics

The study of the process $\text{e}^+\text{e}^- \to \text{e}^+\text{e}^-$ + hadrons will be of interest in particular at LEP200, where the "background" of events $\text{e}^+\text{e}^- \to Z^0 \to$ hadrons is reduced [286, 12, 273]. The available

momentum transfer Q^2 will be very large, exceeding 1000 GeV^2. A measurement of the Q^2 dependence of the photon structure function F_2^γ over a wide range is an important test of asymptotic freedom. An accurate measurement of F_2^γ at large Q^2 allows a determination of α_s with an uncertainty of 10% or better [287].

8. Summary and conclusions

The experiments ALEPH, DELPHI, L3 and OPAL at LEP have performed a large number of measurements of the process $e^+e^- \to Z^0 \to$ hadrons with the following results:
- The strong coupling constant is measured to be $\alpha_s = 0.119 \pm 0.007$ at the Z^0 mass. This value is an average of the results obtained from (i) the ratio of the hadronic and leptonic Z^0 widths and (ii) from analyzing the event topology. The strong coupling strength of bottom quarks agrees with that of the lighter quarks. The running of α_s, as predicted by QCD, is confirmed by the observed $\sqrt{s}$ dependence of the 3-jet fraction.
- Various distributions for 3-jet and 4-jet events have been measured precisely. They agree with the prediction of QCD calculated to second order in α_s. Alternative models with scalar gluons or without gluon self interaction can be ruled out. The triple gluon coupling strength has been measured and agrees with the QCD predictions.
- String and cluster fragmentation models describe hadronic events well. All distributions at the hadron level are reproduced by QCD Monte Carlo programs or analytical calculations. There is no evidence for any "failure" of QCD in reproducing the LEP data.

The studies of hadronic Z^0 decays at LEP have increased significantly our confidence in QCD as *the* theory of strong interactions.

Future *experimental* progress will come mainly from an increase of statistics at the Z^0 resonance, which will lead to the following improvements:

(a) The error in the ratio R_Z of the hadronic and leptonic Z^0 widths will be reduced, so that α_s can be determined with an uncertainty of about 0.005 from R_Z.

(b) Precise QCD tests with identified quark and gluon jets will become possible.

(c) More detailed studies of "soft" phenomena will be performed.

A further increase in precision of α_s determined from 3-jet like observables will be possible by comparing the data to the improved *theoretical* calculations [141]. Hopefully, a full third order calculation will become available in the next few years.

Acknowledgements

This article was written while I was a working in the hadron analysis group of the L3 experiment. I would like to thank all members of this team, in particular Sunanda Banerjee, Mourad Dhina, Elisabetta Gallo, Giorgio Gratta, David Kirkby, Stephan Müller, Jianming Qian, Andreas Ricker, Sergej Shevchenkov and Georgi Sultanov for their cooperation, their engagement and the numerous things I learned from them.

I also benefited from discussions with and help from my colleagues Harm Fesefeldt, John Field, Ulrich Herten, Joachim Rose and Howard Stone.

Particular thanks go to Albrecht Böhm for his continuous support and encouragement and many fruitful discussions.

The QCD analysis would obviously not have been possible without the efforts of all members of the L3 collaboration to build and operate the detector. In particular I would like to acknowledge the leadership of Samuel C.C. Ting.

I would like to thank my colleagues from the ALEPH, DELPHI and OPAL collaborations, in particular Siegfried Bethke, Wim de Boer, Jürgen Drees, Fabrizio Fabbri, Bill Gary, Klaus Hamacher, Peter Mättig, Stefano Marcellini and Michael Schmelling, for many helpful discussions and for providing me with unpublished material.

I am grateful to Valery Khoze, Zoltan Kunszt, Torbjörn Sjöstrand, James Stirling and Peter Zerwas for many lessons they taught me on the theory of QCD. Also several discussions with Guido Altarelli, Stefano Catani, Gustav Kramer, Hans Kühn, Antonio Pich, Lalit Sehgal and Bryan Webber were of great help for me.

I would like to thank David Kirkby, James Stirling and Andreas Ricker for the critical reading of the manuscript, and Yvette Bernard for drawing some of the figures.

This work is supported by the German Bundesministerium für Forschung und Technologie. The L3 detector is financed by many nations from all continents. In the years 1989–1991 I spent a large fraction of my time as a visitor at the European Center for High Energy Physics CERN. I would like to thank all tax payers for their contributions.

Appendix A. QCD correction to Γ_{had}

In the following I will briefly resume the calculation of the coefficients in the expansion (4.7) and discuss theoretical uncertainties for the quantity δ_{QCD}.

The calculations of δ_{QCD} are based on the optical theorem

$$\sigma_{\mathrm{tot}} \sim \mathrm{Im}\, \Pi\,, \tag{A.1}$$

where Π is the inverse Z^0 propagator [42]. Therefore these computations are not done in the same way in which jet cross sections are calculated, see section 4.4.

To third order in α_s the QCD correction to the hadronic Z^0 width can be written in the form

$$\delta_{\mathrm{QCD}} = \sum_q \{B_v^q [v_1^q \alpha_s/\pi + v_2^q (\alpha_s/\pi)^2 + v_3^q (\alpha_s/\pi)^3] + B_a^q [a_1^q \alpha_s/\pi + a_2^q (\alpha_s/\pi)^2 + a_3^q (\alpha_s/\pi)^3]\}, \tag{A.2}$$

where B_v^q and B_a^q denote the vector and axial vector contributions to the branching fractions of Z^0 into quarks of type q,

$$B_v^q = V_q^2 \left(\sum_q (V_q^2 + A_q^2) \right)^{-1}, \quad B_a^q = A_q^2 \left(\sum_q (V_q^2 + A_q^2) \right)^{-1}, \tag{A.3}$$

without QCD correction, see section 2.2.1. The sum $\sum_q$ extends over all five quark flavors u, d, s, c, b. The relative uncertainties of the numbers B_v^q, B_a^q are smaller than 3% (for 90 GeV $< m_t <$ 200 GeV and 50 GeV $< m_H <$ 1000 GeV) and can be neglected in the context of this paper.

The quark mass dependence of the first order coefficients can be approximated in lowest order by [131, 129]

$$v_1^q = 1 + 12 (m_q/m_Z)^2, \tag{A.4}$$

$$a_1^q = 1 - 24(m_q/m_Z)^2 \ln(m_q/m_Z)\,. \tag{A.5}$$

With $m_c = 1.5$ GeV and $m_b = 4.8$ GeV one gets

$$v_1^c = 1.00, \quad a_1^c = 1.03, \tag{A.6}$$

$$v_1^b = 1.03, \quad a_1^b = 1.20. \tag{A.7}$$

Taking into account next to leading corrections [130] one obtains [127]

$$a_1^c \approx 1.03, \quad a_1^b \approx 1.28. \tag{A.8}$$

Therefore the first order mass correction is dominated by the axial vector part for bottom production.

For the second order coefficients [288] the dependence of the top mass for a_2^b (due to the large top–bottom mass splitting) has been calculated, while the other quarks are assumed to be massless [131]

$$v_2^q = 1.985 - 0.115 N_F = 1.410, \quad a_2^q = v_2^q - \delta^t, \tag{A.9}$$

where I use $N_F = 5$. The top mass dependent correction δ^t is nonzero only for b quarks. Approximately [131]:

$$\delta^t = 3.083 - 0.0865(m_Z/m_t)^2 - 0.0132(m_Z/m_t)^4 - 2\ln(m_Z/m_t)\,. \tag{A.10}$$

For $m_t = 124^{+32}_{-36}$ GeV [36] *) one obtains

$$\delta^t = 3.6 \pm 0.6. \tag{A.11}$$

This correction to a_2^b is therefore very large!

The third order coefficients are [124, 129]

$$v_3^q = -6.637 - 1.200 N_F - 0.005 N_F^2 - 0.41 \left(\sum V_q\right)^2 / \sum V_q^2 = -13.16, \tag{A.12}$$

$$a_3^q = -6.637 - 1.200 N_F - 0.005 N_F^2 = -12.76. \tag{A.13}$$

The difference between vector and axial vector coefficients is small and can be neglected:

$$v_3^q \approx a_3^q \approx -13. \tag{A.14}$$

With the definitions

$$c_i = \sum_q (B_v^q v_i^q + B_a^q a_i^q), \tag{A.15}$$

the QCD correction to the hadronic final width can be written in the form

$$\delta_{QCD} = c_1 \alpha_s/\pi + c_2(\alpha_s/\pi)^2 + c_3(\alpha_s/\pi)^3, \tag{A.16}$$

*) Here the value for m_t is used which is obtained from a fit to LEP, $p\bar{p}$ collider and neutrino data with α_s being a free parameter.

with

$$c_1 = 1.05 \pm 0.01\,, \quad c_2 = 0.9 \pm 0.1\,, \quad c_3 = -13\,. \tag{A.17}$$

The error estimate for c_1 is based on the difference between first order and higher order mass corrections and a bottom mass uncertainty of ± 0.3 GeV. The error on c_2 is dominated by the error on the top mass. An uncertainty of $\Delta m_{\text{top}} = \pm 35$ GeV corresponds to $\Delta c_2 = 0.01$.

Using $\alpha_s = 0.115$ the total relative error for δ_{QCD} is estimated to be $\approx 2\%$ with the following contributions:

- First order bottom mass correction: 1%.
- Second order top mass correction: < 0.5%.
- Missing higher order corrections: 1%. In ref. [285] (see also ref. [289]) the fourth and fifth order coefficients have been estimated to be ≈ -160 and ≈ -2600, respectively. In spite of their size the corresponding correction to α_s is only about -1%. This result is consistent with an estimate of the higher order corrections from the energy scale dependence as shown in fig. 4.1a. Also an analysis of the renormalization scheme dependence leads to similar conclusions [290].
- Non perturbative corrections are expected to be of the order $\Delta\delta_{\text{QCD}} = \text{O}((\Lambda/m_Z)^2) = \text{O}(10^{-5})$ and therefore negligible [291]. In ref. [292] the possible effect of coherence of $u\bar{u}$ and $d\bar{d}$ final states on the Z^0 hadronic decay width has been estimated to be as large as 10 MeV, depending on the model used. However, this correction, which is strongly $\sqrt{s}$ dependent, is predicted to be even larger in size and negative at 35 GeV. This model is therefore strongly disfavored experimentally [22–24].
- The QED correction to Γ_{had} is given to first order in α by $\delta_{\text{QED}} = \frac{3}{4}(\alpha/\pi)Q_q^2$. Averaged over the five flavors (as produced at the Z^0) the correction amounts to 0.0004 and is therefore small. However, the interplay of gluon and photon radiation could increase the (combined strong and electromagnetic) correction to the hadronic cross section. These effects have not yet been calculated, but are assumed here to be small.

The uncertainty $\Delta R_Z = \pm 0.02$ in the electroweak part of the calculation of R_Z translates into $\Delta\alpha_s = 3\%$ and is therefore currently the biggest theoretical uncertainty in the determination of the strong coupling constant from the hadronic Z width. However, this error will shrink to about 2% as soon as the top mass is known to some 10 GeV, and to about 1% if also the Higgs mass is known.

References

[1] M. Gell-Mann, Acta Physica Austriaca Suppl. IX (1972) 733;
H. Fritzsch and M. Gell-Mann, 16th International Conference on High Energy Physics, Batavia, 1972, eds J.D. Jackson and A. Roberts, National Accelerator Laboratory (1972);
H. Fritzsch, M. Gell-Mann and H. Leytwyler, Phys. Lett. B 47 (1973) 365.
[2] D.J. Gross and F. Wilczek, Phys. Rev. Lett. 30 (1973) 1343; Phys. Rev. D 8 (1973) 3633;
H.D. Politzer, Phys. Rev. Lett. 30 (1973) 1346.
[3] G. 't Hooft, Nucl. Phys. B 33 (1971) 173.
[4] G. Altarelli, Annu. Rev. Nucl. Part. Sci. 39 (1989) 357; QCD and Experiment, CERN preprint CERN-TH 5760/90.
[5] J.D. Bjorken and S.D. Drell, Relativistic Quantum Mechanics, (McGraw-Hill, New York, 1964).
[6] R.K. Ellis and W.J. Stirling, QCD and Collider Physics, Fermilab Report FERMILAB-Conf-90-164-T.
[7] T. Muta, Foundation of QCD (World Scientific, Singapore, 1987);
R.D. Field, Applications of Perturbative QCD (Addison-Wesley, Reading, 1989);
A.H. Mueller, ed., Perturbative QCD (World Scientific, Singapore, 1989);
Y.L. Dokshitzer et al., Basics of Perturbative QCD (Editions Frontières, Paris 1991).
[8] Z. Kunszt and P. Nason, in: Z Physics at LEP 1, CERN Report CERN-89-08, Vol. I, p. 373.

[9] V.A. Khoze, Color Coherence Physics at the Z^0, CERN preprint CERN-TH 5849-90;
V.A. Khoze, Y.L. Dokshitzer and S.I. Troyan, Color Coherence in QCD Jets, Lund preprint LU TP 90-12;
Y.L. Dokshitzer, V.A. Khoze and S.I. Troyan, Phenomenology of the Particle Spectra in QCD Jets in a Modified Leading Logarithmic Approximation, Durham preprint DTP/91/82.
[10] B.R. Webber, J. Phys. G 17 (1991) 1493.
[11] T. Sjöstrand, Int. J. Mod. Phys. A 3 (1988) 751; in: Z Physics at LEP 1, CERN Report CERN-89-08, Vol. III, p. 143.
[12] P.M. Zerwas, QCD, $\gamma\gamma$ and Heavy Quarks in e^+e^- Collisions, Aachen Report PITHA 89/23.
[13] A. Ali and F. Barreiro, in: High Energy Electron Positron Physics, eds A. Ali and P. Söding, (World Scientific, Singapore, 1988) p. 611.
[14] P. Mättig, Phys. Rep. 177 (1989) 142.
[15] R. Petronzio, Lattice Quantum Chromodynamics, CERN preprint CERN-TH-4858/87;
A. Ukawa, Status of Lattice Field Theory and Computer Simulations, 25th International Conf. on High Energy Physics, Singapore, 1990, eds K.K. Phua and Y. Yamaguchi (World Scientific, Singapore, 1990) p. 79.
[16] M. Gell-Mann, Phys. Lett. 8 (1964) 214;
G. Zweig, An SU_3 Model for Strong Interaction Symmetry and its Breaking I, CERN preprint CERN-TH-401 (1964);
An SU_3 Model for Strong Interaction Symmetry and its Breaking II, CERN preprint CERN-TH-412 (1964).
[17] R.P. Feynman, Photon–Hadron Interactions (Benjamin, New York, 1972).
[18] E.D. Bloom et al., Phys. Rev. Lett. 23 (1969) 930;
M. Breidenbach et al., Phys. Rev. Lett. 23 (1969) 935;
J.I. Friedman and H.W. Kendall, Annu. Rev. Nucl. Part. Sci. 22 (1972) 203;
J.I. Friedman, Rev. Mod. Phys. 63 (1991) 615.
[19] M.Y. Han and Y. Nambu, Phys. Rev. B 139 (1965) 1006.
[20] M. Aguilar-Benitez et al., Phys. Lett. B 239 (1990) 1.
[21] M. Aguilar-Benitez et al., Phys. Lett. B 204 (1988) 1.
[22] G. d'Agostini, W. de Boer and G. Grindhammer, Phys. Lett. B 229 (1989) 160;
W. de Boer, Results on R from PEP, PETRA, TRISTAN and SLC, DESY preprint DESY 89-111.
[23] R. Marshall, Z. Phys. C 43 (1989) 595.
[24] V. Branchina et al., Phys. Rev. Lett. 65 (1990) 3237; A Combined Fit to $R(e^+e^- \rightarrow \text{hadrons})$ and LEP DATA, Catania preprint (1991).
[25] S. Weinberg, Phys. Rev. Lett. 31 (1973) 494; Phys. Rev. D 8 (1973) 4482.
[26] G. 't Hooft, Nucl. Phys. B 61 (1973) 455;
W.A. Bardeen et al., Phys. Rev. D 18 (1978) 3998.
[27] W. Caswell, Phys. Rev. Lett. 33 (1974) 244;
D.R.T. Jones, Nucl. Phys. B 75 (1974) 531.
[28] O.V. Tarasov, A.A. Vladimirov and A.Y. Zharkov, Phys. Lett. B 93 (1980) 429.
[29] T. Hebbeker, Remarks on Relations between α_s and Λ, L3 note 958 (1991).
[30] W.J. Marciano, Phys. Rev. D 29 (1984) 580.
[31] R.F. Schwitters et al., Phys. Rev. Lett. 35 (1975) 1320;
G. Hanson et al., Phys. Rev. Lett. 35 (1975) 1609.
[32] TASSO Collaboration, R. Brandelik et al., Phys. Lett. B 86 (1979) 243;
MARK J Collaboration, D.P. Barber et al., Phys. Rev. Lett. 43 (1979) 830;
PLUTO Collaboration, C. Berger et al., Phys. Lett. B 86 (1979) 418;
JADE Collaboration, W. Bartel et al., Phys. Lett. B 91 (1980) 142.
[33] TASSO Collaboration, R. Brandelik et al., Phys. Lett. B 97 (1980) 453;
D. Lüke (TASSO Collaboration), Recent Results from TASSO, 21st International Conference on High Energy Physics, Paris, 1982; eds P. Petiau and M. Porneuf, J. Phys. (Paris) C 3 (1982) 67;
PLUTO Collaboration, C. Berger et al., Phys. Lett. B 97 (1980) 459;
CELLO Collaboration, H.-J. Behrend et al., Phys. Lett. B 110 (1982) 329;
R. Clare (MARK J Collaboration), QCD Properties of Jets, MIT Ph.D. Thesis (1982).
S.L. Wu, Phys. Rep. 107 (1984) 59.
[34] JADE Collaboration, W. Bartel et al., Phys. Lett. B 101 (1981) 129; Z. Phys. C 21 (1983) 37;
JADE Collaboration, F. Ould-Saada et al., Z. Phys. C 39 (1988) 1.
[35] TASSO Collaboration, M. Althoff et al., Z. Phys. C 22 (1984) 307;
HRS Collaboration, D. Bender et al., Phys. Rev. D 31 (1985) 1;
TPC Collaboration, H. Aihara et al., Phys. Rev. Lett. 52 (1984) 577.
[36] The LEP Collaborations: ALEPH, DELPHI, L3 and OPAL, Phys. Lett. B 276 (1992) 247.

[37] M. Consoli and W. Hollik in Z Physics at LEP 1, CERN Report CERN-89-08, Vol. I, p. 7.
[38] F.A. Berends, in: Z Physics at LEP 1, CERN Report CERN-89-08, Vol. I, p. 89.
[39] D. Bardin et al., program ZFITTER 4.0; Nucl. Phys. B 351 (1991) 1; Z. Phys. C 44 (1989) 493; Phys. Lett. B 255 (1991) 290.
[40] CDF Collaboration, F. Abe et al., Phys. Rev. Lett. 68 (1992) 447.
[41] T. Sjöstrand, Comput. Phys. Commun. 39 (1986) 347;
T. Sjöstrand and M. Bengtsson, Comput. Phys. Commun. 43 (1987) 367.
[42] G. Kramer, Theory of Jets in Electron–Positron Annihilation, Springer Tracts of Modern Physics 102 (Springer, Berlin, 1984).
[43] R.K. Ellis, D.A. Ross and A.E. Terrano, Nucl. Phys. B 178 (1981) 421.
[44] K. Fabricius et al., Phys. Lett. B 97 (1980) 431; Z. Phys. C 11 (1982) 315.
[45] F. Gutbrod, G. Kramer, G. Schierholz, Z. Phys. C 21 (1984) 235.
[46] G. Kramer and B. Lampe, Z. Phys. C 39 (1988) 101; Fortschr. Phys. 37 (1989) 161.
[47] J. Ellis, M.K. Gaillard and G.G. Ross, Nucl. Phys. B 111 (1976) 253, 516 (Erratum).
[48] B.L. Ioffe, Phys. Lett. B 78 (1978) 277.
[49] J.G. Körner and G.A. Schuler, Z. Phys. C 26 (1985) 559;
J.G. Körner, G.A. Schuler and F. Barreiro, Phys. Lett. B 188 (1987) 272;
G.A. Schuler and J.G. Körner, Nucl. Phys. B 325 (1989) 557.
[50] B.A. Kniehl and J.H. Kühn, Phys. Lett. B 224 (1989) 229.
[51] L3 Collaboration, B. Adeva et al., Phys. Lett. B 263 (1991) 551.
[52] F.A. Berends, W.T. Giele and H. Kuijf, Nucl. Phys. B 321 (1989) 39;
K. Hagiwara and D. Zeppenfeld, Nucl. Phys. B 313 (1989) 560;
N.K. Falck, D. Graudenz and G. Kramer, Phys. Lett. B 220 (1989) 299; Nucl. Phys. B 328 (1989) 317;
C.J. Maxwell, Phys. Lett. B 192 (1987) 190; 225 (1989) 425;
C.J. Maxwell and J.A. Nicholls, Nucl. Phys. B 316 (1989) 321;
M. Mangano and S. Parke, Phys. Rev. D 39 (1989) 758;
W.T. Giele and E.W.N. Glover, Higher Order Corrections to Jet Cross Sections in e^+e^- Annihilation, Fermilab preprint FERMILAB-Pub-91/100-T.
[53] OPAL Collaboration, P.D. Acton et al., Phys. Lett. B 276 (1992) 547.
[54] B.R. Webber, Annu. Rev. Nucl. Part. Sci. 36 (1986) 253.
[55] K. Konishi, A. Ukawa and G. Veneziano, Nucl. Phys. B 157 (1979) 45;
R. Odorico, Nucl. Phys. B 172 (1980) 157;
G.C. Fox and S. Wolfram, Nucl. Phys. B 168 (1980) 285;
T.D. Gottschalk, Nucl. Phys. B 14 (1983) 201;
G. Marchesini and B.R. Webber, Nucl. Phys. B 238 (1984) 1;
B.R. Webber, Nucl. Phys. B 238 (1984) 492.
[56] G. Altarelli and G. Parisi, Nucl. Phys. B 126 (1977) 298.
[57] A.H. Mueller, Phys. Lett. B 104 (1981) 161;
A. Bassetto et al., Nucl. Phys. B 207 (1982) 189;
B.I. Ermolaev and V.S. Fadin, JETP Lett. 33 (1981) 269;
Y.L. Dokshitzer, V.S. Fadin and V.A. Khoze, Phys. Lett. B 115 (1982) 242.
[58] B. Andersson et al., Phys. Rep. 97 (1983) 31;
X. Artru, Phys. Rep. 97 (1983) 147.
[59] G.C. Fox and S. Wolfram, Nucl. Phys. B 213 (1983) 65.
[60] G.Marchesini and B.R. Webber, Nucl. Phys. B 310 (1988) 461;
I.G. Knowles, Nucl. Phys. B 310 (1988) 571.
[61] R.D. Field and R.P. Feynman, Nucl. Phys. B 136 (1978) 1.
[62] P. Hoyer et al., Nucl. Phys. B 161 (1979) 349.
[63] A. Ali et al., Nucl. Phys. B 168 (1980) 409; Phys. Lett. B 93 (1980) 155.
[64] G. Flügge, Jet Fragmentation, The Quark Structure of Matter, Strasbourg-Karlsruhe, 1985, eds M. Jacob and K. Winter (World Scientific, Singapore, 1986) p. 79;
D.H. Saxon in High Energy Electron Positron Physics, eds A. Ali and P. Söding (World Scientific, Singapore, 1988) p. 540.
[65] J.H. Kühn and P.M. Zerwas, in: Z Physics at LEP 1, CERN Report CERN-89-08, Vol. I, p. 267.
[66] T. Sjöstrand, Comput. Phys. Commun. 28 (1983) 229.
[67] TPC/Two-Gamma Collaboration, H. Aihara et al., Phys. Rev. D 41 (1990) 2667.
[68] F.C. Erné, private communication (1992).

[69] F.A. Berends, P.H. Daverveldt and R. Kleiss, Comput. Phys. Commun. 40 (1986) 271, 285, 309.
[70] LEP Technical Notebook, CERN, 1989.
[71] ALEPH Collaboration, D. Decamp et al., Nucl. Instrum. Methods A 294 (1990) 121;
M. Schmelling (ALEPH Collaboration), private communication (1991).
[72] DELPHI Collaboration, P. Aarnio et al., Nucl. Instrum. Methods A 303 (1991) 233;
K. Hamacher (DELPHI Collaboration), private communication (1991).
[73] L3 Collaboration, B. Adeva et al., Nucl. Instrum. Methods A 289 (1990) 35.
[74] OPAL Collaboration, K. Ahmet et al., Nucl. Instrum. Methods A 305 (1991) 275;
S. Bethke (OPAL Collaboration), private communication (1991).
[75] C.Y. Prescott, The SLC program, SLAC preprint SLAC-PUB 3570 (1985).
[76] MARK II Collaboration, G. Abrams et al., Nucl. Instrum. Methods A 281 (1989) 55.
[77] M. Breidenbach, Status of SLC, LEPC meeting, CERN, Geneva, November 1991.
[78] U. Pettersson, ARIADNE: A Monte Carlo for QCD Cascades in the Color Dipole Formulation, Lund preprint LU TP 88-5;
L. Lönnblad, ARIADNE 3: A Monte Carlo for QCD Cascades in the Color Dipole Formulation, Lund preprint LU TP 89-10 (1988); The Color Dipole Cascade Model and the Ariadne Program, Lund preprint LU TP 91-11 (1991).
[79] K. Kato and T. Munehisa, Phys. Rev. D 36 (1987) 61; Comput. Phys. Commun. 64 (1991) 67.
[80] J. Kalinowski, K. Konishi and T.R. Taylor, Nucl. Phys. B 181 (1981) 221;
J. Kalinowski et al., Nucl. Phys. B 181 (1981) 253;
J.F. Gunion and J. Kalinowski, Phys. Rev. D 29 (1984) 1545;
J.F. Gunion, J. Kalinowski and L. Szymanowski, Phys. Rev. D 32 (1985) 2303.
[81] N. Magnussen, Measurement of Jet Cross Sections in e^+e^- Annihilation at 44 GeV Center of Mass Energy, DESY Internal Report F22-89-01 (1989).
[82] R. Odorico, Nucl. Phys. B 228 (1983) 381; Comput. Phys. Commun. 32 (1984) 139; 34 (1985) 43 (Erratum); 59 (1990) 527;
P. Mazzanti and R. Odorico, Nucl. Phys. B 370 (1992) 23.
[83] ALEPH Collaboration, D. Decamp et al., Phys. Lett. B 234 (1990) 209.
[84] ALEPH Collaboration, D. Decamp et al., Properties of Hadronic Z^0 Decays and Test of QCD Generators, ALEPH internal note, February 1991.
[85] DELPHI Collaboration, P. Aarnio et al., Phys. Lett. B 240 (1990) 271.
[86] DELPHI Collaboration, P. Abreu et al., Comparison of Data with QCD Models, DELPHI note 91-74 PHYS 128, paper contributed to the Joint International Lepton-Photon Symposium and Europhysics Conference on High Energy Physics, Geneva, 1991.
[87] DELPHI Collaboration, P. Abreu et al., Z. Phys. C 54 (1992) 45.
[88] L3 Collaboration, B. Adeva et al., Phys. Lett. B 249 (1990) 341.
[89] L3 Collaboration, B. Adeva et al., Phys. Lett. B 257 (1991) 469.
[90] OPAL Collaboration, M.Z. Akrawy et al., Z. Phys. C 47 (1990) 505.
[91] MARK II Collaboration, G.S. Abrams et al., Phys. Rev. Lett. 63 (1989) 1558; 64 (1990) 1334.
[92] W. de Boer, H. Fürstenau and J.H. Köhne, Z. Phys. C 49 (1991) 141.
[93] L3 Collaboration, B. Adeva et al., Phys. Lett. B 241 (1990) 416; 261 (1991) 177.
[94] ALEPH Collaboration, D. Decamp et al., Phys. Lett. B 244 (1990) 551; 266 (1991) 218; Measurement of the Leptonic Decay Rates and Fragmentation Parameters for b and c States Produced in Z Decay, ALEPH internal note, July 1991, paper contributed to the Joint International Lepton-Photon Symposium and Europhysics Conference on High Energy Physics, Geneva, 1991.
[95] C. Peterson et al., Phys. Rev. D 27 (1983) 105.
[96] S. Brandt et al., Phys. Lett. 12 (1964) 57;
E. Farhi, Phys. Rev. Lett. 39 (1977) 1587.
[97] PLUTO Collaboration, C. Berger et al., Z. Phys. C 12 (1982) 297;
HRS Collaboration, D. Bender et al., Phys Rev. D 31 (1985) 1;
MARK II Collaboration, A. Peterson et al., Phys. Rev. D 37 (1988) 1;
CELLO Collaboration, H.J. Behrend et al., Z. Phys. C 44 (1989) 63;
TASSO Collaboration, W. Braunschweig et al., Z. Phys. C 47 (1990) 187;
AMY Collaboration, Y.K. Li et al., Phys. Rev. D 41 (1990) 2675.
[98] DELPHI Collaboration, P. Abreu et al., A Measurement of D^{*+} Production in Hadronic Z^0 Decays, DELPHI note 91-63 PHYS 117, paper contributed to the Joint International Lepton-Photon Symposium and Europhysics Conference on High Energy Physics, Geneva, 1991;
DELPHI Collaboration, P. Abreu et al., Partial Width of the Z^0 into $b\bar{b}$ Final States and Mean b Semileptonic

Branching Fraction, DELPHI note 91-49 PHYS 104, paper contributed to the Joint International Lepton-Photon Symposium and Europhysics Conference on High Energy Physics, Geneva, 1991.
[99] OPAL Collaboration, M.Z. Akrawy et al., Phys. Lett. 263 (1991) 311;
OPAL Collaboration, G. Alexander et al., Phys. Lett. 262 (1991) 341.
[100] P. Mättig, QCD Measurements with Heavy Quarks at LEP, Bonn preprint Bonn-He-91-19;
P. Roudeau, Heavy Flavour Physics at LEP, Joint International Lepton-Photon Symposium and Europhysics Conference on High Energy Physics, Geneva, 1991; Orsay preprint LAL 91-49.
[101] I. Bigi et al., Phys. Lett. B 181 (1986) 157.
[102] Y.I. Azimov, Y.L. Dokshitzer and V.A. Khoze, Yad. Fiz. 36 (1982) 1510;
V.G. Kartvelishvili, A.K. Likhoded and S.R. Slabospitskii, Yad. Fiz. 38 (1983) 1563;
Y.I. Azimov et al., Yad. Fiz. 40 (1984) 777.
[103] B. Mele and P. Nason, Phys. Lett. B 245 (1990) 635; Nucl. Phys. B 361 (1991) 626.
[104] T.F. Walsh and P. Zerwas, Phys. Lett. B 44 (1973) 195;
S.J. Brodsky, C.E. Carlson and R. Suaya, Phys. Rev. D 14 (1976) 2264;
K. Koller, T.F. Walsh and P.M. Zerwas, Z. Phys. C 2 (1979) 197;
E. Laermann et al., Nucl. Phys. B 207 (1982) 205;
P. Mättig and W. Zeuner, Z. Phys. C 52 (1991) 31.
[105] ALEPH Collaboration, D. Decamp et al., Phys. Lett. B 264 (1991) 476;
DELPHI Collaboration, P. Abreu et al., Z. Phys. C 53 (1992) 555;
L3 Collaboration, B. Adeva et al., Measurement of Final State Photon Radiation in Hadronic Z^0 Decays, L3 internal note 971, July 1991;
OPAL Collaboration, M.Z. Akrawy et al., Phys. Lett. B 246 (1990) 285;
OPAL Collaboration, G. Alexander et al., Phys. Lett. B 264 (1991) 219.
[106] OPAL Collaboration, P.D. Acton et al., Z. Phys. C 54 (1992) 193.
[107] G. Kramer and B. Lampe, Phys. Lett. B 269 (1991) 401.
[108] M Seymour, Photon Implementation in HERWIG, Workshop on Photon Radiation from Quarks, Annecy 1991.
[109] D. Kirkby, Photon Implementation in SPLASH, Workshop on Photon Radiation from Quarks, Annecy 1991;
SPLASH: Simulation of Photons in Leading-Log Approximation Showers, CALTECH preprint CALT-68-1761 (1991).
[110] T. Sjöstrand, Photons as a Tool to Study Gluon Fragmentation, Workshop on Photon Radiation from Quarks, Annecy 1991; Photon Implementation in JETSET, Workshop on Photon Radiation from Quarks, Annecy 1991.
[111] B. Andersson, G. Gustafson and C. Sjögren, Prompt Photon Production in e^+e^--Annihilation, Lund preprint LU TP 91-31;
B. Andersson, Photons and Jet Evaluation, Workshop on Photon Radiation from Quarks, Annecy 1991;
L. Lönnblad, Photon Implementation in ARIADNE, Workshop on Photon Radiation from Quarks, Annecy 1991.
[112] G.G. Ross, Beyond the Standard Model, Joint International Lepton-Photon Symposium and Europhysics Conference on High Energy Physics, Geneva, 1991;
U. Amaldi et al., Phys. Lett. B 281 (1992) 374.
[113] J.C. Collins and D.E. Soper, Annu. Rev. Nucl. Part. Sci. 37 (1987) 383.
[114] D.W. Duke and R.G. Roberts, Phys. Rep. 120 (1985) 275.
[115] T. Hebbeker, Renormalization Scale Dependence in QCD, L3 note 959 (1991).
[116] G. Kramer, Nucl. Phys. B 16 (Proc. Suppl.) (1990) 254;
J. Stirling, private communication (1991).
[117] P.M. Stevenson, Phys. Rev. D 23 (1981) 2916; Nucl. Phys. B 203 (1982) 472; 231 (1984) 65.
[118] G. Grunberg, Phys. Lett. B 95 (1980) 70; Phys. Rev. D 29 (1984) 2315.
[119] S.J. Brodsky, G.P. Lepage and P.B. Mackenzie, Phys. Rev. D 28 (1983) 228.
[120] S. Bethke, Z. Phys. C 43 (1989) 331.
[121] OPAL Collaboration, M.Z. Akrawy et al., Phys. Lett. B 235 (1990) 389; Z. Phys. C 49 (1991) 375.
[122] DELPHI Collaboration, P. Abreu et al., Phys. Lett. B 247 (1990) 167;
K. Hamacher (DELPHI Collaboration), private communication (1991).
[123] N. Brown and W.J. Stirling, Phys. Lett. B 252 (1990) 657.
[124] L.R. Surguladze and M.A. Samuel, Phys. Rev. Lett. 66 (1991) 560, 2416 (Erratum);
S.G. Gorishny, A.L. Kataev and S.A. Larin, Phys. Lett. B 259 (1991) 144.
[125] F.A. Berends et al, program ZBATCH/ZHADRO;
F.A. Berends, G. Burgers and W.L. van Neerven, Nucl. Phys. B 297 (1988) 429;
G. Burgers, CERN preprint CERN-TH-5119/88 (1988).
[126] M. Martinez et al., program MIZA; Z. Phys. C 49 (1991) 645.
[127] T. Hebbeker, QCD correction to Γ_{had}, Aachen Report PITHA 91/08 (revised version).

[128] S.G. Gorishny, A.L. Kataev and S.A. Larin, Phys. Lett. B 212 (1988) 238.
[129] J. Jérsak, E. Laermann and P. Zerwas, Phys. Rev. D 25 (1982) 1218;
A. Djouadi, J.H. Kühn and P.M. Zerwas, Z. Phys. C 46 (1990) 411.
[130] K.G. Chetyrkin and J.H. Kühn, Phys. Lett. B 248 (1990) 359.
[131] B.A. Kniehl and J.H. Kühn, Phys. Lett. B 224 (1989) 229; Nucl. Phys. B 329 (1990) 547.
[132] ALEPH Collaboration, D. Decamp et al., Z. Phys. C 53 (1992) 1.
[133] DELPHI Collaboration, P. Abreu et al., Nucl. Phys. B 367 (1991) 3.
[134] L3 Collaboration, B. Adeva et al., Z. Phys. C 51 (1991) 179.
[135] OPAL Collaboration, G. Alexander et al., Z. Phys. C 52 (1991) 175.
[136] UA2 Collaboration, J. Alitti et al., Phys. Lett. B 241 (1990) 150; 276 (1992) 354.
[137] CDF Collaboration, F. Abe et al., Phys. Rev. Lett. 65 (1990) 2243.
[138] CDHS Collaboration, H. Abramowicz et al., Phys. Lett. B 241 (1990) 150;
CDHS Collaboration, A. Blondel et al., Z. Phys. C 45 (1990) 361.
[139] CHARM Collaboration, J.V. Allaby et al., Phys. Lett. B 177 (1986) 446; Z. Phys. C 36 (1987) 611.
[140] G. Sterman, Phys. Rev. D 17 (1978) 2773, 2789.
[141] S. Catani et al., Phys. Lett. B 263 (1991) 491; Average Number of Jets in e^+e^- Annihilation, CERN preprint CERN-TH.6328/91 (revised version);
S. Catani, G. Turnock and B.R. Webber, Phys. Lett. B 272 (1991) 368.
[142] J.C. Collins and D.E. Soper, Nucl. Phys. B 193 (1981) 381; 197 (1982) 446; 284 (1987) 253;
J. Kodaira and L. Trentadue, Phys. Lett. B 123 (1983) 335.
[143] K. Tesima and M.F. Wade, Z. Phys. C 52 (1991) 31.
[144] Y.L. Dokshitzer, D.I. Dyakonov and S.I. Troyan, Phys. Lett. 78 (1978) 290;
C.L. Basham et al., Phys. Rev. Lett. 41 (1978) 1585; Phys. Rev. D 17 (1978) 2298; 19 (1979) 2018.
[145] F. Csikor, G. Pócsik and A. Tóth, Phys. Rev. D 31 (1985) 1025;
F. Csikor et al., Phys. Rev. D 34 (1986) 129.
[146] G.C. Fox and S. Wolfram, Phys. Rev. Lett. 41 (1978) 1581; Nucl. Phys. B 149 (1979) 413; Phys. Lett. B 82 (1979) 134.
[147] L3 Collaboration, B. Adeva et al., Phys. Lett. B 248 (1990) 464.
[148] ALEPH Collaboration, D. Decamp et al., Phys. Lett. B 255 (1991) 623;
T. Lohse (ALEPH Collaboration), private communication (1991).
[149] J. Ellis, M.K. Gaillard and G.G. Ross, Nucl. Phys. 111 (1976) 253, 516 (Erratum);
A. de Rújula et al., Nucl. Phys. B 138 (1978) 387;
G. Sterman and S. Weinberg, Phys. Rev. Lett. 39 (1977) 1436.
[150] JADE Collaboration, W. Bartel et al., Z. Phys. C 33 (1986) 23;
JADE Collaboration, S. Bethke et al., Phys. Lett. B 213 (1988) 235.
[151] Y.L. Dokshitzer, Contribution to the Workshop on Jets at LEP and HERA, Durham (1990);
N. Brown and W.J. Stirling, Z. Phys. C 53 (1992) 629;
S. Catani et al., Phys. Lett. B 269 (1991) 432.
[152] S. Bethke et al., Nucl. Phys. B 370 (1992) 310.
[153] MARK II Collaboration, S. Komamiya et al., Phys. Rev. Lett. 64 (1990) 987.
[154] L. Clavelli, Phys. Lett. B 85 (1979) 111;
MARK II Collaboration, A. Peterson et al., Phys. Rev. D 37 (1988) 1;
TASSO Collaboration, W. Braunschweig et al., Z. Phys. C 45 (1989) 11.
[155] A. Ali and F. Barreiro, Phys. Lett. B 118 (1982) 155; Nucl. Phys. B 236 (1984) 269.
[156] D.G. Richards, W.J. Stirling and S.D. Ellis, Phys. Lett. B 119 (1982) 193; Nucl. Phys. B 229 (1983) 317.
[157] N.K. Falck and G. Kramer, Z. Phys. C 42 (1989) 459.
[158] DELPHI Collaboration, P. Abreu et al., Phys. Lett. B 252 (1990) 149;
K. Hamacher (DELPHI Collaboration), private communication (1991).
[159] ALEPH Collaboration, D. Decamp et al., Phys. Lett. B 257 (1991) 479.
[160] OPAL Collaboration, M.Z. Akrawy et al., Phys. Lett. B 252 (1990) 159.
[161] OPAL Collaboration, G. Azuelos, Measurement of α_s from Planar Triple-Energy Correlations in Hadronic Decays of the Z^0, OPAL internal note PN032, March 1991.
[162] OPAL Collaboration, S. Sanghera, A Measurement of $\alpha_s(M_Z)$ from C Planarity, Oblateness and Thrust at the Z^0 Peak, OPAL internal note PN033, April 1991.
[163] N. Magnoli, P. Nason and R. Rattazi, Phys. Lett. B 252 (1990) 271.
[164] T. Hebbeker, QCD at LEP/SLC, Aachen Report PITHA 91/11.
[165] S. Bethke, J. Phys. G 17 (1991) 1455; Tests of QCD at LEP, OPAL internal report OPAL-CR045 (1991).

[166] M. Schmelling (ALEPH Collaboration), private communication (1991).
[167] S. Bethke (OPAL Collaboration), private communication (1991).
[168] J. Ellis, D.V. Nanopoulos and D.A. Ross, Phys. Lett. B 267 (1991) 132.
[169] A. Pich, Hadronic τ Decays and QCD, CERN preprint CERN-TH-5940/90.
[170] W. Bernreuther and W. Wetzel, Nucl. Phys. B 197 (1982) 228.
[171] S. Narison and A. Pich, Phys. Lett. B 211 (1988) 183;
E. Braaten, Phys. Rev. D 39 (1989) 1458;
M.A. Samuel and L.R. Surguladze, Phys. Rev. D 44 (1991) 1602;
A. Pich, Tau Physics, CERN preprint CERN-TH.6237/91.
[172] E. Braaten, S. Narison and A. Pich, Nucl. Phys. B 373 (1992) 581.
[173] A.D. Martin, R.G. Roberts and W.J. Stirling, Phys. Rev. D 43 (1991) 3648; Phys. Lett. B 266 (1991) 173.
[174] M. Virchaux and A. Milsztajn, Phys. Lett. B 274 (1992) 221.
[175] UA2 Collaboration, J. Alitti et al., Phys. Lett. 263 (1991) 563;
M. Lindgren et al., Phys. Rev. D 45 (1992) 3038.
[176] W. Kwong et al., Phys. Rev. D 37 (1988) 3210.
[177] TASSO Collaboration, W. Braunschweig et al., Phys. Lett. B 138 (1984) 317.
[178] TASSO Collaboration, W. Braunschweig et al., Z. Phys. C 42 (1989) 17.
[179] TASSO Collaboration, W. Braunschweig et al., Z. Phys. C 44 (1989) 365.
[180] N. Magnussen (JADE Collaboration), Latest PETRA results on QCD, XX. International Symposium on Multiparticle Dynamics, Dortmund 1990, eds R. Baier and D. Wegener (World Scientific, Singapore, 1991) p. 273.
[181] L3 Collaboration, B. Adeva et al., Phys. Lett. B 271 (1991) 461.
[182] MARK II Collaboration, S. Bethke et al., Z. Phys. C 43 (1989) 325.
[183] TASSO Collaboration, W. Braunschweig et al., Phys. Lett. B 214 (1988) 286.
[184] AMY Collaboration, I.H. Park et al., Phys. Rev. Lett. 62 (1989) 1713.
[185] VENUS Collaboration, K. Abe et al., Phys. Lett. B 240 (1990) 232.
[186] MARK J Collaboration, B. Adeva et al., Phys. Rev. Lett. 50 (1983) 2051; 54 (1985) 1750;
CELLO Collaboration, H.-J. Behrend et al., Phys. Lett. B 138 (1984) 311;
TASSO Collaboration, M. Althoff et al., Z. Phys. C 26 (1984) 157;
MAC Collaboration, E. Fernandez et al., Phys. Rev. D 31 (1985) 2724;
PLUTO Collaboration, C. Berger et al., Z. Phys. C 28 (1985) 365;
TASSO Collaboration, W. Braunschweig et al., Z. Phys. C 36 (1987) 349;
MARK II Collaboration, D.R. Wood et al., Phys. Rev. D 37 (1988) 3091;
TOPAZ Collaboration, I. Adachi et al., Phys. Lett. B 227 (1989) 495.
[187] E. Laermann, K.H. Streng and P.M. Zerwas, Z. Phys. C 3 (1980) 289; to be published (Erratum);
K. Koller et al., Z. Phys. C 6 (1980) 131.
[188] N.M. Avram and D.H. Schiller, Nucl. Phys. B 70 (1974) 272;
A.C. Hirshfeld and G. Kramer, Nucl. Phys. B 74 (1974) 211;
G. Kramer, G. Schierholz and J. Willrodt, Phys. Lett. B 79 (1978) 249; 80 (1979) 433 (Erratum).
[189] G. Kramer, G. Schierholz and J. Willrodt, Z. Phys. C 4 (1980) 149.
[190] J.G. Körner and D.H. Schiller, Helicity Description of $e^+e^- \to q\bar{q}g$ and $e^+e^- \to Q\bar{Q}(1^{--}) \to ggg$ on and off the Z^0: Quark, Gluon and Beam Polarization Effects, DESY Report 81-043 (1981).
[191] J. Ellis and I. Karliner, Nucl. Phys. B 148 (1979) 141.
[192] OPAL Collaboration, G. Alexander et al, Z. Phys. C 52 (1991) 543.
[193] DELPHI Collaboration, P. Abreu et al., Phys. Lett. B 274 (1992) 498.
[194] TASSO Collaboration, W. Braunschweig et al., Z. Phys. C 47 (1990) 181.
[195] K. Koller and H. Krasemann, Phys. Lett. B 88 (1979) 119;
UA1 Collaboration, G. Arnison et al., Phys. Lett. B 136 (1984) 294;
UA2 Collaboration, P. Bagnaia et al., Phys. Lett. B 144 (1984) 283;
N. Artega-Romero, A. Nicolaidis and J. Silva, Phys. Rev. Lett. 52 (1984) 172.
[196] K.J.F. Gaemers and J.A.M. Vermaseren, Z. Phys. C 7 (1980) 81.
[197] J.G. Körner, G. Schierholz and J. Willrodt, Nucl. Phys. B 185 (1981) 365.
[198] O. Nachtmann and A. Reiter, Z. Phys. C 16 (1982) 45;
G. Rudolph, in: Physics at LEP, CERN Report CERN-86-02, Vol. II, p. 150.
[199] M. Bengtsson and P.M. Zerwas, Phys. Lett. B 208 (1988) 306.
[200] DELPHI Collaboration, P. Abreu et al., Phys. Lett. B 255 (1991) 466; Evidence for the Triple-Gluon Vertex by Measuring the Color-Factor, DELPHI note 91-52 PHYS 107, paper contributed to the Joint International Lepton-Photon Symposium and Europhysics Conference on High Energy Physics, Geneva, 1991.

[201] A. Duff and D. Zeppenfeld, Probing QCD via Four-Jet Decays of the Z^0 Boson, Madison preprint MAD/PH/651 (1991).
[202] S. Bethke, A. Ricker and P.M. Zerwas, Z. Phys. C 49 (1991) 59.
[203] L. Lerner Z. Phys. C 45 (1990) 399; 46 (1990) 489.
[204] L3 Collaboration, B. Adeva et al., Phys. Lett. B 248 (1990) 227.
[205] 181 OPAL Collaboration, M.Z. Akrawy et al., Z. Phys. C 49 (1991) 49.
[206] AMY Collaboration, I.H. Park et al., Phys. Rev. Lett. 62 (1989) 1713;
VENUS Collaboration, K. Abe et al., Phys. Rev. Lett. 66 (1991) 280;
R. Itoh, Recent Results from TRISTAN, Joint International Lepton-Photon Symposium and Europhysics Conference on High Energy Physics, Geneva, 1991.
[207] L. DiLella, Annu. Rev. Nucl. Part. Sci. 35 (1985) 107.
[208] A. Breakstone et al., Phys. Lett. B 248 (1990) 220.
[209] ALEPH Collaboration, D. Decamp et al., Testing the Non-Abelian Structure of QCD Based on Four-Jet Events – Evidence for the Triple Gluon Vertex, ALEPH internal note 91-84, June 1991.
[210] UA2 Collaboration, J.Alitti et al., Phys. Lett. B 277 (1992) 194.
[211] V. Khoze and L. Lönnblad, Phys. Lett. B 241 (1990) 123.
[212] D. Amati and G. Veneziano, Phys. Lett. B 83 (1979) 87;
G. Marchesini, L. Trentadue and G. Veneziano, Nucl. Phys. B 181 (1981) 335.
[213] Y.L. Dokshitzer and S.I. Troyan, Nonleading Perturbative Corrections to the Dynamics of Quark-Gluon Cascades and Soft Hadron Spectra in e^+e^- Annihilation, Leningrad preprint LNPI-922 (1984);
Y.I. Azimov et al., Z. Phys. C 27 (1985) 65; 31 (1986) 213.
[214] ALEPH Collaboration, D. Decamp et al., Phys. Lett. B 273 (1991) 181.
[215] DELPHI Collaboration, P. Aarnio et al., Charged Multiplicity and Rapidity Distributions in Z^0 Hadronic Decays, CERN preprint CERN-PPE/90-117;
DELPHI Collaboration, P. Abreu et al., Z. Phys. C 50 (1991) 185; 52 (1991) 271; Phys. Lett. B 276 (1992) 254.
[216] L3 Collaboration, B. Adeva et al., Phys. Lett. B 259 (1991) 199.
[217] OPAL Collaboration, P.D. Acton et al., Z. Phys. C 53 (1992) 535.
[218] S. Carius and G. Ingelman, Phys. Lett. B 252 (1990) 647;
R. Szwed, G. Wrochna and A.K. Wróblewski, Mod. Phys. Lett. A 5 (1990) 1851.
[219] Z. Koba, H.B. Nielsen and P. Olesen, Nucl. Phys. B 40 (1972) 317.
[220] DELPHI Collaboration, P. Abreu et al., Charged Particle Multiplicity of Quarks and Gluon Jets in Z^0 Hadronic Decays, DELPHI note 91-58 PHYS 113.
[221] A.H. Mueller, Nucl. Phys. B 213 (1983) 85; 228 (1983) 351.
[222] B.R. Webber, Phys. Lett. B 143 (1984) 501.
[223] E.D. Malaza and B.R. Webber, Phys. Lett. B 149 (1984) 501; Nucl. Phys. B 267 (1986) 702;
E.D. Malaza et al., Phys. Lett. B 266 (1991) 169.
[224] E.D. Malaza, Z. Phys. C 31 (1986) 143.
[225] K. Tesima, Phys. Lett. B 221 (1989) 91; 224 (1989) 450 (Erratum);
F. Cuypers and K. Tesima, Z. Phys. C 52 (1991) 69.
[226] AMY Collaboration, H.W. Zheng et al., Phys. Rev. D 42 (1990) 737.
[227] HRS Collaboration, D. Bender et al., Phys. Rev. D 34 (1986) 3304.
[228] JADE Collaboration, W. Bartel et al., Z. Phys. C 20 (1983) 187.
[229] PLUTO Collaboration, C. Berger et al., Phys. Lett. B 95 (1980) 313.
[230] TASSO Collaboration, W. Braunschweig et al., Z. Phys. C 45 (1989) 193.
[231] TPC Collaboration, H. Aihara et al., Phys. Lett. B 184 (1987) 299.
[232] TOPAZ Collaboration, I. Adachi et al., Phys. Lett. B 227 (1989) 495.
[233] B.R. Webber, private communication (1991).
[234] OPAL Collaboration, G. Alexander et al., Phys. Lett. B 264 (1991) 467.
[235] DELPHI Collaboration, P. Abreu et al., Phys. Lett. B 275 (1992) 231.
[236] C.P. Fong and B.R. Webber, Phys. Lett. B 229 (1989) 289; Nucl. Phys. B 355 (1991) 54.
[237] ALEPH Collaboration, D. Decamp et al., Measurement of Charged Particle Distributions Sensitive to QCD Coherence in Hadronic Z Decays, ALEPH internal note 91-103, July 1991.
[238] OPAL Collaboration, M.Z. Akrawy et al., Phys. Lett. B 247 (1990) 617.
[239] V.A. Khoze and Y.L. Dokshitzer, private communication (1991).
[240] Y.L. Dokshitzer et al., Rev. Mod. Phys. 60 (1988) 373.
[241] P. Mazzanti and R. Odorico, Nucl. Phys. B 370 (1992) 23.
[242] ARGUS Collaboration, H. Albrecht et al., Z. Phys. C 46 (1990) 15.

[243] CRYSTAL BALL Collaboration, C. Bieler et al., Z. Phys. C 49 (1991) 225.
[244] HRS Collaboration, D. Bender et al., Phys. Rev. D 31 (1985) 1.
[245] MARK II Collaboration, J.F. Patrick et al., Phys. Rev. Lett. 49 (1982) 1232.
[246] JADE Collaboration, W. Bartel et al., Z. Phys. C 28 (1985) 343;
JADE Collaboration, D.D. Pitzl et al., Z. Phys. C 46 (1990) 1.
[247] TASSO Collaboration, W. Braunschweig et al., Z. Phys. C 33 (1986) 13; 42 (1989) 189; 47 (1990) 187.
[248] R. Itoh, Recent Results from TRISTAN, Joint International Lepton-Photon Symposium and Europhysics Conference on High Energy Physics, Geneva, 1991.
[249] TPC Collaboration, H. Aihara et al., Z. Phys. C 28 (1985) 31;
TPC/Two-Gamma Collaboration, H. Aihara et al., Phys. Rev. Lett. 57 (1986) 945;
TASSO Collaboration, M. Althoff et al., Z. Phys. C 29 (1985) 29;
MARK II Collaboration, P.D. Sheldon et al., Phys. Rev. Lett. 57 (1986) 1398.
[250] B. Andersson, G. Gustafson and T. Sjöstrand, Phys. Lett. B 94 (1980) 211; Z. Phys. C 6 (1980) 235.
[251] Y.I. Azimov et al., Phys. Lett. B 165 (1985) 147; Yad. Fiz. 43 (1986) 147.
[252] T. Sjöstrand, QCD and Jets at LEP, Cargèse, 1990, eds M. Lévy et al., (Plenum Press, New York, 1991) p. 367.
[253] OPAL Collaboration, M.Z. Akrawy et al., Phys. Lett. B 261 (1991) 334.
[254] OPAL Collaboration, G. Alexander et al., Phys. Lett. B 265 (1991) 462.
[255] Y.L. Dokshitzer at al., Phys. Lett. B 245 (1990) 243.
[256] DELPHI Collaboration, P. Abreu et al., Interjet Correlations in Hadronic Jets from Z^0 Decays, DELPHI note 91-53 PHYS 108, paper contributed to the Joint International Lepton-Photon Symposium and Europhysics Conference on High Energy Physics, Geneva, 1991.
[257] B. Loerstad (DELPHI Collaboration), Charged Multiplicities and their Dependences Measured by DELPHI, Joint International Lepton-Photon Symposium and Europhysics Conference on High Energy Physics, Geneva, 1991.
[258] S.J. Brodsky and J.F. Gunion, Phys. Rev. Lett. 37 (1976) 402;
K. Shizuya and S.-H.H. Tye, Phys. Rev. Lett. 41 (1978) 787;
M.B. Einhorn and B.G. Weeks, Nucl. Phys. B 146 (1978) 445.
[259] A.H. Mueller, Nucl. Phys. B 241 (1984) 141;
J.B. Gaffney and A.H. Mueller, Nucl. Phys. B 250 (1985) 109.
[260] JADE Collaboration, W. Bartel et al., Phys. Lett. B 123 (1983) 460;
HRS Collaboration, M. Derrick et al., Phys. Lett. B 165 (1985) 449;
MARK II Collaboration, A. Petersen et al., Phys. Rev. Lett. 55 (1985) 1954;
TASSO Collaboration, W. Braunschweig et al., Z. Phys. C 45 (1989) 1;
AMY Collaboration, Y.K. Kim et al., Phys. Rev. Lett. 63 (1989) 1772.
[261] W. Kittel, Experimental Results on Intermittency, XX. International Symposium on Multiparticle Dynamics, Dortmund 1990, eds R. Baier and D. Wegener, (World Scientific, Singapore, 1991) p. 401.
[262] A. Białas, Theory of Intermittency, XX. International Symposium on Multiparticle Dynamics, Dortmund 1990, eds R. Baier and D. Wegener, (World Scientific, Singapore, 1991) p. 669.
[263] TASSO Collaboration, W. Braunschweig et al., Phys. Lett. B 231 (1989) 548.
[264] CELLO Collaboration, H.J. Behrend et al., Phys. Lett. B 256 (1991) 97.
[265] A. Białas and R. Peschanski, Nucl. Phys. B 273 (1986) 703; 308 (1988) 857.
[266] ALEPH Collaboration, D. Decamp et al., Z. Phys. C 53 (1992) 21.
[267] DELPHI Collaboration, P. Aarnio et al., Phys. Lett. B 247 (1990) 137.
[268] OPAL Collaboration, M.Z. Akrawy et al., Phys. Lett. 262 (1991) 351.
[269] ALEPH Collaboration, D. Decamp et al., Z. Phys. C 54 (1992) 75.
[270] DELPHI Collaboration, P. Abreu et al., Bose–Einstein Correlations at LEP, DELPHI note 91-57 PHYS 112, paper contributed to the Joint International Lepton-Photon Symposium and Europhysics Conference on High Energy Physics, Geneva, 1991.
[271] OPAL Collaboration, P.D. Acton et al., Phys. Lett. B 267 (1991) 143.
[272] S. Marcellini (OPAL Collaboration), Bose–Einstein Correlations in High Energy Collisions, Joint International Lepton-Photon Symposium and Europhysics Conference on High Energy Physics, Geneva, 1991.
[273] I. Bergström et al., Report of the Working Group on High Luminosity at LEP, CERN Report CERN-91-02, p. 182.
[274] M. Mjaed and J. Prorriol, Phys. Lett. B 217 (1989) 560.
[275] L.M. Jones, Phys. Rev. D 39 (1989) 2550; 42 (1990) 811.
[276] L. Lönnblad, C. Peterson and T. Rögnvaldsson, Nucl. Phys. B 349 (1991) 675; Phys. Rev. Lett. 65 (1990) 1321.
[277] Z. Fodor, Phys. Rev. D 41 (1990) 1726; Phys. Lett. 263 (1991) 305;
I. Csabai, F. Czakó and Z. Fodor, Phys. Rev. D 44 (1991) 1905; Nucl. Phys. B 374 (1992) 288.

[278] J. Pumplin, Variables for Distinguishing Between Quark Jets and Gluon Jets, Michigan preprint (1990); Phys. Rev. D 44 (1991) 2025.
[279] L. Bellantoni et al., Nucl. Instrum. Methods A 310 (1992) 618.
[280] Z. Fodor, Phys. Rev. D 40 (1989) 267.
[281] D. Michelsen, Angular Correlations of 4 Jets in e^+e^- Annihilation: Asymmetries and the 3-Gluon Vertex, DESY Report DESY 90-090.
[282] M. Bengtsson and T. Sjöstrand, Nucl. Phys. B 289 (1987) 810.
[283] A. Djouadi, F.M. Renard and C. Verzegnassi, Phys. Lett. B 241 (1990) 260.
[284] A. Pich, private communication (1991).
[285] G.B. West, Phys. Rev. Lett. 67 (1991) 1388.
[286] D.J. Miller et al., in: ECFA Workshop on LEP 200, CERN Report CERN-87-08, p. 202.
[287] A. Cordier and P.M. Zerwas, in: ECFA Workshop on LEP 200, CERN Report CERN-87-08, p. 242.
[288] K.G. Chetyrkin, A.L. Kataev and F.V. Tkachov, Phys. Lett. B 85 (1979) 277;
M. Dine and J. Sapirstein, Phys. Rev. Lett. 43 (1979) 668;
W. Celmaster and R.J. Gonsalves, Phys. Rev. Lett. 44 (1980) 560; Phys. Rev. D 21 (1980) 3112.
[289] L.S. Brown and L.G. Yaffe, Phys. Rev. D 45 (1992) 398;
D.T. Barclay and C.J. Maxwell, On a proposed Asymptotic Estimate on the n Loop Correction to the e^+e^- Total Hadronic Cross Section, Durham preprint DTP/91/72.
[290] J. Chyla, A. Kataev and S. Larin, Phys. Lett. B 267 (1991) 269.
[291] P. Zerwas, private communication (1991).
[292] S. Barshay, P. Heiliger and L.M. Sehgal, Z. Phys. C 49 (1991) 261.